Site U1345[1]

Expedition 323 Scientists[2]

Chapter contents

[1] Expedition 323 Scientists, 2011. Site U1345. *In* Takahashi, K., Ravelo, A.C., Alvarez Zarikian, C.A., and the Expedition 323 Scientists, *Proc. IODP,* 323: Tokyo (Integrated Ocean Drilling Program Management International, Inc.). doi:10.2204/iodp.proc.323.109.2011
[2] Expedition 323 Scientists' addresses.

Background and objectives

The primary objective of drilling at Integrated Ocean Drilling Program (IODP) Site U1345 (proposed Site NAV-1B; Takahashi et al., 2009) was to study high-resolution Holocene–late Pleistocene paleoceanography at a location proximal to the gateway to the Arctic Ocean at a water depth of ~1008 m. Site U1345 is located on an interfluve ridge near the large, broad head of the Navarin submarine channel off the Bering Sea shelf (Figs. F1, F2, F3, F4, F5) (Normark and Carlson, 2003). This site was anticipated to have had high fluxes of terrigenous sediment from the shelf during glacials and deglacials. This site is also in an area of high biological productivity known as the "Green Belt," which is formed by nutrients brought to the photic zone by tidal mixing and transverse circulation at the shelf edge and eddies in the Bering Slope Current (BSC). The BSC originates in the incoming Alaskan Stream water that flows through the western Aleutians into the Bering Sea (Taniguchi, 1984; Springer et al., 1996). Site U1345 is located at the center of the modern oxygen minimum zone (OMZ) and is expected to record past changes in OMZ intensity. Given high biogenic and terrigenous flux, sedimentation rates at this site are expected to be high, with intermittent millimeter to submillimeter laminations (see below), and future work should allow for the reconstruction of detailed climate change on submillennial timescales. This record can then be compared with high-resolution records from Ocean Drilling Program (ODP) Sites 893 (Santa Barbara Basin) and 1002 (Cariaco Basin) and the Greenland Ice Sheet Project 2 (GISP2). Site U1345 provides the northernmost constraint on the vertical structure of watermasses in the Aleutian Basin in relation to the sites at Bowers Ridge and Umnak Plateau.

Site U1345 is located close to the maximum extent of present-day seasonal sea ice cover. Thus, this site is sensitive to changes in seasonal and perennial sea ice cover during glacial–interglacial cycles. Because of its proximity to the location of sea ice formation and brine production, this site, as well as IODP Site U1344, may provide crucial information regarding the formation of intermediate or deep watermasses in the Bering Sea in the past.

Site U1345 has high surface-ocean productivity and can also be used to study the impact of subseafloor microbes on biogeochemical fluxes. Organic carbon–fueled respiration and its impact on sediment geochemistry in such a highly productive region have not previously been quantified. Sediments from this site can also

doi:10.2204/iodp.proc.323.109.2011

be used to investigate the link between subseafloor microbial communities and export production from the surface ocean (Takahashi et al., 2000).

Reports of sedimentation rates at this site vary significantly, ranging from 14 cm/k.y. during the Holocene and 91 cm/k.y. during the Last Glacial Maximum (LGM) to as much as 242 cm/k.y. during the last deglaciation (Cook et al., 2005). Thus, before drilling, we expected to recover sections from the Holocene to late Pleistocene.

Operations

Five holes were cored at Site U1345 (Table T1). With the exception of Hole U1345B, which was cored for microbiological sampling to 36.7 m drilling depth below seafloor (DSF), four holes were cored to ~150 m DSF. A complete set of site-specific tide tables was provided by the science party to make coring adjustments relative to the initial mudline core and each successive core in each hole. Coring was generally routine, except for encountering biogenic methane in the cores, which complicated the curation of all cores at this site. Two complete splices were obtained at Site U1345 to ~150 meters below seafloor (mbsf). Advanced piston corer (APC) coring for Site U1345 totaled 68 cores, 632.1 m penetrated, and 648.65 m recovered, for 102.6% core recovery. The time spent at Site U1345 was 2.2 days.

Hole U1345A

Hole U1345A was spudded at 0045 h on 23 August 2009 (all times are ship local time, Universal Time Coordinated [UTC] – 11 h). The first APC core barrel recovered 4.39 m of sediment, establishing the seafloor depth at 1019.1 m drilling depth below rig floor (DRF). APC coring using nonmagnetic coring assemblies continued through Core 323-U1345A-16H to 146.9 m DSF. Temperature measurements were taken on Cores 323-U1345A-5H, 8H, and 12H with the third-generation advanced piston corer temperature tool (APCT-3). APC core recovery for Hole U1345A was 101.1%, with 148.24 m recovered.

Hole U1345B

The ship was offset 20 m northwest of Hole U1345A. Both perfluorocarbon tracer (PFT) and microspheres were deployed for contamination testing. Four APC cores were recovered to 36.7 m DSF for use as microbiology samples. Average APC core recovery for Hole U1345B was 105.7%, with 38.79 m of sediment recovered.

Hole U1345C

The ship was offset 20 m northwest of Hole U1345B. APC coring using nonmagnetic coring assemblies continued through Core 323-U1345C-16H to 148.5 m DSF. APC core recovery for Hole U1345C was 102.9%, with 152.85 m recovered.

Hole U1345D

The ship was offset 20 m northwest of Hole U1345C. APC coring using nonmagnetic coring assemblies continued through Core 323-U1345D-16H to 150.0 m DSF. APC core recovery for Hole U1345D was 103.1%, with 154.62 m recovered.

Hole U1345E

The ship was offset 20 m northwest of Hole U1345D. APC coring using nonmagnetic coring assemblies continued through Core 323-U1345E-16H to 150.0 m DSF. APC core recovery for Hole U1345E was 102.8%, with 154.15 m recovered.

Lithostratigraphy

Five holes were cored at Site U1345, reaching a maximum depth of 150.89 mbsf in Hole U1345E. The sediments at this site are primarily siliciclastic with varying amounts of diatoms and minor amounts of foraminifers and calcareous nannofossils. Authigenic carbonates occur frequently at this site in all holes deeper than 30 mbsf. The sediments are predominantly dark/very dark gray and dark/very dark greenish gray. One lithologic unit spanning the middle Pleistocene to the Holocene was defined at this site.

Description of unit

Unit I

Intervals: Sections 323-U1345A-1H-1, 0 cm, through 16H-CC, 58 cm; 323-U1345B-1H-1, 0 cm, through 4H-CC, 24 cm; 323-U1345C-1H-1, 0 cm, through 16H-CC, 34 cm; 323-U1345D-1H-1, 0 cm, through 16H-CC, 42 cm; and 323-U1345E-1H-1, 0 cm, through 16H-CC, 55 cm

Depths: Hole U1345A, 0–147.43 mbsf; Hole U1345B, 0–35.26 mbsf; Hole U1345C, 0–148.53 mbsf; Hole U1345D, 0–150.51 mbsf; and Hole U1345E, 0–150.89 mbsf

Age: mid-Pleistocene to Holocene

The lithologies at this site are mostly diatom-rich and diatom-bearing siliciclastic sediments, with frequent thinly laminated to thinly bedded 5–40 cm thick intervals that characterize ~10% of the sediments collected at this site (Figs. F6, F7, F8, F9). The

siliciclastic sediments are mostly diatom-rich clayey silt, diatom-bearing sandy silt/silty clay/silt and silt/sandy silt/silty clay (see **"Site U1345 smear slides"** in "Core descriptions"). The sediments range in color from very dark greenish gray (10Y 3/1 and 5GY 3/1) and dark greenish gray (5GY 4/1) to dark gray (4/N) and very dark gray (3/N). The laminated/thinly bedded sediments typically are composed of alternating lithologies and layers that contain a higher fraction of diatoms. In general, the laminated/thinly bedded intervals have higher abundances of foraminifers and calcareous nannofossils than nonlaminated sediments. The lithologies consisting of laminations/thin beds are commonly diatom-bearing silty clay/clayey silt, diatom-rich silty/clayey silt, and diatom ooze.

In the main lithologies, the siliciclastic fraction is primarily composed of quartz, feldspar, rock fragments, and clay minerals (see **"Site U1345 smear slides"** in "Core descriptions"). Millimeter- to centimeter-scale pyrite mottles and specks are frequent, particularly in sediments with high proportions of biogenic grains. In smear slides, pyrite often appears as framboids within and among diatom frustules. The abundance of foraminifers and calcareous nannofossils is generally <10%. There are numerous sandy patches and layers at Site U1345.

The transitions between lithologies are gradational, and the color changes are subtle. The boundaries between laminated and nonlaminated sediment are often gradational, although sharp boundaries at the base of laminated intervals were also observed. The contacts between individual thin laminae are mostly sharp, but contacts in thin-bedded lithologies often have gradational boundaries.

In the laminated portions there are three small intervals of soft-sediment deformation characterized by folded or truncated laminations: intervals 323-U1345A-13H-7, 115–121 cm; 323-U1345D-6H-2, 85–96 cm; and 323-U1345D-1H-3, 99–105 cm (Fig. **F10**). Note that possible soft-sediment deformation in massive, homogeneous sediment could not be easily detected because of the lack of structures.

The induration of sediments at Site U1345 is soft throughout, with the exception of one hard dolostone layer in interval 323-U1345A-5H-5, 130–137 cm. The original sediment fabric, consisting of thin laminations, is preserved in the dolostone. The sediment above and below the dolostone is thinly laminated as well.

The laminated and thinly bedded intervals that occur at this site can be correlated between Holes U1345A, U1345C, U1345D, and U1345E based on visual observations, reflectance, and magnetic susceptibility data (Fig. **F11**). Most laminations and thin bedding include diatom-rich lithologies; however, several laminated intervals include only alternations of siliciclastic lithologies. The former intervals are often associated with lower magnetic susceptibility, lower density, lower natural gamma radiation (NGR), and higher values of color reflectance parameter b*. The siliciclastic-rich laminations are also associated with lower magnetic susceptibility but not with other coherent changes in physical properties.

Bioturbation is slight to moderate throughout the cores, except for some laminated intervals in which bioturbation is absent. The transitions between sediments with different colors or textures sometimes have centimeter-scale mottling and are occasionally gradational. In general, millimeter- to centimeter-scale mottles composed of pyrite or sand occur throughout the site and probably represent filled bioturbation burrows.

Subrounded to well-rounded granule- to pebble-sized clasts occur frequently at Site U1345. There are no patterns in the frequency or clustering of clasts in any of the holes. The sediments at Site U1345 contain the highest proportion of sand observed during Expedition 323.

Ash is less common at this site than at sites farther south. However there are thin ash layers in Holes U1345A, U1345C, and U1345D, in addition to ash-filled mottles. A 2 cm × 6 cm subvertical ash layer at interval 323-U1345A-1H-2, 0–10 cm, can be correlated to a 2 cm × 2 cm ash plug at the top of interval 323-U1345C-1H-2, 0–10 cm. In the latter, the majority of the tilted ash layer is in the working half of the split core. This ash is not present in Hole U1345D because coring began deeper than the ash layer. Core 323-U1345E-1H was not split in order to preserve it for shore-based whole-round analysis. The ash is denser and firmer than the surrounding very soft sediment, which probably accounts for its tilting during splitting or coring. Two other thin, light gray to white, disseminated, bioturbated ash layers occur. One is found only in Core 323-U1345C-12H; the other is found in Cores 323-U1345D-14H and 323-U1345E-14H.

Finely disseminated authigenic carbonates occur frequently at Site U1345 below 30 mbsf. Euhedral crystal shapes such as rhombs, acicular crystals, and globular crystals with extreme birefringence are usually 4–10 µm long but reach 50 µm in some of samples. The sediment containing authigenic carbonates tends to be slightly lighter or more yellowish in color than the surrounding sediment. Authigenic carbonates occasionally occur in laminated sediments.

A mold of a tube worm colony was found in interval 323-U1345C-16H-3, 105–118 cm, surrounded by authigenic carbonate–rich sediments (Fig. F12). The tube walls appear to have originally been flexible, as evidenced by the partial collapse of some tubes. Thin section petrographic analysis suggests that the tube walls could have been remineralized to a partially amorphous material with low birefringence that extinguishes parallel to the tube walls. X-ray diffraction (XRD) analysis of a decalcified sample (see XRD in "Supplementary material") shows the presence of amorphous silica, which may be the mineral that composes the tube walls. The cavities within the mold have been filled by diatom clayey silt. Sparry calcite (possibly siderite; Fig. F12C) precipitates from the tube walls toward the center of the cavities. The tube walls, the sediment in the cavities, and the sparry calcite are completely or partially replaced by a mosaic of very fine (<5 µm) carbonate rhombs (possibly dolomite).

The presence of gas in the sediments caused several types of coring disturbance that affect stratigraphic integrity. Sediment at the top or bottom of the cores below Cores 323-U1345A-7H, 323-U1345C-6H, 323-U1345D-5H, and 323-U1345E-5H was ejected out of the core barrel by gas expansion; 20–150 cm of sediment was extruded onto the rig floor. This sediment was pushed back into a core liner; however, some sediment pieces may be out of order or upside down. Punctures were made in Core 2H and in every core thereafter for all holes, potentially causing a significant loss of sediment from extrusion. Punctures were not always noted in core descriptions because they were not always visible on the cut surface of the core. Numerous cracks and voids occur in all holes between 5 and 20 mbsf and deeper. In addition, wafers of sediment between wide voids were broken and jumbled during core splitting. The resulting gaps affected the measurements of physical properties (gamma ray attenuation [GRA] bulk density, in particular) and color reflectance.

Discussion

Unit I spans the mid-Pleistocene to Holocene. As such, it corresponds to the upper portion of Unit I at other sites, which includes sediments deposited since the early Pleistocene. Site U1345 is distinct among the near-shelf sites because of the abundance and generally coarser texture of the siliciclastic component in the sediments as well as the higher frequency of laminated intervals. Intervals characterized by >25% sand and thin sandy layers occur at all depths in all holes drilled at this site. The laminations and thin-bedded sediments are numerous and well correlated between holes.

Site U1345 is located in the central portion of the modern OMZ. As such, the sediments deposited at this site can provide important information concerning Pleistocene to Holocene variability of bottom water oxygen concentrations. The preservation of laminated and thinly bedded sediments (beds <10 cm in thickness) could be interpreted to result from a reduction in or cessation of the activity of benthic macrofauna as a result of low oxygen concentrations in the bottom waters and surface sediments. Hereafter, references to "laminations" or "laminated intervals" include these thin beds.

Laminations do not have a clear signature in the physical properties or color reflectance data (Figs. F6, F7, F8, F9) like that observed at Site U1342. This is probably because of the dominant presence of the siliciclastic fraction and the fact that the relatively small changes in the relative proportion of biogenic grains have a smaller influence on physical properties and color than they do at sites with more drastic lithologic contrasts between laminated and nonlaminated intervals.

The laminated intervals can be divided into two categories based on the abundance of biogenic grains:

1. Couplets or triplets of diatom oozes, mixed siliciclastic/biogenic sediments, and siliciclastic sediments; or
2. Couplets of siliciclastic sediments of alternating textures that may include minor (<40%) amounts of diatoms (Fig. F13; see "Site U1345 smear slides" in "Core descriptions").

Laminated sediments of the first category are similar to laminated intervals at other sites, which are typically biogenic rich and olive-green, dark olive-gray, or very dark greenish gray. This category of lamination seems to occur mainly during interglacials (Fig. F11). This relationship supports previous observations of a higher flux of diatoms during interglacials than during glacial periods (Okazaki et al., 2005). The variable bottom water oxygen concentrations are probably influenced by the magnitude of the export production and the associated consumption of oxygen by organic matter remineralization, in addition to changes in the ventilation of intermediate watermasses.

The second category of laminated sediments is mainly siliciclastic and is unique to Site U1345. This type of lamination occurs in sediments that are tentatively identified as having been deposited during glacial conditions (Fig. F13). Because these sediments are not biogenic rich, changes in intermediate water ventilation may have been the controlling parameter for bottom water oxygen concentrations during these periods. Detailed reconstructions of productiv-

ity and export production as well as ocean circulation proxy records will be required to elucidate the mechanisms responsible for the fluctuations in OMZ intensity and position that occurred in the past.

Intermittent finely disseminated authigenic carbonates are present in sediment below ~30 mbsf in all holes at this site. The sulfate–methane transition zone (SMTZ) is at ~6.5 mbsf, the shallowest observed during Expedition 323 (see **"Geochemistry and microbiology"**). Calcium and magnesium concentrations in the pore water decrease toward the SMTZ, suggesting active authigenic carbonate precipitation at and below this depth today (see **"Geochemistry and microbiology"**). Smear slide analysis indicates the presence of authigenic carbonate crystals large enough to be identified at relatively low magnification (400×). Therefore, it is possible that carbonate crystals <2–4 µm were not observed and recorded, even if they were present.

Sediment intervals containing authigenic carbonates are subtly paler or more yellowish in color than the surrounding sediment; however, authigenic carbonates were observed in smear slides even in sediments without an obvious color change. Therefore, it is likely that the occurrence of authigenic carbonates was underestimated, and further study of the mineralogical and isotopic composition of the sediment will be required to comprehensively determine the distribution of authigenic minerals. The remineralized and dolotomized tube worm colony may be evidence of a methane cold seep if it is found to be of a type that generally has chemosynthetic symbionts and/or is found near cold seeps today (e.g., Vanreusel et al., 2009).

In several cases, authigenic carbonates were observed in laminated intervals (Fig. **F13**). The authigenic carbonates do not appear to preferentially occur in laminations, but they are associated with laminated sediments that are tentatively estimated as having been deposited during marine isotope Stage (MIS) 5 (Fig. **F13**). A bulk sediment carbonate measurement taken in the MIS 5 interval is the highest $CaCO_3$ measurement recorded at this site (see **"Geochemistry and microbiology"**).

Few ash layers were observed at Site U1345, but the ash that occurs is light colored, suggesting that its source is explosive rhyolitic volcanism. This site is distant from the nearest likely source of volcaniclastic grains, the Aleutian arc, so the transport mechanism must have been one capable of widespread dissemination.

The lithologies at Site U1345 are sandier than those at any other site from Expedition 323. Lithologies with >25% sand (Figs. **F6, F7, F8, F9**) and thin sandy layers occur throughout all holes. The presence of this coarse material is probably related to the position of Site U1345 at the crest of an interfluve at the mouth of Navarin Canyon. In contrast, other sites on the continental slope, Sites U1343 and U1344, are more distant from the mouths of major canyons that intersect the shelf. Sand deposition at these latter two sites may be limited to large, singular mass movement events. The proximity of Site U1345 to the center of the canyon may allow for the deposition of sediment being transported downslope.

The siliciclastic grain sizes at Site U1345 contrast even more strongly with those from Site U1339, located on a submarine plateau isolated from the continental shelf. Virtually no sand-sized grains were recorded at Site U1339. This may be due to either less transport of terrigenous material to the site or a high biogenic flux to Site U1339 sediments.

Biostratigraphy

Diatoms dominate the microfossil assemblage; however, diatom abundance and preservation are relatively variable, with high to moderate abundance and good to poor preservation. Other siliceous microfossils, radiolarians, and silicoflagellates are also present throughout, with low abundance and poor preservation. These fossils are mainly composed of high-latitude pelagic species, indicating changes to surface water productivity. Core catcher samples from Site U1345 contain well-preserved assemblages of calcareous microfossils throughout the majority of the section (0–168 m core composite depth below seafloor [CCSF-A]). The diversity of planktonic foraminifers and calcareous nannofossils is relatively low, as expected in high-latitude regions, and is consistent with all other sites. Benthic foraminifer diversity is high and consists of calcareous species associated with oxygen-limited environments. Organic-walled microfossils are present in high abundances and have very good preservation. Dinoflagellate assemblages indicate changes between low and high primary productivity, together with generally low sea-surface temperatures (SST) and short seasonal sea ice coverage. Six biostratigraphic datum events based on radiolarians, diatoms, and silicoflagellates reveal a relatively high average sedimentation rate of ~30 cm/k.y. and an age of ~0.5 ± 0.1 Ma for the base of the section (Fig. **F14;** Table **T2**).

Calcareous nannofossils

The abundance and state of preservation of calcareous nannofossils at Site U1345 were assessed by examining all core catcher samples from Holes U1345A–U1345D and by performing additional ob-

servations of laminated intervals on smear slides from the sedimentology collection (Table T3). The abundances of specific age-marker taxa were also evaluated. Calcareous nannofossils are generally rare or absent in the samples, but they are common to abundant at some horizons (Fig. F15), particularly in samples corresponding to laminated intervals, which are interpreted as belonging to interglacial periods (see "Lithostratigraphy"). Their preservation ranges from good to moderate, with only Sample 323-U1345D-12H-CC containing poorly preserved calcareous nannofossils. Both *Coccolithus pelagicus* and small gephyrocapsids are present throughout the sequence, with the former dominating the assemblage in the topmost samples (Samples 323-U1345A-1H-CC and 323-U1345C-1H-CC, plus additional samples from Cores 323-U1345A-1H and 2H) and the latter being more common in the lower levels that contain abundant calcareous nannofossils. *Coccolithus braarudii*, *Calcidiscus leptoporus* (medium and small forms), medium-sized gephyrocapsids, and *Emiliania huxleyi* are also present. *Emiliania huxleyi* is present in both the large (>4 µm) and small (<4 µm) varieties and is dominant in Sample 323-U1345A-1H-CC.

The presence of *E. huxleyi* in the topmost intervals of Holes U1345A–U1345C (Samples 323-U1345A-1H-CC and 2H-CC, 323-U1345B-1H-CC, and 323-U1345C-1H-CC) allows the assignment of those samples to calcareous nannofossil Zone NN21 (Martini, 1971), which ranges from the first occurrence (FO) datum of this species at 0.29 Ma to the present (Lourens et al., 2004). Barren samples and low calcareous nannofossil abundances prevent the assignment of this FO datum to a specific depth; however, the proposed age model based on other datums (Fig. F14) indicates that the distribution of *E. huxleyi* at Site U1345 seems to reflect its acme interval rather than its occurrence record.

No other biostratigraphic marker species were observed at Site U1345. The absence of *Pseudoemiliania lacunosa* in the bottom samples may indicate an age younger than 0.44 Ma for the oldest sediments at this site. However, other evidence (see "Lithostratigraphy" and "Paleomagnetism") indicates that the recovered sequence surpasses this age, which shows that the distribution of this species in this area might be hampered by environmental factors. More detailed shore-based study is needed to assess this datum.

Planktonic foraminifers

The distribution of planktonic foraminifers (>125 µm) was studied in all core catcher samples from Holes U1345A–U1345D (Table T4). The mudline sample from the top of Core 323-U1345D-1H was also analyzed. The late Quaternary fauna at Site U1345 is dominated by *Neogloboquadrina pachyderma* (sinistral), and, in general, there is a high abundance of well-preserved but commonly yellow-stained planktonic foraminifers at this site. *Neogloboquadrina pachyderma* (sinistral) is a polar species that also dominates modern-day faunas in the Bering Sea (Asahi and Takahashi, 2007). Additional species found in the late Quaternary include the subpolar species *Globigerina bulloides*, *Globigerina umbilicata*, and *Neogloboquadrina pachyderma* (dextral), which appear in low numbers. Samples 323-U1345A-1H-CC, 5H-CC, and 13H-CC contain faunas with an elevated content of subpolar species, with *G. bulloides* being the most frequent. This also applies to Samples 323-U1345C-1H-CC, 4H-CC, and 9H-CC and 323-U1345D-1H-CC. All samples contain siliciclastic grains in varying amounts (few to dominant). Pyrite and mica were also observed in the samples.

Benthic foraminifers

More than 40 species of benthic foraminifers were recovered in 49 samples from Holes U1345A–U1345D (Tables T5, T6, T7). The faunal composition shows no long-term change or trend over the cored interval and is therefore designated as one assemblage characterized by generally medium diversity (typically 8–12 species per sample) and high abundance (typically dominant to abundant), with persistently high occurrences of the species *Bulimina* aff. *exilis*, *Uvigerina* cf. *peregrina*, and *Globobulimina pacifica*. Other common and persistent species include *Cassidulinoides tenuis*, *Elphidium* cf. *batialis*, *Brizalina earlandi*, *Epistominella pulchella*, *Islandiella norcrossi*, *Nonionella labradorica*, and *Valvulineria* sp. The dominance of deep and shallow infaunal species fluctuates, and this is most likely related to changes in the extent of bottom water oxygen concentrations in association with changes to surface water productivity and/or deepwater ventilation.

The species composition is similar to that found in the modern OMZ of the Sea of Okhotsk (Bubenshchikova et al., 2008). Moreover, this site is located within the modern OMZ, and mudline samples contain the majority of species found downcore, supporting our low oxygen interpretation (Table T7). As at previous sites in the Bering Sea, faunal composition exhibits large changes in species dominance within the assemblage (Fig. F14). These changes are interpreted to be responses to changes in local oxygen concentration associated with productivity and/or deepwater ventilation shifts.

Ostracodes

All core catcher samples were examined for the presence of ostracodes, but only one specimen of the genus *Cytheropteron* was found in Sample 323-U1345D-11H-CC (Table T7).

Diatoms

Diatom biostratigraphy is based on the analysis of core catcher samples from each core from Holes U1345A, U1345C, U1345D, and U1345E. The depth positions and age estimates of biostratigraphic marker events are shown in Figure F14 and Tables T8, T9, T10, and T11. Diatom preservation is poor to good in all holes, and abundance is common to very abundant throughout this late Pleistocene record.

In Holes U1345A, U1345C, and U1345D, the last occurrence (LO) of *Proboscia curvirostris* and the LO of *Thalassiosira jouseae* were observed in Samples 323-U1345A-8H-CC (66.25 mbsf), 323-U1345C-8H-CC (67.7 mbsf), and 323-U1345D-8H-CC (69.8 mbsf), giving an age of 0.3 Ma (Barron and Gladenkov, 1995; Yanagisawa and Akiba, 1998). This depth is consistent with nearby gateway Site U1343. In Hole U1345E, *T. jouseae* was observed in abundance in Sample 323-U1345E-9H-CC (79.74 mbsf); however, *P. curvirostris* is absent until Sample 323-U1345E-10H-CC (89.1 mbsf), which may be related to preservation issues.

In general, diversity is lower at this site than at the other gateway sites. The diatom assemblage for this zone (NPD11) is dominated by *Thalassiosira antarctica* spores, *Fragilariopsis* spp., *Paralia sol*, *Paralia sulcata*, *Thalassiothrix longissima*, *Thalassionema nitzschioides*, *Thalassiosira latimarginata* s.l., and, to a lesser extent, *Neodenticula seminae*, *Bacteriosira fragilis*, and *Actinocyclus curvatulus*.

The cored interval above the LO of *P. curvirostris* was assigned to *N. seminae* Zone NPD12. This zone is dominated by *T. antarctica* spores, *T. latimarginata* s.l., *P. sulcata*, *Thalassiosira hyalina*, and *B. fragilis*, with *N. seminae* and *A. curvatulus* having minor presence. In general, this site has a higher proportion of coastal neritics and freshwater species than the other gateway Sites U1343 and U1344.

Silicoflagellates and ebridians

Silicoflagellate and ebridian counting was conducted in Hole U1345A (Table T12). The youngest datum, LO of *Distephanus octonarius* (0.2–0.3 Ma), is estimated to occur in Core 323-U1345A-9H (71.11–80.64 mbsf). *Distephanus speculum* is dominant in all counted samples except Sample 323-U1345A-16H-CC (147.33–147.43 mbsf), which contains many *Distephanus medianoctisol* specimens. Ebridians were not found in any sample slides.

Radiolarians

Radiolarian biostratigraphy is based on the analysis of core catcher samples from Holes U1345A–U1345E. Radiolarian zones at Site U1345 could not be established because *Stylatractus universus* is absent. Four radiolarian datums derived from the subarctic Pacific were identified at this site (Table T13). The LOs of *Lychnocanoma nipponica sakaii* (50 ka) and *Spongodiscus* sp. (280–320 ka) are well determined by their abundant occurrences. In contrast, the LOs of *Amphimelissa setosa* (70–90 ka) and *Axoprunum aquilonium* (250–410 ka) are supported only by seldom occurrences, making precise stratigraphic datums difficult. Estimated sedimentation rates between the LOs of *L. nipponica sakaii* and *Spongodiscus* sp. are ~25 cm/k.y. in each hole.

Radiolarian abundances and preservation are shown in Table T14. Total radiolarian abundances are few to common throughout the cores. Radiolarian preservation is generally moderate. The radiolarian assemblage at Site U1345 is composed mainly of typical subarctic Pacific species such as *Ceratospyris borealis*, *Cycladophora davisiana*, *L. nipponica sakaii*, *Spongodiscus* sp., *Spongotrochus glacialis*, *Stylodictya validispina*, and *Stylochlamydium venustum*. Among these species, the relative abundance of *C. davisiana* fluctuates greatly, possibly in relation to ventilation changes with glacial–interglacial cycles. *Sphaeropyle langii-robusta* group, which is commonly found at Sites U1343 and U1344, has very low abundances. Because the abundances of *S. langii-robusta* group at shallower sites (U1339, U1340, and U1342) are also very low, their dwelling depth might be in deep water below ~1000 m.

Palynology: dinoflagellate cysts, pollen, and other palynomorphs

Core catcher samples from Holes U1345A and U1345C and the mudline sample from Hole U1345B were analyzed for their palynological content (Table T15). Moderately to well-preserved palynomorphs were encountered in all samples. Terrestrial palynomorphs, including pollen grains, spores of pteridophytes, and phycoma of prasinophytes, occur throughout the cores in variable numbers. *Picea* and *Sphagnum* are the most dominant palynomorphs among pollen and spores. Their concentrations are usually >500 grains/cm^3, with variability throughout the sequence.

The concentration of dinoflagellate cysts is highly variable but is usually >1000 cysts/cm^3 (Fig. F16). Di-

nocyst assemblages are composed mainly of heterotrophic-related dinocysts. Eighteen taxa were recorded, but only *Brigantedinium* spp. and *Islandinium minutum* occur in significant numbers, and they dominate the assemblages throughout. The composition of dinoflagellate cyst assemblages is modern in character, suggesting a Pleistocene age for all analyzed samples.

Discussion

High-frequency variation can be seen in the abundance and composition of all microfossil groups. Figures **F15, F16,** and **F17** are marked with shaded boxes at the approximate locations of what appear to be distinct interglacials (~5, 40, 130, and 145 m CCSF-A). This locations are based on the reduction in sea ice diatoms, the increase in dinoflagellates, planktonic foraminifers, and calcareous nannofossil abundances, the increase in the open ocean diatoms *Neodenticula* and *Actinocyclus* spp., and the increase in the high-productivity dinoflagellate *I. minutum* and the associated low-oxygen benthic foraminifer *B.* aff. *exilis*. These intervals also coincide with lower GRA bulk density and are consistent with the age model.

Overall, calcareous nannofossil abundance at Site U1345 (Fig. **F15**) seems to follow glacial–interglacial cyclicity (with higher numbers during interglacials) and generally appears to reflect environmental factors such as temperature and nutrients rather than an overprinted diagenetic signal. Calcareous nannofossils do not proliferate in areas of sea ice.

Elevated contents of subpolar planktonic foraminifer species, including *G. bulloides*, appear at ~5, 40, 90, 130, and 145 m CCSF-A, largely coinciding with the interglacials defined (Fig. **F15**). This reveals increased SST during these intervals because *G. bulloides* is controlled by temperature rather than food availability in the Bering Sea (Reynolds and Thunell, 1985; Asahi and Takahashi, 2007). These periods of elevated SST probably reflect interglacial conditions.

As at previous sites in the Bering Sea, the benthic foraminifer faunal composition shows large changes in species dominance within the assemblage (Tables **T5, T6, T7**). These changes are interpreted as responses to shifts in local oxygen concentration associated with productivity and/or deepwater ventilation. *Bulimina* aff. *exilis* is generally regarded as a low-oxygen/deep infaunal species (e.g., Kaiho, 1994; Bubenshchikova et al., 2008) and occurs in samples associated with high productivity and low sea ice. This suggests that higher productivity during some interglacials caused an expanded, more intense OMZ. Deepwater ventilation may also affect these faunas.

Among all radiolarian species, *C. davisiana* has the highest fluctuations in abundance, possibly related to ventilation changes with glacial–interglacial cycles (Ohkushi et al., 2003).

Low proportions of sea ice diatoms and high proportions of open water diatoms correspond well to the interglacial horizons (Fig. **F17**). In general, this site has a higher proportion of coastal neritic and freshwater species than the other gateway Sites U1343 and U1344. These coastal benthic and freshwater species are regarded as endemic to sea ice and are not a factor of continental run-off and subsequent lateral transport. Several of the species found at Site U1345 have been documented in sea ice from the Chukchi Sea (Von Quillfeldt et al., 2003). Horner (1985) found that these species formed an inverted ecosystem, living in pockets within the ice or attaching themselves to the ice strata.

The dinoflagellate species *Brigantedinium* spp. is one of the most ubiquitous taxa among protoperidinials, and its distribution in modern sediments is closely related to primary productivity in temperate regions such as the northeastern Pacific margins (e.g., Radi and de Vernal, 2004). However, it is also abundant in polar and subpolar regions of the North Atlantic and Arctic oceans, where seasonal sea ice coverage occurs (Rochon et al., 1999). *Islandinium minutum* is one of the principal, if not dominant, components of assemblages in the modern Arctic Ocean (Rochon et al., 1999; Head et al., 2001). It has been found to be very abundant in polar upwelling zones such as the North Water Polynia (Hamel et al., 2002). The overall abundance of dinocysts, and particularly the above-mentioned species, suggests high productivity and upwelling during strong interglacials. Dinocyst abundance also increases from 80 m CCSF-A to the top of the sequence. The extremely high abundance of dinocysts, especially in Samples 323-U1345B-Mudline and 323-U1345A-5H-CC (44.4 m CCSF-A) and Core 323-U1345A-13H (130.6 m CCSF-A), suggests interglacial periods. High dinocyst abundance coincides with relatively low pollen and spore concentrations. Such low terrestrial contribution during these intervals could be due to several mechanisms, including changes in sea level that drastically affected the proximity of land, changes in vegetation in source areas, and changes in the strength and pattern of atmospheric/oceanic circulation trajectories.

Paleomagnetism

The archive halves of all cores recovered at Site U1345 were measured on the three-axis cryogenic magnetometer at 2.5 cm intervals. Natural remanent magnetization (NRM) was measured before (NRM

step) and/or after (demagnetization step) stepwise alternating-field (AF) demagnetization in peak fields up to 20 mT. All cores from Hole U1345A and Cores 323-U1345C-1H through 7H were measured at NRM step and 20 mT demagnetization step; other Site U1345 cores were measured only at 20 mT demagnetization step to keep up with core flow.

Inclination, declination, and intensity of NRM after 20 mT AF demagnetization with magnetic susceptibility for Hole U1345A are plotted in Figure F18. Inclination and intensity of NRM after 20 mT AF demagnetization with magnetic susceptibility for Holes U1345C–U1345E are plotted in Figure F19. In Figure F18, declination is plotted with values corrected using the FlexIt orientation tool (black dots) and with raw values (blue dots). The corrected declinations cluster well around 0°, indicating that the tool functionally worked for this site. The average inclination values are nearly 70° for the normal polarity intervals observed in Site U1345 cores. These values are close to the site axial dipole inclination (~72°), indicating that overprint magnetization caused by the drill pipe and/or core barrel can be effectively removed from the NRM records. Because there are no apparent polarity reversals in the cores at this site, the entire sequence from Site U1345 is assigned to the Brunhes normal polarity zone.

Relative paleointensity of cores was estimated from Site U1345 to examine potential geochronological information during the Brunhes Chron. Figure F20 shows magnetic susceptibility (top) and relative paleointensity (bottom) for Hole U1345A based on normalizing NRM after 20 mT AF demagnetization by magnetic susceptibility. The paleointensity variation has a large amplitude and obviously shows a coherent change with magnetic susceptibility (Fig. F20), suggesting that NRM intensity was largely influenced by environmental change. However, there are differences, and the relative paleointensity pattern is consistent with that seen at all other sites. On the basis of those correlations, MIS 1–12 are tentatively identified in Figure F20.

The dramatic changes in NRM shown in Figure F18 indicate notable effects of early sediment diagenesis, which were also noted at the previous sites. Significant magnetic mineral dissolution starts within 5 mbsf because of anaerobic oxidation of methane (AOM)–sulfate reduction processes (see "Geochemistry and microbiology"). This is also evident at Sites U1344, U1343, and U1339. The active zone of dissolution appears to be limited from the seafloor to ~10 m depth interval, so magnetization does not change significantly at deeper depths. This dissolution complicates our ability to make relative paleointensity estimates but does not appear to hinder us from gaining a reliable sense of directional changes, both in secular variation and in polarity.

Geochemistry and microbiology

Interstitial water chemistry

In Hole U1345A, 17 samples for interstitial water analyses were retrieved at a resolution of two samples per core from Cores 323-U1345A-1H and 2H and one sample per core thereafter to 120.25 mbsf (Core 323-U1345A-14H). High-resolution sampling was conducted at the microbiology-dedicated hole (U1345B), with 77 whole-round samples taken. To prevent oxidation, whole rounds were stored in a nitrogen-filled glove box at 7°C until squeezed. Aliquot samples were processed for routine shipboard analyses (see "Geochemistry" in the "Methods" chapter) and collected for shore-based analyses of sulfur and oxygen isotopes of sulfate and hydrogen sulfide, trace metals, dissolved organic carbon (DOC), and fatty acids.

Chlorinity, salinity, alkalinity, dissolved inorganic carbon, and pH

Salinity at Site U1345 ranges from 35 to 37 (Fig. F21I), and chloride concentrations average 549.3 ± 30.4 mM (Fig. F22C), with no clear trend with depth.

Alkalinity increases significantly in the uppermost ~20 mbsf from 2.8 mM at 0.05 mbsf to ~46 mM, slightly increases and reaches a maximum value of 58.1 mM at 74.3 mbsf, and then decreases to 36.7 mM at the bottom of the hole (Fig. F21C). This trend is similar to the dissolved inorganic carbon (DIC) profile (Fig. F21A). DIC concentrations reach a maximum of 59.2 mM at 74.3 mbsf and decrease below this depth. pH values generally vary between 7.5 and 7.9 (Fig. F21B). A local maximum in pH occurs at ~6.2 mbsf.

Dissolved sulfate and hydrogen sulfide

Interstitial water sulfate concentrations decrease almost linearly from seawater values of 28.4 mM at 0.05 mbsf to values below detection limit at 6.25 mbsf (Fig. F21D). Hydrogen sulfide concentrations are above detection limit from 3 to 8 mbsf, with a maximum value of 2.3 mM at 6.25 mbsf (Fig. F21F).

Dissolved ammonium, phosphate, and silica

Dissolved ammonium concentrations increase throughout the sediment column to a maximum value of 9.1 mM at 139.43 mbsf (Fig. F21H). Dissolved phosphate concentrations increase in the uppermost 8.5 mbsf to 195 µM and then increase subtly to 215 µM from 8.5 to 21.45 mbsf (Fig. F21G). A

local minimum of <200 µM occurs between 22.25 and 27.25 mbsf. Phosphate concentrations are ~280 µM at greater depths. Dissolved silica concentrations at Site U1345 are very scattered in the uppermost 40 mbsf and increase to >1000 µM between ~80 and 120 mbsf (Fig. F22K).

Dissolved calcium, magnesium, sodium, and potassium

Dissolved calcium concentrations decrease pronouncedly in the uppermost 7.75 mbsf to 2.7 mM (Fig. F22A). Below this depth, calcium concentrations continue to decrease, reaching a minimum value of 1.6 mM at 35.8 mbsf. Calcium concentrations increase slightly to >3 mM below ~40 mbsf. Dissolved magnesium concentrations decrease from 50 mM at 0.05 mbsf to 44.1 mM at 7.75 mbsf (Fig. F22B). Between 7.75 and 36.25 mbsf, magnesium concentrations have a scattered distribution but an overall trend to values higher than those in the uppermost layer. Below 74.31 mbsf, magnesium concentrations decrease again and reach a minimum of 42.1 mM at 120.21 mbsf. Dissolved sodium and potassium concentrations at Site U1345 are in the range of 464.8 ± 19.4 mM and 11.1 ± 0.8 mM, respectively (Fig. F22D, F22E).

Dissolved manganese, iron, barium, boron, lithium, and strontium

The dissolved iron profile has a distinct concentration peak between 8.3 and 15.8 mbsf, with a maximum value of 24.2 µM at 10.5 mbsf and a second, less defined, peak at ~35 mbsf (Fig. F22H). Below 40 mbsf, dissolved iron concentrations have scattered, high values. Despite its lower concentrations, dissolved manganese (Fig. F22G) constrains the two peaks in the iron profile. Peaks in manganese concentrations occur at ~15 and 25 mbsf. Maximum concentrations at these two peaks are 4.6 and 5.12 µM, respectively.

Dissolved barium concentrations increase just above the depth of the current SMTZ at ~5 mbsf and show the most pronounced increase between 5 and 9 mbsf. Below this layer, barium concentrations remain almost unchanged at <20 µM (Fig. F22L). Boron concentrations increase in the uppermost 20 m to ~730 µM and reach a maximum value of 880 µM at 83 mbsf. Lithium concentrations decrease in the uppermost 15 mbsf to <5 µM but steadily increase throughout the rest of the sediment column (Fig. F22I). Overall, dissolved strontium concentrations display a similar trend, with decreasing concentrations in the uppermost 35 m and increasing values below this depth, although the uppermost 40 m of this profile is scattered (Fig. F22F).

Volatile hydrocarbons

Samples for volatile hydrocarbon analyses were taken from Hole U1345A at the same resolution as interstitial water samples described above. Methane is detectable at all depths at Site U1345 except the uppermost 6 mbsf of the sediment column (Fig. F21E). Ethane and other volatile hydrocarbons were not detected at Site U1345.

Sedimentary bulk geochemistry

Eighteen samples from Hole U1345A were used for the preliminary analysis of solid-phase total carbon (TC), total nitrogen (TN), total sulfur (TS), and total inorganic carbon (TIC). From these analyses, total organic carbon (TOC) and calcium carbonate ($CaCO_3$) concentrations were calculated (see "Geochemistry" in the "Methods" chapter). $CaCO_3$ content at Site U1345 ranges from 1.2 to 6.1 wt% (average = 2.1 wt%) (Fig. F23A). TOC and TN values range from 0.40 to 1.43 wt% (average = 0.75 wt%) and from 0.07 to 0.14 wt% (average = 0.10 wt%), respectively (Fig. F23B, F23C). TS values range from 0.21 to 0.82 wt% (average = 0.42 wt%) (Fig. F23D). Splits of squeeze cakes were also collected and treated for shore-based analyses of bulk elemental composition, iron mineral phases, and iron-monosulfide and pyrite content and sulfur isotope composition.

Microbiology

Samples for community structure and total prokaryotic cell abundance were collected adjacent to interstitial water whole rounds. High-resolution sampling took place in the microbiology-dedicated cores, and additional samples were taken once per core to APC refusal.

Microbial activity and diversity in the uppermost 25 m of sediment column will be examined during postcruise study. We will focus on the function of Archaea in the uppermost zone of organoclastic sulfate reduction, the SMTZ, and the methanogenesis zone. The SMTZ is a "hot spot" for microbial activity and abundance in the subseafloor (D'Hondt, Jørgensen, Miller, et al., 2003), and we expect an increase in the abundance and activity of microorganisms there. To estimate the abundance of living microorganisms, samples were also taken at low resolution for catalyzed reporter deposition-fluorescence in situ hybridization (CARD-FISH) within the three zones and in the deepest section of Hole U1345A.

We will examine bacterial and archaeal diversity by a combination of conventional 16S ribosomal ribonucleic acid (rRNA) clone libraries, quantitative polymerase chain reaction (qPCR), and/or a new quantitative community fingerprinting method involving

automated ribosomal intergenic spacer analysis (ARISA) (Ramette, 2009).

Conclusion

Of all the sites investigated, Site U1345 has the shallowest SMTZ, at 6–7 mbsf. This site is characterized by the steepest flux of methane into this zone and the highest interstitial water hydrogen sulfide concentrations. Similar to other shelf Sites U1343 and U1344, the almost linear sulfate and methane concentration profiles suggest that sulfate reduction coupled to AOM accounts for most of the sulfate consumption in the sediment column. Preliminary modeling of the DIC profile (data not shown) suggests that net DIC production in the SMTZ accounts for as much as 70% of DIC production in the uppermost sediment layers.

The occurrence of high concentrations of dissolved hydrogen sulfide in the SMTZ can be attributed to very high sulfate reduction rates at this depth and probably to an insufficient pool of reactive Fe mineral phases, such as Fe (oxyhydr)oxides, which can react with hydrogen sulfide on short timescales. Distinct peaks in dissolved iron and manganese concentrations immediately below the SMTZ might result from microbial dissimilatory iron reduction, which releases Fe^{2+}, whereas the concurrent liberation of manganese might be attributed to the reoxidation of ferrous iron by Mn oxides (Canfield et al., 1993). Alternatively, downward-diffusing hydrogen sulfide from the SMTZ may react with the remaining Fe mineral phases to form FeS minerals and release dissolved Fe^{2+}.

The organic matter degradation products phosphate and ammonium accumulate in the interstitial water. The distinct minimum in phosphate concentration between 22.25 and 27.25 mbsf, however, indicates that the consumption of this species is most likely caused by the formation of phosphate-bearing minerals such as apatite.

The calcium and magnesium profiles (Fig. **F22A, F22B**) show depletion at the depth of the present SMTZ. This suggests the formation of authigenic Mg-rich carbonate, such as dolomite, driven by the production of DIC during AOM and increased pH and alkalinity, leading to the oversaturation of interstitial water with respect to carbonate. Interestingly, dissolved calcium concentrations continue to decrease with depth to a minimum concentration at ~40 mbsf. This depth corresponds to a dolostone layer found at 40.27 mbsf (see **"Lithostratigraphy"**).

Sites U1343, U1344, and U1345 also have high concentrations of dissolved barium in the interstitial water, indicating a sink of this ion just above the SMTZ. The distribution of barium at these sites can be attributed to diagenetic remobilization of barium, deposited as biogenic barite, into the sulfate-depleted interstitial water (von Breymann et al., 1992). The upper end of the SMTZ, where the sulfate and dissolved barium profiles overlap, marks the present front of authigenic barite formation.

Physical properties

Site U1345 was spudded at a water depth of ~1008 m along the uppermost sector of the Beringian margin near the large, broad head of the Navarin submarine channel (Normark and Carlson, 2003). The underlying stratigraphic section, which exhibits sediment-filled canyon axes, is ~1 km thick and overlies a deeply subsided wave-cut platform of early Tertiary age. The platform is underlain by basement units of Cretaceous and Jurassic age (Cooper et al., 1987).

Five holes were drilled at Site U1345. Four of these holes (U1345A, U1345C, U1345D, and U1345E) were drilled to similar depths ranging from ~147 to 150 mbsf; the microbiology-dedicated hole (U1345B) was drilled to 36.7 mbsf. Cores from Holes U1345A, U1345C, U1345D, and U1345E were placed sequentially on the "fast track" Special Task Multisensor Logger (STMSL) and the Whole-Round Multisensor Logger (WRMSL) systems to measure bulk density and magnetic susceptibility; cores from Hole U1345B were scanned only on the STMSL before being stored in the cold room for microbiological sampling. These same cores were scanned for NGR, and at least one section, commonly the undisturbed Section 2, of each core was selected for thermal conductivity measurement. Determination of moisture and density (MAD) physical properties was conducted only on cores retrieved from Hole U1345A. Core continuity was typically broken and disturbed by gas-expansion cracking and gapping. As a consequence, WRMSL *P*-wave measurements were not taken for cores collected from Site U1345 holes.

Only one lithologic unit, Unit I, was defined for the sediment penetrated at Site U1345 (see **"Lithostratigraphy"**). Unit I is composed of silt and clay with subordinate but important volumes of sand. Lesser components are provided by diatom frustules and lesser amounts of other microfossils. The section recovered at Site U1345 is the most coarse grained and siliciclastic of all stratigraphic sequences drilled during Expedition 323.

GRA and MAD (discrete-sample) wet bulk density

Wet bulk density recorded by the WRMSL GRA densitometer is indicated by the continuous line in Figure F24A. Also shown on this figure are discrete sample measurements of bulk density by the MAD methodology (open circles). Figure F24B is a line plot of only MAD bulk density readings. The two profiles of downhole bulk density are generally similar in the uppermost ~70 mbsf but are dissimilar at greater depths, where MAD density readings are significantly higher than GRA measurements. Both profiles display a small downhole increase in density. GRA measurements increase from a near-seafloor value of ~1.65 to 1.75 g/cm³ at the bottom of the hole, and MAD determinations increase from a near-seafloor value of 1.64 g/cm³ to a hole-bottom average of ~1.85 g/cm³ (Fig. F24). The reason for the difference between the two profiles in the lower part of the hole is not understood. Calculation or calibration errors may have affected the accuracy of MAD density determination for the lower half of Hole U1345A. However, wet bulk densities in Hole U1345A appear to be higher by 0.1–0.2 g/cm³ compared to density measurements from Hole U1344A in the uppermost 150 m of the sedimentary section; the higher densities in Hole U1345A probably reflect the sediment's higher sand content.

Similar to stratigraphic sections drilled at Beringian margin sites (U1343 and U1344), GRA density values in Hole U1345A also document rhythmic fluctuations, with readings as high as ~2.05 g/cm³ and as low as ~1.40 g/cm³. The longer wavelength between oscillations is ~25–50 m. The change in wavelength presumably reflects time changes in the deposition rate and texture of siliciclastic material.

Magnetic susceptibility

The downhole distribution of magnetic susceptibility is displayed in Figure F25. The profile recorded by the WRMSL scanner outlines sharply defined highs separated by broad, low-relief lows. The profile is similar to the blade contour of a logger's high-toothed felling saw. Peak values rise to ~170 SI units, above lows averaging ~20 SI units. Although core sections that passed by the magnetic susceptibility detection coils were disrupted by gas-expansion cracks, the measurements seem to have realistically recorded downhole variations in magnetic susceptibility, which are functions of many factors (see "Paleomagnetism").

Natural gamma radiation

The downhole profile of NGR readings displayed in Figure F26 is broadly similar to that of GRA bulk density (Fig. F24A). Recorded NGR values are lowest (~25 counts/s) in poorly consolidated and relatively porous near-seafloor sediment. Below ~15 mbsf, average NGR readings increase rhythmically from ~33 to 38 counts/s at the bottom of Hole U1345A (~145 mbsf). The slight increase may reflect a downsection increase in clay mineral content, but it most likely also reflects sediment compaction and densification tracked by a downsection increase in GRA bulk density and a matching decrease in porosity and water content (Fig. F27). The estimated hole-average NGR reading of ~35 counts/s is slightly higher than the ~30 counts/s of the uppermost ~150 m of section cored at other Beringian margin sites (U1343 and U1344). The higher NGR in Hole U1345A may result from the coarser and higher content of siliciclastic mineral debris.

MAD porosity and water content

Downsection profiles of MAD-measured porosity and water content record a progressive decrease in average values (Fig. F27; Table T16). Near-surface porosity is ~68%, lower than that estimated (75%) for the finer grained sediment of nearby Hole U1344A. Porosity in the lower 15 m of Hole U1345A decreases to ~53%, the lowest average recorded at Beringian margin drilling sites. The downhole distribution of water content and porosity is rhythmic. Within the lithologically similar deposits of Unit I, the trend of downhole-decreasing porosity and water content is surmised to reflect compaction and dewatering. Oscillations about these general gradients are likely caused by textural variations in the dominantly siliciclastic clay, silt, and sand beds of Unit I.

Grain density

Figure F28 documents little change in average grain density with depth. The estimated hole average is 2.75 g/cm³, which is higher than that observed (2.69 g/cm³) in the uppermost 150 m of Hole U1344A. The higher average grain density of Unit I in Hole U1345A is interpreted to be a consequence of its greater abundance of coarse siliciclastic grains.

Thermal conductivity

The downhole distribution of thermal conductivity readings (Fig. F29) displays an overall trend of increasing conductivity, from a near-surface value near ~1.00 W/(m·K) to ~1.23 W/(m·K) at the deepest measurement just above ~140 mbsf. Oscillations about

the average are high, ranging from 1.32 to ~0.810 W/(m·K). The estimated thermal conductivity hole average is ~1.07 W/(m·K), which is higher than the average thermal conductivity value (0.942 W/[m·K]) for the uppermost ~150 m cored in Hole U1344A. With respect to Unit I of Hole U1343A, the higher thermal conductivity of Unit I of Hole U1345A can be attributed to its higher sand and silt content and lower porosity.

Stratigraphic correlation

The composite depth scale and primary splice at Site U1345 is complete and continuous from 0.0 to 168.0 m CCSF-D (as defined in **"Stratigraphic correlation"** in the "Methods" chapter). The splice ranges from the top of Core 323-U1345A-1H (0 m CCSF-D) to horizon 323-U1345D-16H-7, 150.57 cm (168.0 m CCSF-D) (Tables **T17, T18**). There are no appended intervals. The splice is composed of intervals from Holes U1345A, U1345C, and U1345D. Parts of Hole U1345E were preserved as pristine whole-round sections for postcruise analyses. These cores are not included in the primary splice; however, they were considered when constructing composite depths and are thus included in the affine table (Table **T17**). The secondary splice at Site U1345 was constructed during the postcruise sampling party from 0.0 to 166.39 m CCSF-A, ranging from the top of Core 323-U1345C-1H (0.0 m CCSF-A) to the bottom of Core 323-U1345E-16H (166.39 m CCSF-A) (Table **T19**). The secondary splice is composed of intervals from Holes U1345A, U1345C, U1345D, and U1345E and includes none of the same intervals used in the primary splice. The secondary splice was constructed using a depth framework that is consistent with the primary splice, so the affine table (Table **T17**) is universal for both the primary and secondary splices.

Correlations were accomplished using IODP Correlator software (version 1.656), and where possible some intervals were checked with digital line-scan images with Corelyzer (version 1.3.3). The composite (CCSF-A) and splice (CCSF-D) depth scales are based primarily on the stratigraphic correlation of WRMSL magnetic susceptibility data (Fig. **F30**). Correlations were checked with WRMSL GRA bulk density (Fig. **F31**), whole-round NGR (Fig. **F32**), and color reflectance parameter b* (Fig. **F33**) data. However, these data were less useful for correlation than WRMSL magnetic susceptibility data because of noise induced by extensive voids (WRMSL GRA and b*) or low signal amplitudes (NGR). In many cores, Section 1 needed to be reconstructed on the catwalk after gas expansion pushed material out of the core liner, so the intervals in Section 1 of all cores except Core 323-U1345A-1H are not included in the splice unless no other copy of the interval was available.

The CCSF-A and CCSF-D scales were constructed by assuming that the uppermost sediment (the mudline) in Core 323-U1345A-1H represents the sediment/water interface in the primary splice. The mudline was also recovered in Cores 323-U1345C-1H and 323-U1345E-1H, confirming the fidelity of the top of the recovered section. Core 323-U1345A-1H serves as the anchor in the composite depth scale and is the only core with depths that are the same on the mbsf, CCSF-A, and CCSF-D scales. From this anchor we worked downhole, correlating the variations in core logging data on a core-by-core basis using Correlator.

Most of the splice points in the primary splice are clear and convincing based on multiple copies of the section recovered in five holes. The splice tie point between intervals 323-U1345A-10H-4, 48.75 cm, and 323-U1345C-10H-1, 92.95 cm (92.66 m CCSF-A), is uncertain because Core 323-U1345A-10H contains disturbed flow-in that starts approximately in the middle of Section 10H-4 and extends through the bottom of Section 10H-7. The disturbed section is not included in the splice; however, as a result of this disturbance, the composite depths in this interval could not be verified by multiple realizations. The splice tie point between horizons 323-U1345D-10H-7, 54.48 cm, and 323-U1335A-11H-3, 115.4 cm (103.02 m CCSF-A), is tentative because of low signal amplitudes in WRMSL magnetic susceptibility.

Within the splice, the composite CCSF-A depth scale is defined as the CCSF-D depth scale. Note that CCSF-D rigorously applies only to the spliced interval. Intervals outside the splice, although available with CCSF-A composite depth assignments, should not be expected to correlate precisely with fine-scale details within the splice or with other holes because of normal variation in the relative spacing of features in different holes. Such apparent depth differences may reflect coring artifacts or fine-scale variations in sediment accumulation and preservation at and below the seafloor.

The cumulative offset between the mbsf and CCSF-A depth scales is roughly linear (Figs. **F34, F35**). The affine growth factor (a measure of the fractional stretching of the composite section relative to the drilled interval; see **"Stratigraphic correlation"** in the "Methods" chapter) at Site U1345 is 1.11. A few significant anomalies around this relatively uniform affine growth relationship are unexplained but may indicate uncertainties in the assignment of composite depths. Calculation of mass accumulation rates (MARs) based on the CCSF-A or CCSF-D scales

should account for the affine growth factor by dividing apparent depth intervals by the appropriate growth factor. After it is divided by the growth factor (accounting for the different depth intervals), this scaled depth scale should be referred to as CCSF-B.

Downhole measurements

The only downhole measurements made at Site U1345 were three deployments of the APCT-3 tool in Hole U1345A. The measured temperatures range from 4.92°C at 42.4 m DSF to 8.15°C at 108.9 m DSF (Table **T20**), indicating a local geothermal gradient of 48.5°C/km (Fig. **F36**). A simple estimate of heat flow can be obtained from the product of the geothermal gradient by the average thermal conductivity (1.064 W/[m·K]; see **"Physical properties"**), which gives a value of 51.6 mW/m^2, which agrees with existing measurement in the area (the global heat flow database of the International Heat Flow Commission can be found at **www.heatflow.und.edu/index.html**).

Considering the variations in thermal conductivity with depth, a more accurate measure of heat flow in a conductive regime can be given by a "Bullard plot," in which the thermal resistance of an interval is calculated by integrating the inverse of thermal conductivity over depth. If the thermal regime is purely conductive, heat flow will be the slope of temperature versus the thermal resistance profile (Bullard, 1939). Thermal resistance calculated over the intervals overlying each APCT-3 measurement is shown in Table **T20,** and the resulting linear fit of temperature to thermal resistance gives a slightly lower heat flow value of 50.9 mW/m^2.

References

Asahi, H., and Takahashi, K., 2007. A 9-year time-series of planktonic foraminifer fluxes and environmental change in the Bering Sea and the central subarctic Pacific Ocean, 1990–1999. *Prog. Oceanogr.,* 72(4):343–363. **doi:10.1016/j.pocean.2006.03.021**

Barron, J.A., and Gladenkov, A.Y., 1995. Early Miocene to Pleistocene diatom stratigraphy of Leg 145. *In* Rea, D.K., Basov, I.A., Scholl, D.W., and Allan, J.F. (Eds.), *Proc. ODP, Sci. Results,* 145: College Station, TX (Ocean Drilling Program), 3–19. **doi:10.2973/odp.proc.sr.145.101.1995**

Bubenshchikova, N., Nürnberg, D., Lembke-Jene, L., and Pavlova, G., 2008. Living benthic foraminifera of the Okhotsk Sea: faunal composition, standing stocks and microhabitats. *Mar. Micropaleontol.,* 69(3–4):314–333. **doi:10.1016/j.marmicro.2008.09.002**

Bullard, E.C., 1939. Heat flow in South Africa. *Proc. R. Soc. London, Ser. A,* 173:474–502.

Canfield, D.E., Thamdrup, B., and Hansen, J.W., 1993. The anaerobic degradation of organic matter in Danish coastal sediments: iron reduction, manganese reduction, and sulfate reduction. *Geochim. Cosmochim. Acta,* 57(6):3867–3883. **doi:10.1016/0016-7037(93)90340-3**

Cook, M.S., Keigwin, L.D., and Sancetta, C.A., 2005. The deglacial history of surface and intermediate water of the Bering Sea. *Deep-Sea Res., Part II,* 52(16–18):2163–2173. **doi:10.1016/j.dsr2.2005.07.004**

Cooper, A.K., Scholl, D.W., and Marlow, M.S., 1987. Structural framework, sedimentary sequences, and hydrocarbon potential of the Aleutian and Bowers Basins, Bering Sea. *In* Scholl, D.W., Grantz, A., and Vedder, J. (Eds.), *Geology and Resource Potential of the Continental Margin of Western North America and Adjacent Ocean Basins—Beaufort Sea to Baja California* (Vol. 6): *Earth Sci. Ser.* Houston (Circum-Pacific Council for Energy and Mineral Resources), 476–502.

D'Hondt, S.L., Jørgensen, B.B., Miller, D.J., et al., 2003. *Proc. ODP, Init. Repts.,* 201: College Station, TX (Ocean Drilling Program). **doi:10.2973/odp.proc.ir.201.2003**

Hamel, D., de Vernal, A., Gosselin, M., and Hillaire-Marcel, C., 2002. Organic-walled microfossils and geochemical tracers: sedimentary indicators of productivity changes in the North Water and northern Baffin Bay during the last centuries. *Deep-Sea Res., Part II,* 49(22–23):5277–5295. **doi:10.1016/S0967-0645(02)00190-X**

Head, M.J., Harland, R., and Matthiessen, J., 2001. Cold marine indicators of the late Quaternary: the new dinoflagellate cyst genus *Islandinium* and related morphotypes. *J. Quat. Sci.,* 16(7):621–636. **doi:10.1002/jqs.657**

Horner, R.A. (Ed.), 1985. *Sea-ice Biota.* Boca Raton, FL (CRC Press).

Kaiho, K., 1994. Benthic foraminiferal dissolved-oxygen index and dissolved-oxygen levels in the modern ocean. *Geology,* 22(8):719–722. **doi:10.1130/0091-7613(1994)022<0719:BFDOIA>2.3.CO;2**

Ling, H.Y., 1992. Late Neogene silicoflagellates and ebridians from Leg 128, Sea of Japan. *In* Pisciotto, K.A., Ingle, J.C., Jr., von Breymann, M.T., and Barron, J., et al. (Eds.), *Proc. ODP, Sci. Results,* 127/128, Pt. 1: College Station, TX (Ocean Drilling Program), 237–248. **doi:10.2973/odp.proc.sr.127128-1.126.1992**

Lourens, L.J., Hilgen, F.J., Shackleton, N.J., Laskar, J., and Wilson, D., 2004. The Neogene period. *In* Gradstein, F.M., Ogg, J.G., and Smith, A.G. (Eds.), *A Geological Time Scale 2004*. Cambridge (Cambridge Univ. Press), 409–440.

Martini, E., 1971. Standard Tertiary and Quaternary calcareous nannoplankton zonation. *In* Farinacci, A. (Ed.), *Proc. 2nd Int. Conf. Planktonic Microfossils Roma:* Rome (Ed. Tecnosci.), 2:739–785.

Normark, W.R., and Carlson, P.R., 2003. Giant submarine canyons: is size any clue to their importance in the rock record? *In* Chan, M.A., and Archer, A.W. (Eds.), *Extreme Depositional Environments: Mega end Members in Geologic Time*. Spec. Pap.—Geol. Soc. Am., 370:175–190. **doi:10.1130/0-8137-2370-1.175**

Ohkushi, K., Itaki, T., and Nemoto, N., 2003. Last Glacial–Holocene change in intermediate-water ventilation in

the northwestern Pacific. *Quat. Sci. Rev.,* 22(14):1477–1484. doi:10.1016/S0277-3791(03)00082-9

Okazaki, Y., Takahashi, K., Asahi, H., Katsuki, K., Hori, J., Yasuda, H., Sagawa, Y., and Tokuyama, H., 2005. Productivity changes in the Bering Sea during the late Quaternary. *Deep-Sea Res., Part II,* 52(16–18):2150–2162. doi:10.1016/j.dsr2.2005.07.003

Radi, T., and de Vernal, A., 2004. Dinocyst distribution in surface sediments from the northeastern Pacific margin (40–60°N) in relation to hydrographic conditions, productivity and upwelling. *Rev. Palaeobot. Palynol.,* 128(1–2):169–193. doi:10.1016/S0034-6667(03)00118-0

Ramette, A., 2009. Quantitative community fingerprinting methods for estimating the abundance of operational taxonomic units in natural microbial communities. *Appl. Environ. Microbiol.,* 75(8):2495–2505. doi:10.1128/AEM.02409-08

Reynolds, L., and Thunell, R.C., 1985. Seasonal succession of planktonic foraminifera in the subpolar North Pacific. *J. Foraminiferal Res.,* 15(4):282–301. doi:10.2113/gsjfr.15.4.282

Rochon, A., de Vernal, A., Turon, J.L., Mathiessen, J., and Head, M.J., 1999. Distribution of recent dinoflagellate cysts in surface sediments from the North Atlantic Ocean and adjacent seas in relation to sea-surface parameters. *Am. Assoc. Strat. Palynol. Found. Contrib. Ser.,* Vol. 35.

Springer, A.M., McRoy, C.P., and Flint, M.V., 1996. The Bering Sea Green Belt: shelf-edge processes and ecosystem production. *Fish. Oceanogr.,* 5(3–4):205–223. doi:10.1111/j.1365-2419.1996.tb00118.x

Takahashi, K., Fujitani, N., Yanada, M., and Maita, Y., 2000. Long-term biogenic particle fluxes in the Bering Sea and the central subarctic Pacific Ocean, 1990–1995. *Deep-Sea Res., Part I,* 47(9):1723–1759. doi:10.1016/S0967-0637(00)00002-9

Takahashi, K., Ravelo, A.C., and Alvarez Zarikian, C.A., 2009. Pliocene–Pleistocene paleoceanography and climate history of the Bering Sea. *IODP Sci. Prosp.,* 323. doi:10.2204/iodp.sp.323.2009

Taniguchi, A., 1984. Microzooplankton biomass in the arctic and subarctic Pacific Ocean in summer. *In* Hoshiai, T., and Fukuchi, M., *Proc. Sixth Symp. Polar Biol.* Mem. Natl. Inst. Polar Res. Spec. Issue (Jpn.), 32:63–76.

Vanreusel, A. Andersen, A.C., Boetius, A., Connelly, D., Cunha, M.R., Decker, C., Hilario, A., Kormas, K.A., Maignien, L., Olu, K., Pachiadaki, M., Ritt, B., Rodrigues, C., Sarrazin, J., Tyler, P., Van Gaever, S., Pierre, C., and Vanneste, H., 2009. Biodiversity of cold seep ecosystems along the European margins. *Oceanography,* 22(1):110–127. http://www.tos.org/oceanography/issues/issue_archive/issue_pdfs/22_1/22-1_vanreusel.pdf

von Breymann, M.T., Brumsack, H., and Emeis, K.C., 1992. Depositional and diagenetic behavior of barium in the Japan Sea. *In* Pisciotto, K.A., Ingle, J.C., Jr., von Breymann, M.T., Barron, J., et al., *Proc. ODP, Sci. Results,* 127/128 (Pt. 1): College Station, TX (Ocean Drilling Program), 651–665. doi:10.2973/odp.proc.sr.127128-1.168.1992

Von Quillfeldt, C.H., Ambrose, W.G., Jr., and Clough, L.M., 2003. High number of diatom species in first-year ice from the Chukchi Sea. *Polar Biol.,* 26(12):806–818. doi:10.1007/s00300-003-0549-1

Yanagisawa, Y., and Akiba, F., 1998. Refined Neogene diatom biostratigraphy for the northwest Pacific around Japan, with an introduction of code numbers for selected diatom biohorizons. *Chishitsugaku Zasshi,* 104:395–414.

Publication: 15 March 2011
MS 323-109

Figure F1. Location map showing Site U1345, on a topographic high off the northern Bering Sea shelf.

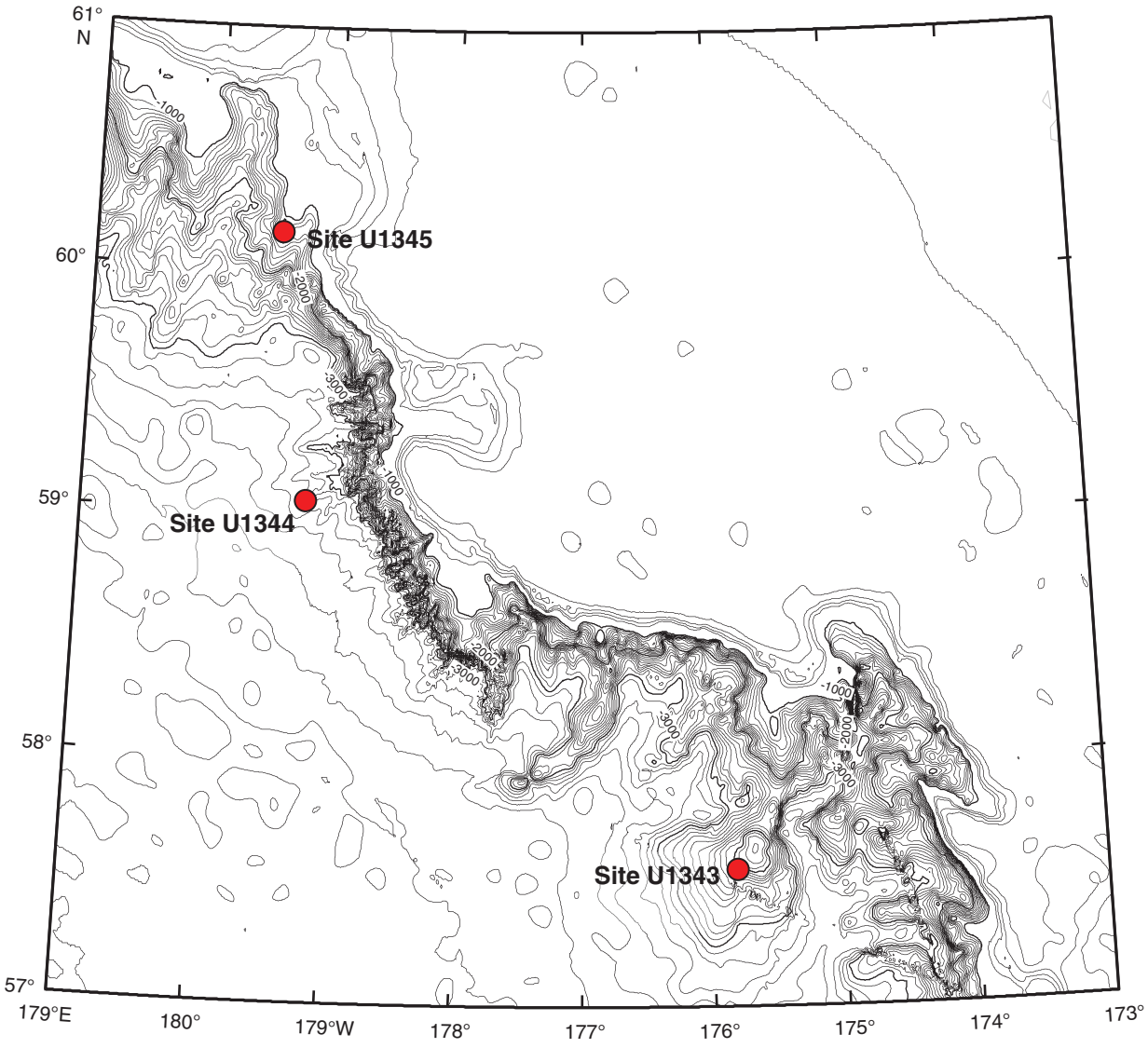

Figure F2. Navigation map for *Discoverer* 4-80-BS Line 18 and *Farnella* 2-86-BS Line 4A around Site U1345 and HLY02-02-3JPC. CDP = common depth point.

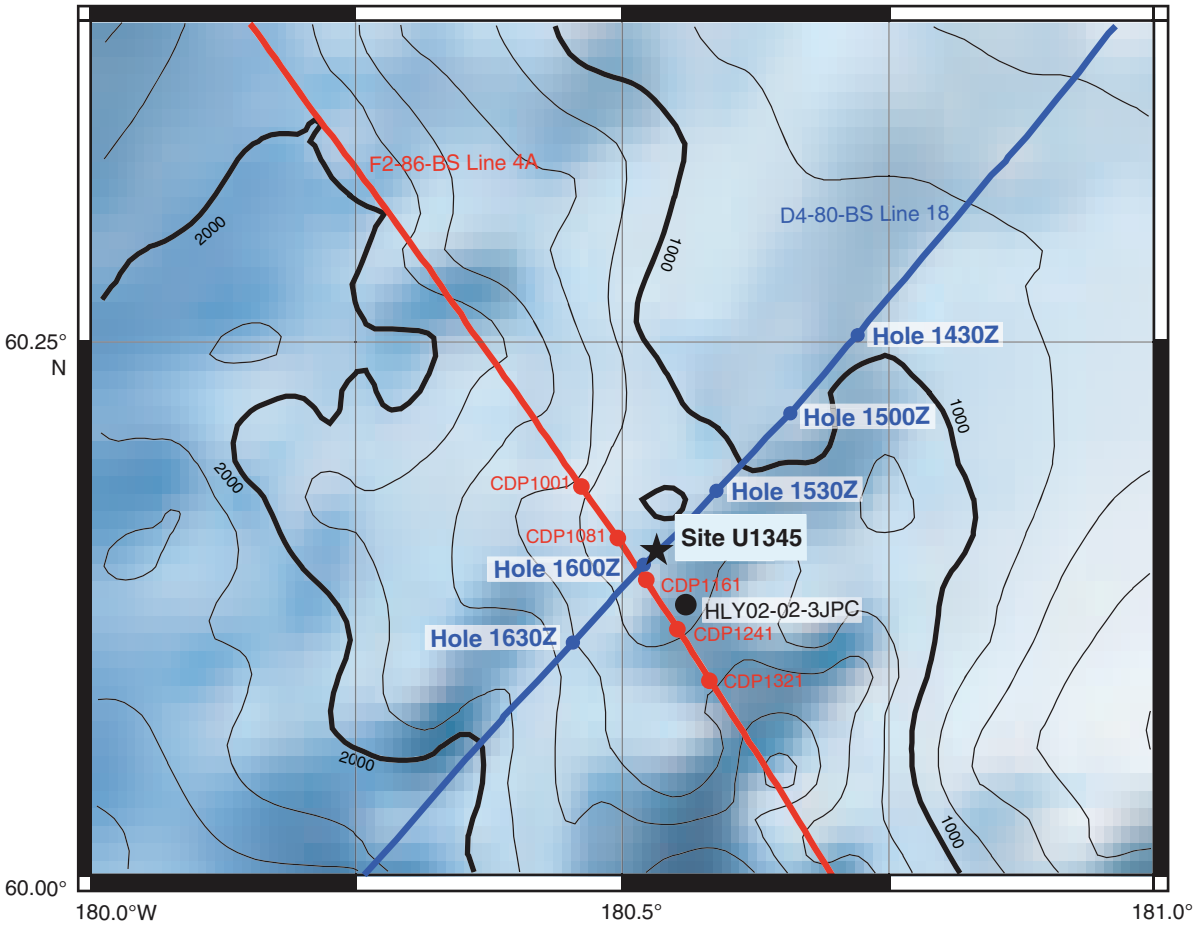

Figure F3. Seismic profile of *Farnella* 2-86-BS Line 4A (northwest–southeast) showing the location of Site U1345. CDP = common depth point.

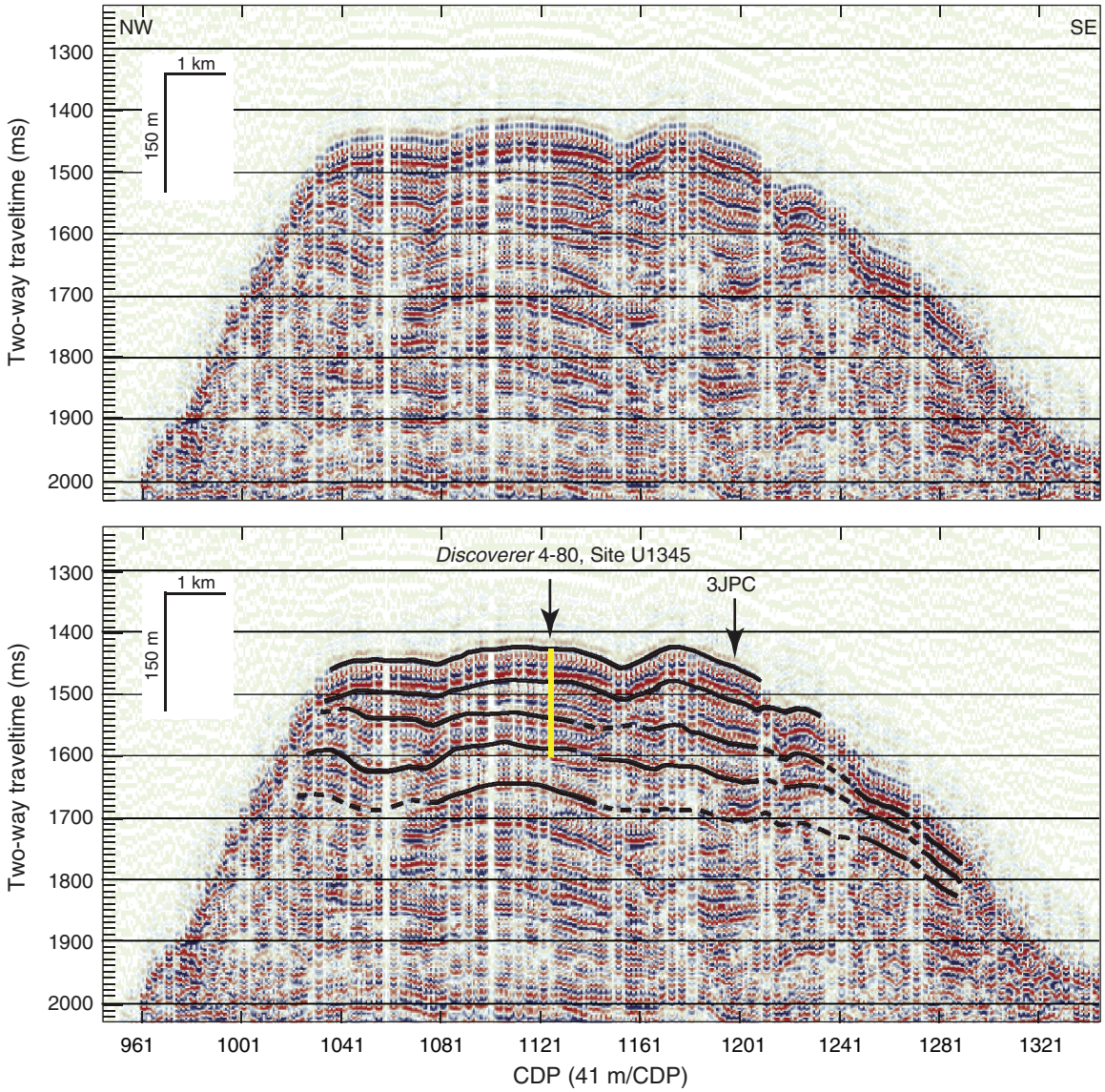

Figure F4. Seismic profile of *Discoverer* 4-80-BS Line 18 (northeast–southwest) showing the location of Site U1345.

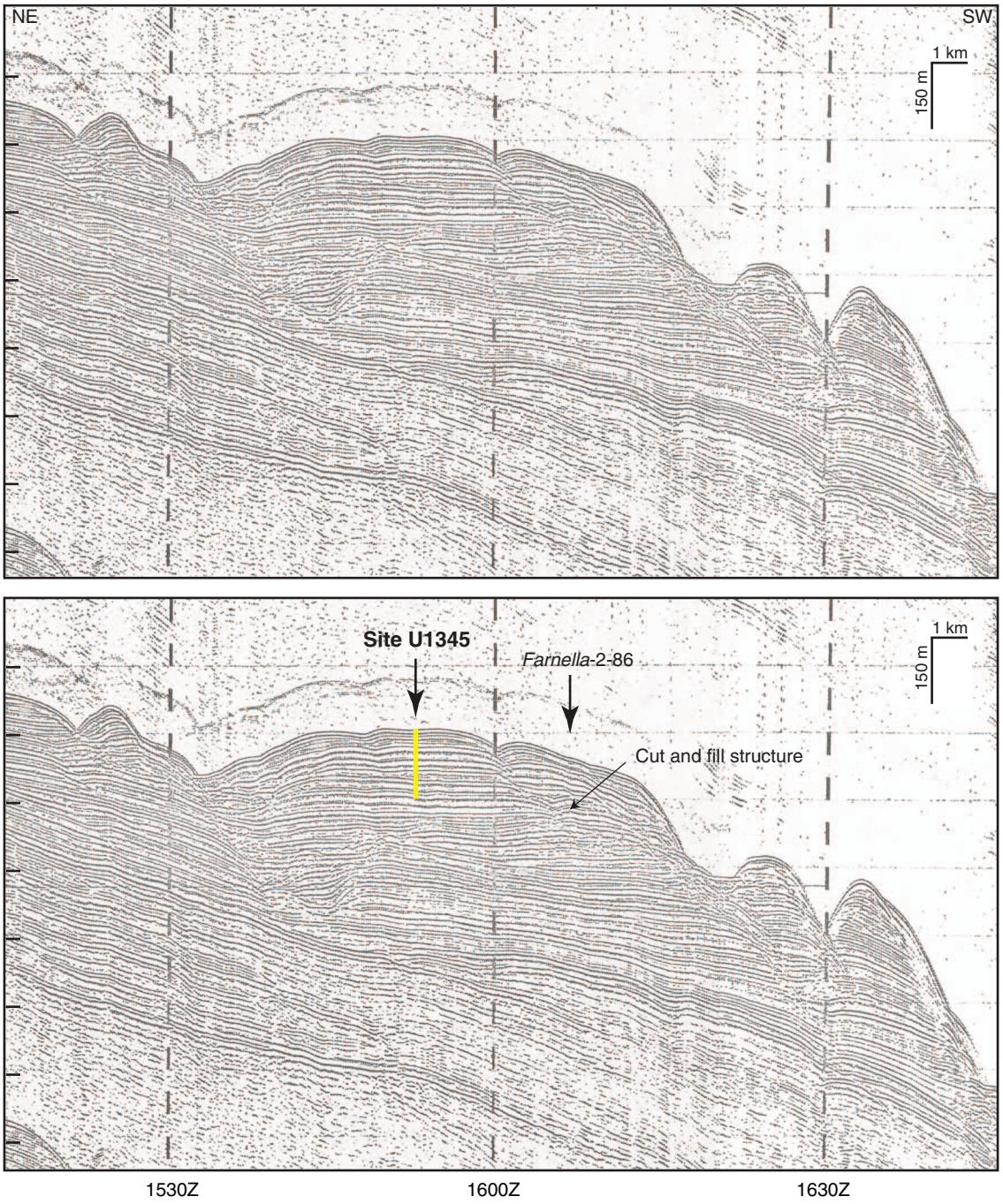

Figure F5. Minisparker profile of *Discoverer* 4-80-BS Line 18 (northeast–southwest) showing the location of Site U1345.

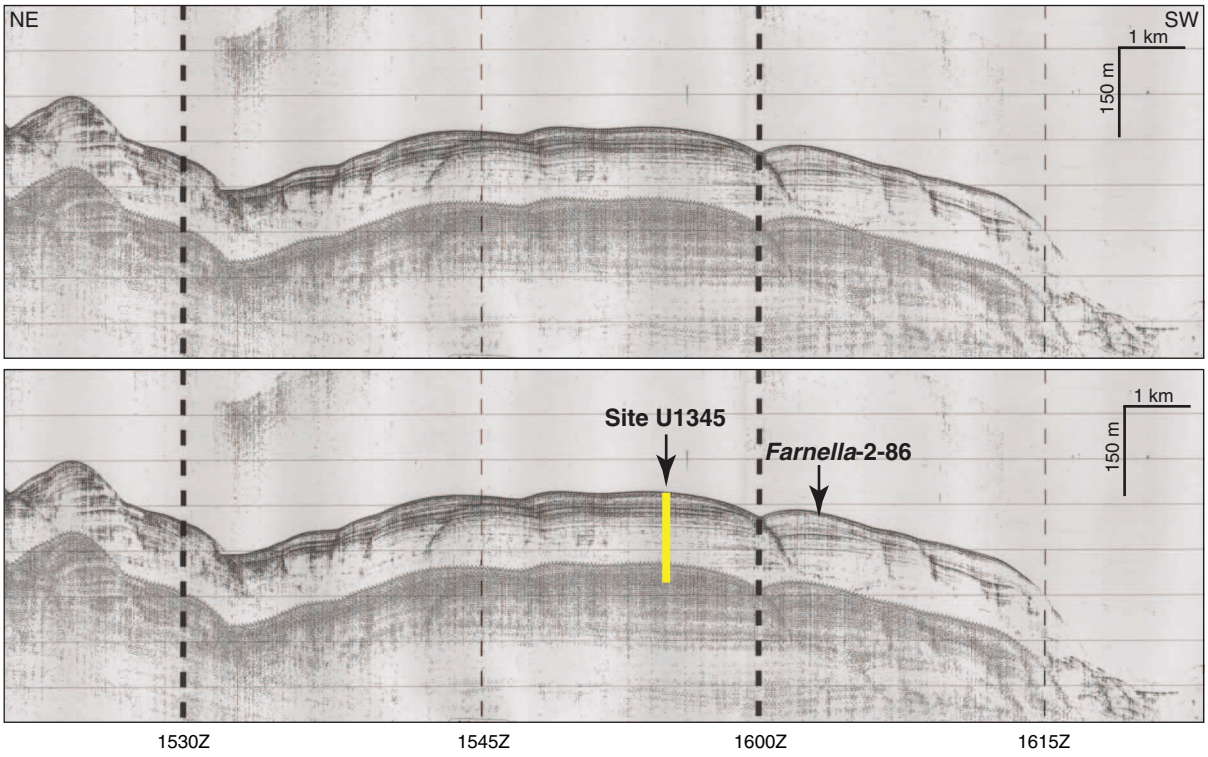

Figure F6. Summary of lithology, structures, accessories, microfossils, and physical properties, Hole U1345A. See legend in Figure F6 in the "Methods" chapter. Soft-sed = soft-sediment, auth = authigenic, calc = calcareous, NGR = natural gamma radiation, GRA = gamma ray attenuation, sed rate = sedimentation rate.

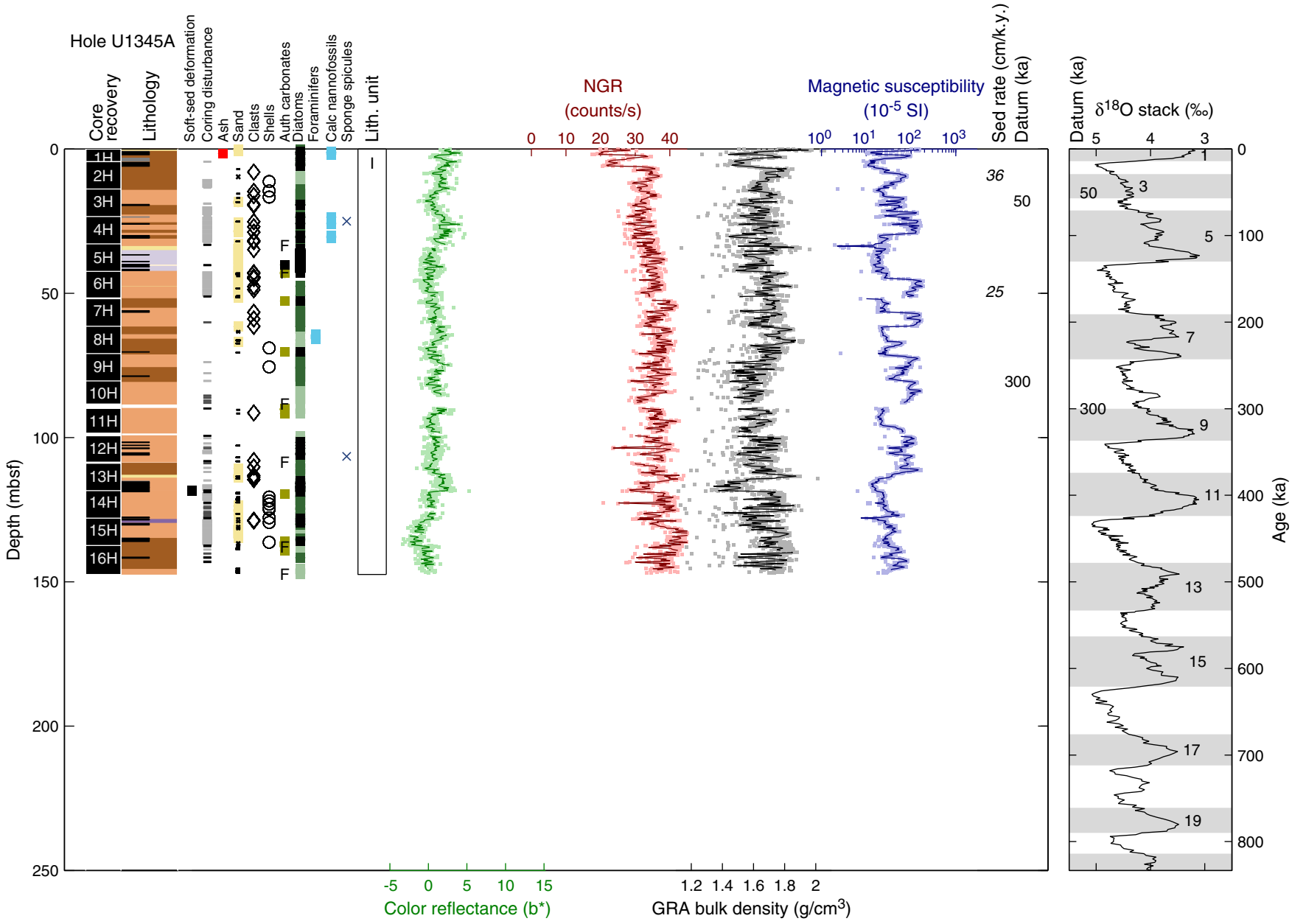

Figure F7. Summary of lithology, structures, accessories, microfossils, and physical properties, Hole U1345C. See legend in Figure F6 in the "Methods" chapter. Soft-sed = soft-sediment, auth = authigenic, calc = calcareous, NGR = natural gamma radiation, GRA = gamma ray attenuation, sed rate = sedimentation rate.

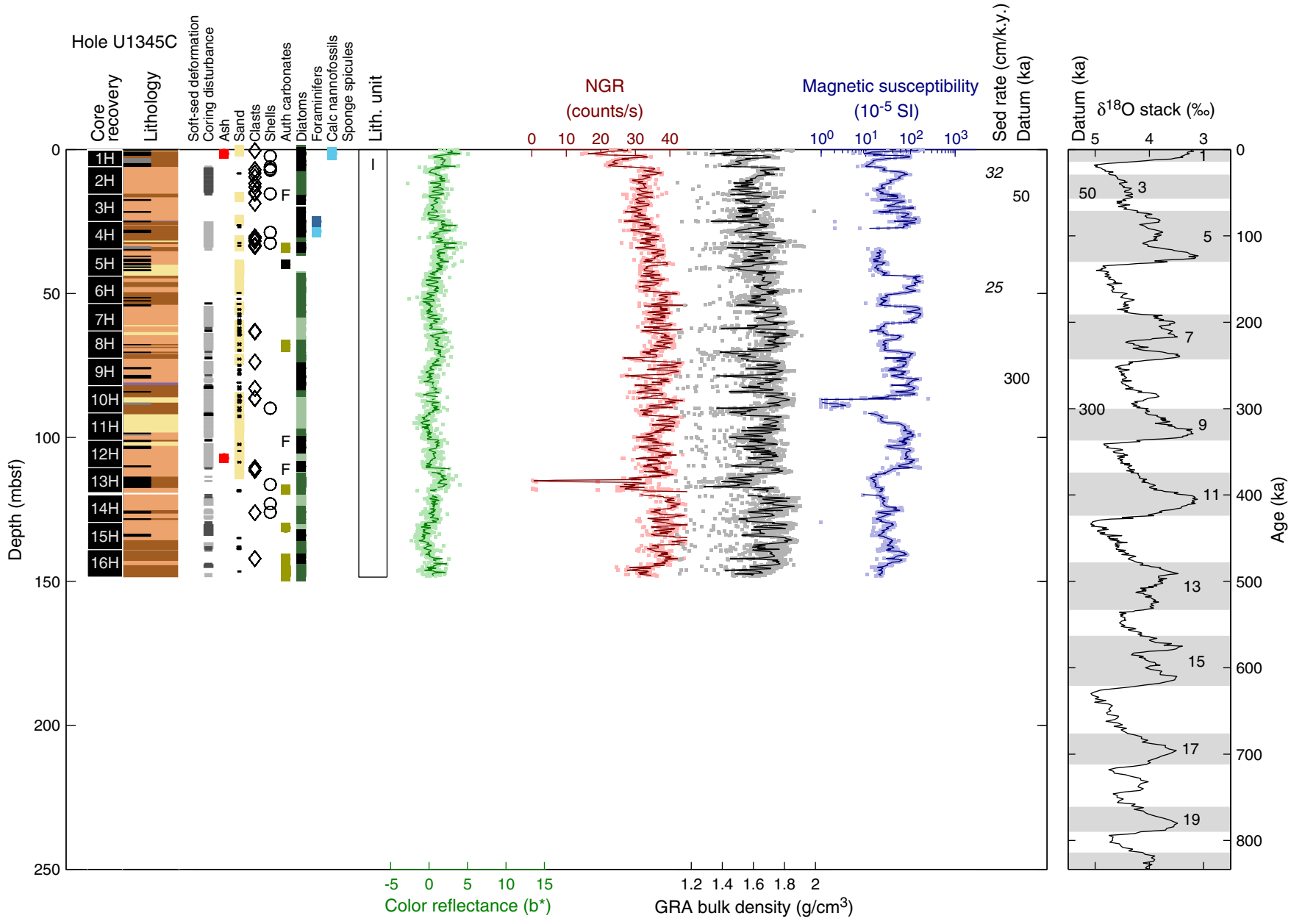

Figure F8. Summary of lithology, structures, accessories, microfossils, and physical properties, Hole U1345D. See legend in Figure F6 in the "Methods" chapter. Soft-sed = soft-sediment, auth = authigenic, calc = calcareous, NGR = natural gamma radiation, GRA = gamma ray attenuation, sed rate = sedimentation rate.

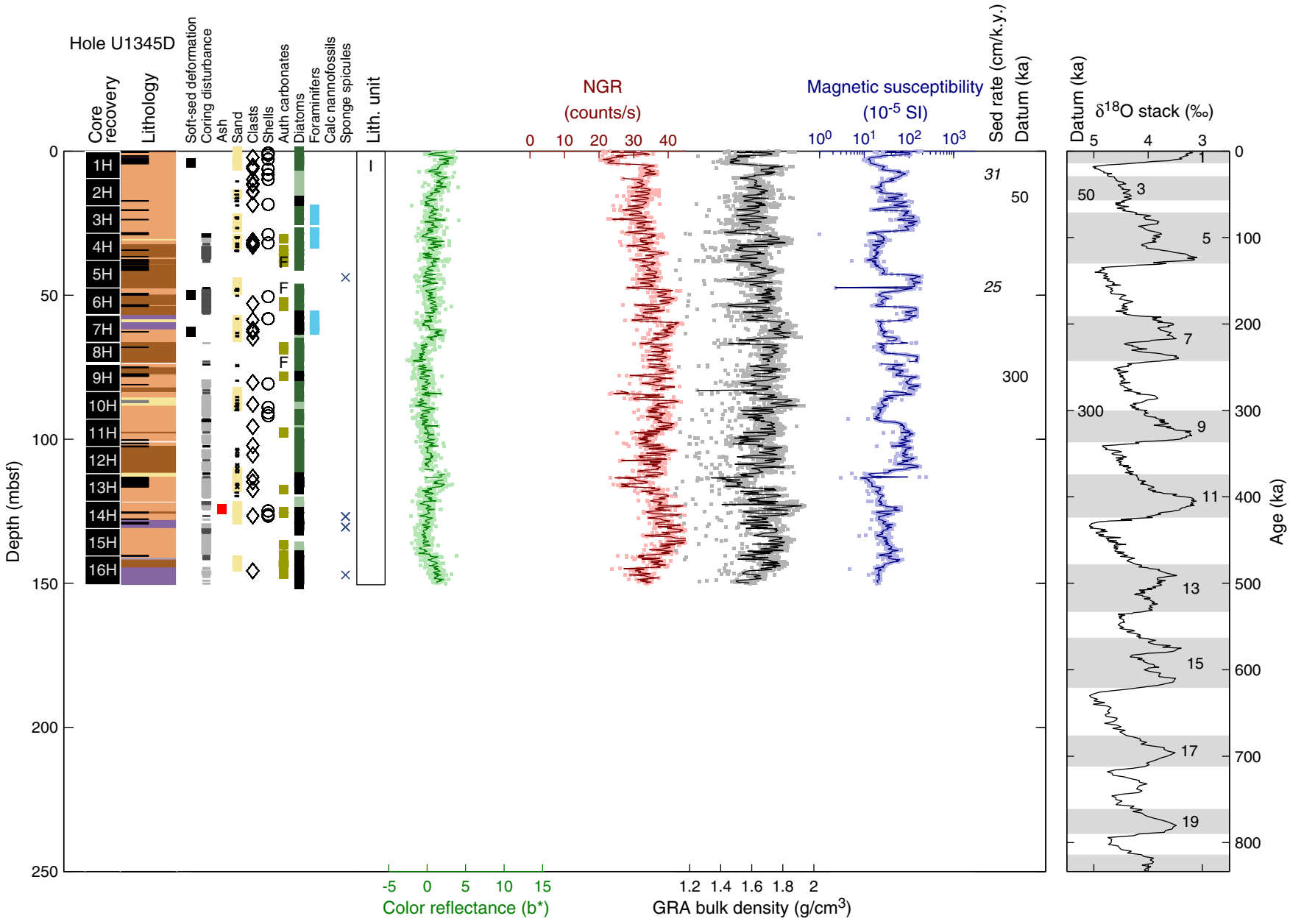

Figure F9. Summary of lithology, structures, accessories, microfossils, and physical properties, Hole U1345E. See legend in Figure F6 in the "Methods" chapter. Soft-sed = soft-sediment, auth = authigenic, calc = calcareous, NGR = natural gamma radiation, GRA = gamma ray attenuation, sed rate = sedimentation rate.

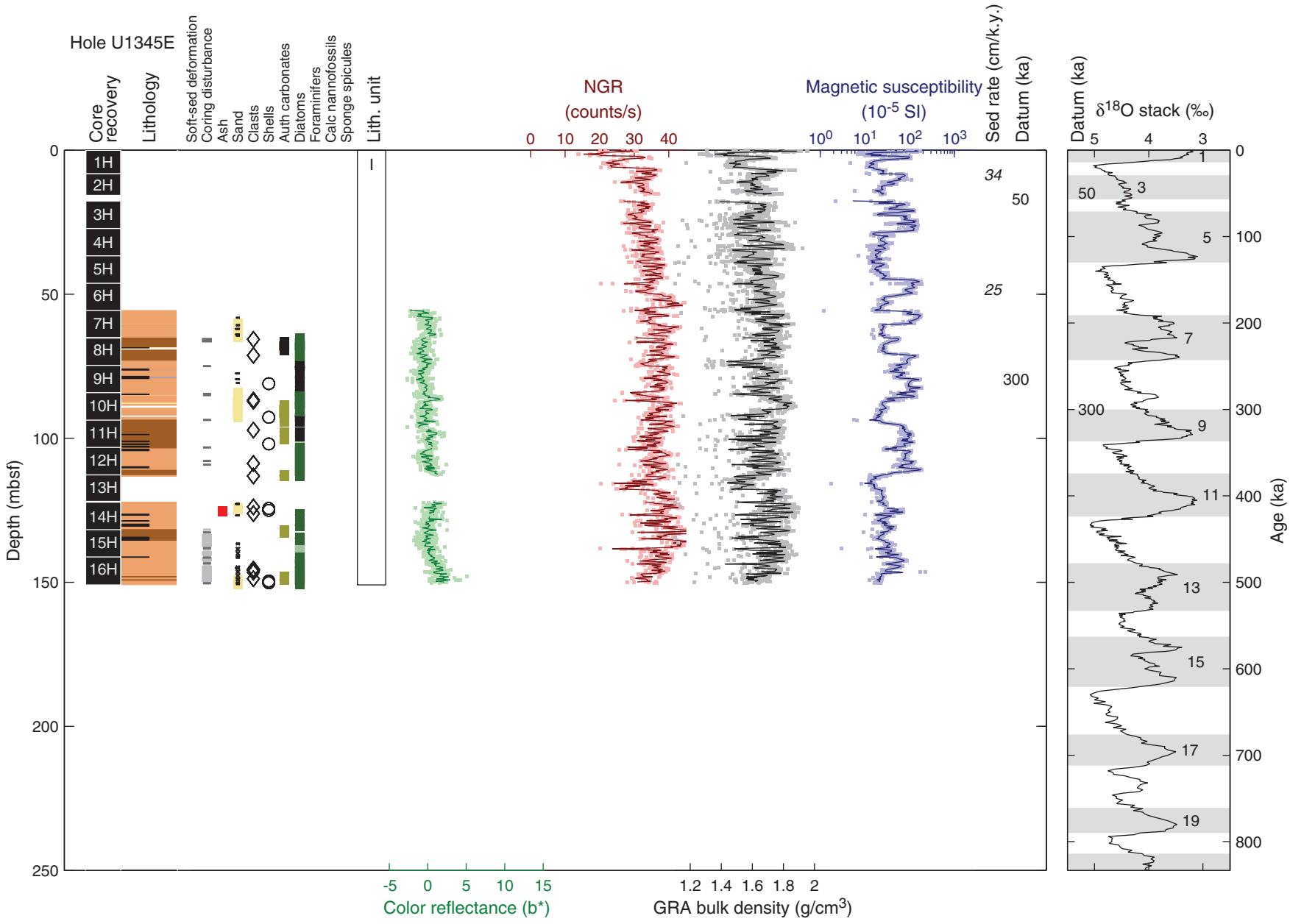

Figure F10. Core photographs of soft-sediment deformation, Site U1345. **A.** Undulating, chaotic laminations (interval 323-U1345A-13H-7, 110–124 cm). **B.** Truncated laminae (interval 323-U1345D-1H-3, 94–107 cm).

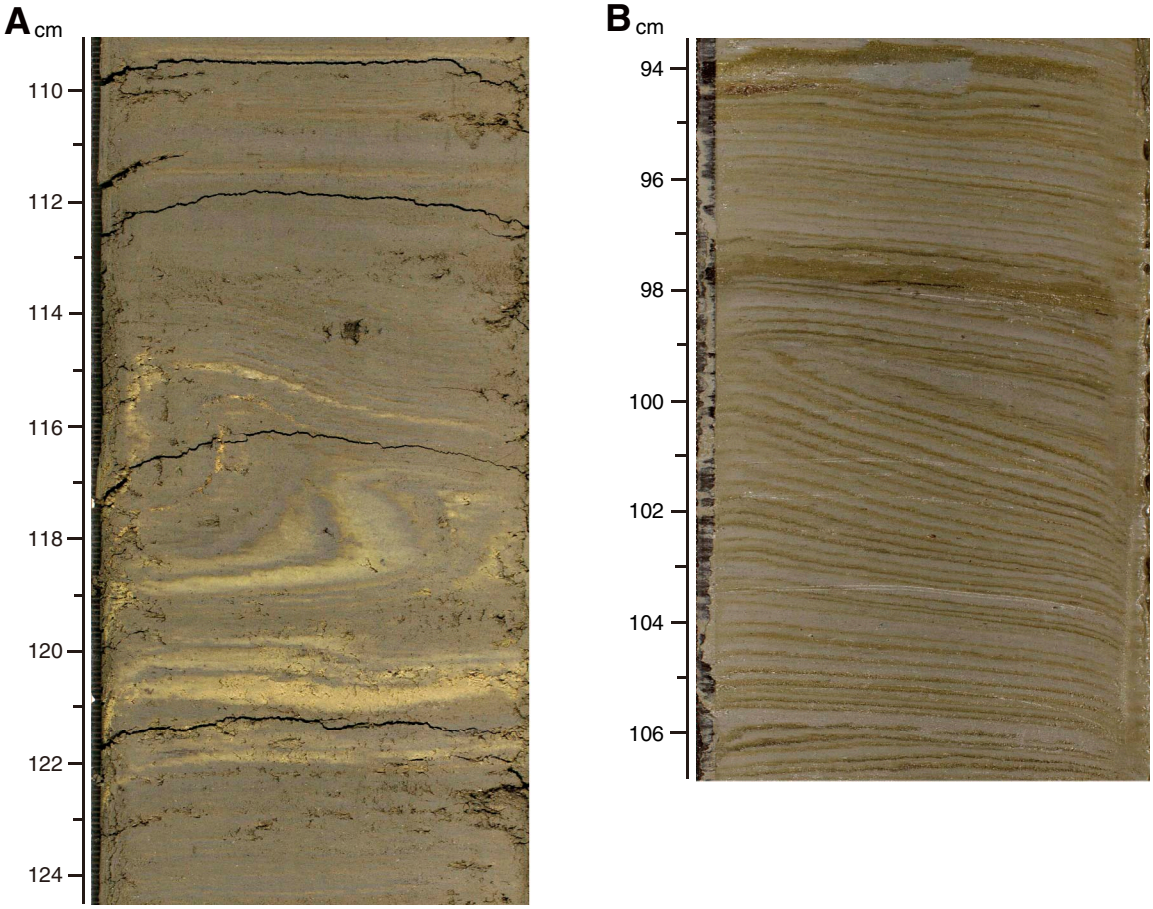

Figure F11. Correlation of laminated intervals in Holes U1345A, U1345C, U1345D, and U1345E, plotted with magnetic susceptibility. Pink bars = biogenic-rich laminations, blue bars = siliciclastic-rich laminations, green bars = laminations with authigenic carbonates.

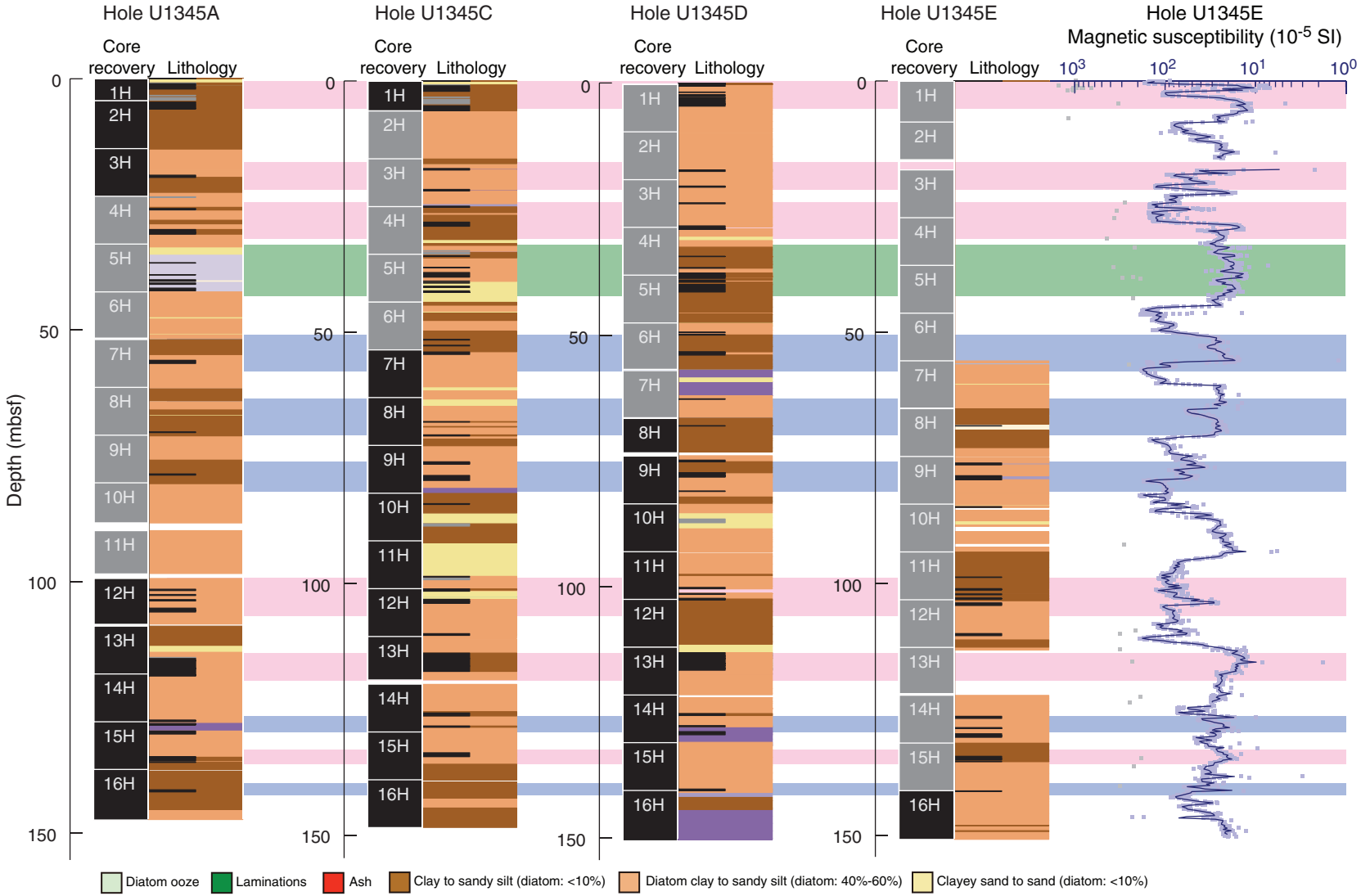

Figure F12. Tube worm colony mold. **A.** Image of colony in place in the core (interval 323-U1345C-16H-3, 102–124 cm). **B.** Photomicrographs of the colony in thin section under plane-polarized light (above) and cross-polarized light (below). Numbers and arrows indicate areas where (1) dolomitization impinges on the tube walls, (2) minerals occur at the intersection of tube walls, (3) diatoms are visible as part of the diatom clayey silt sediment infill, and (4) birefringence occurs parallel to the tube walls. **C.** X-ray diffractogram showing mineral composition of the colony after digesting carbonates with 10% HCl (Sample 323-U1345C-16H-3, 108–110 cm). Q = quartz, T = tridymite, Cr = cristobalite, S = siderite, Fsp = feldspar. Note that peaks are shifted 0.3° too high, so there may be Ca or Mg replacement of Fe.

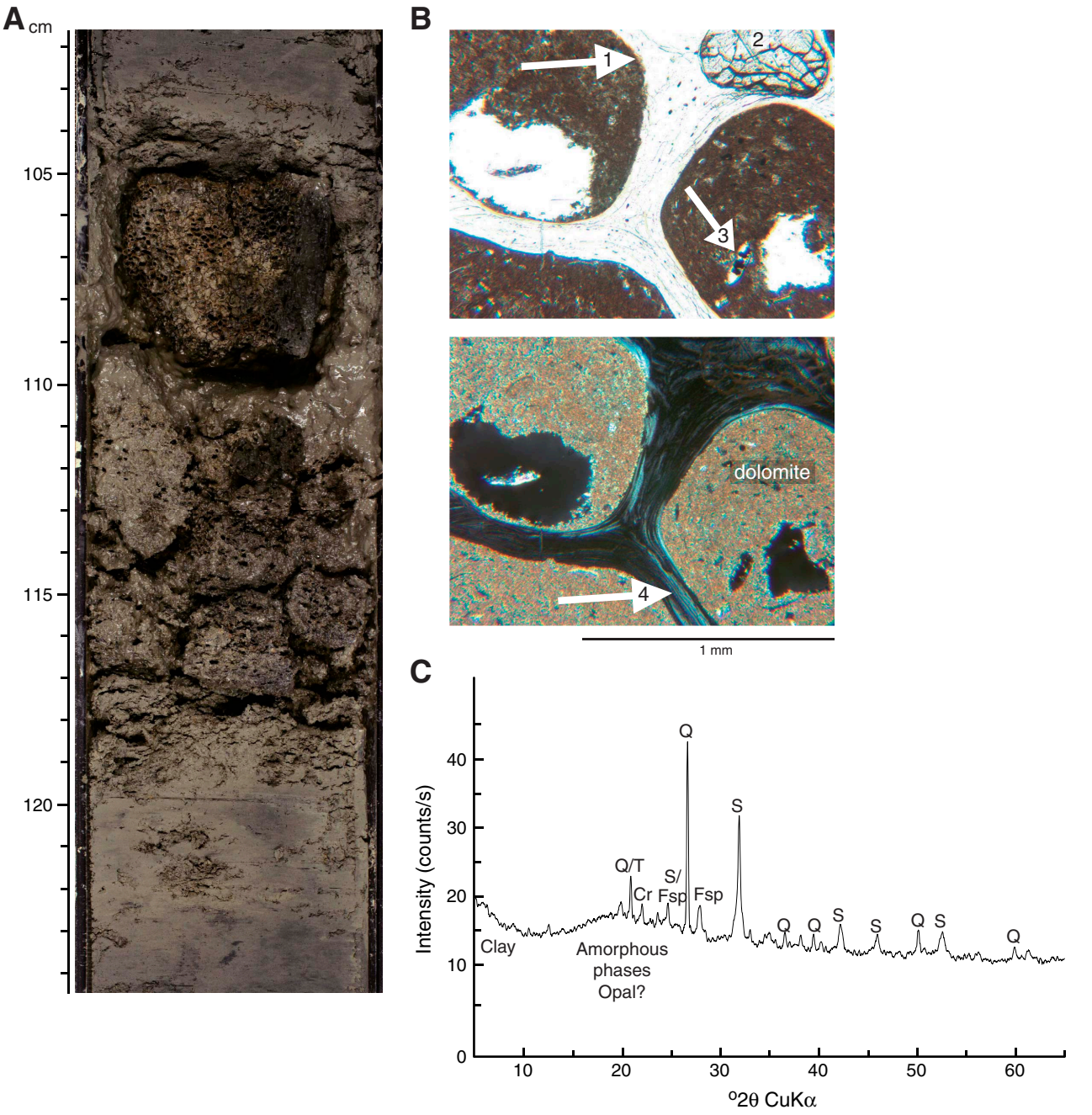

Figure F13. Core photographs of laminations, Site U1345. **A.** Type I (biogenic-rich laminations) (interval 323-U1345A-2H-1, 96–125 cm). **B.** Type II (siliciclastic-rich laminations) (interval 323-U1345A-9H-7, 11–28 cm). **C.** Type IA (Type I laminations with authigenic carbonate) (interval 323-U1345A-9H-4, 11–36 cm).

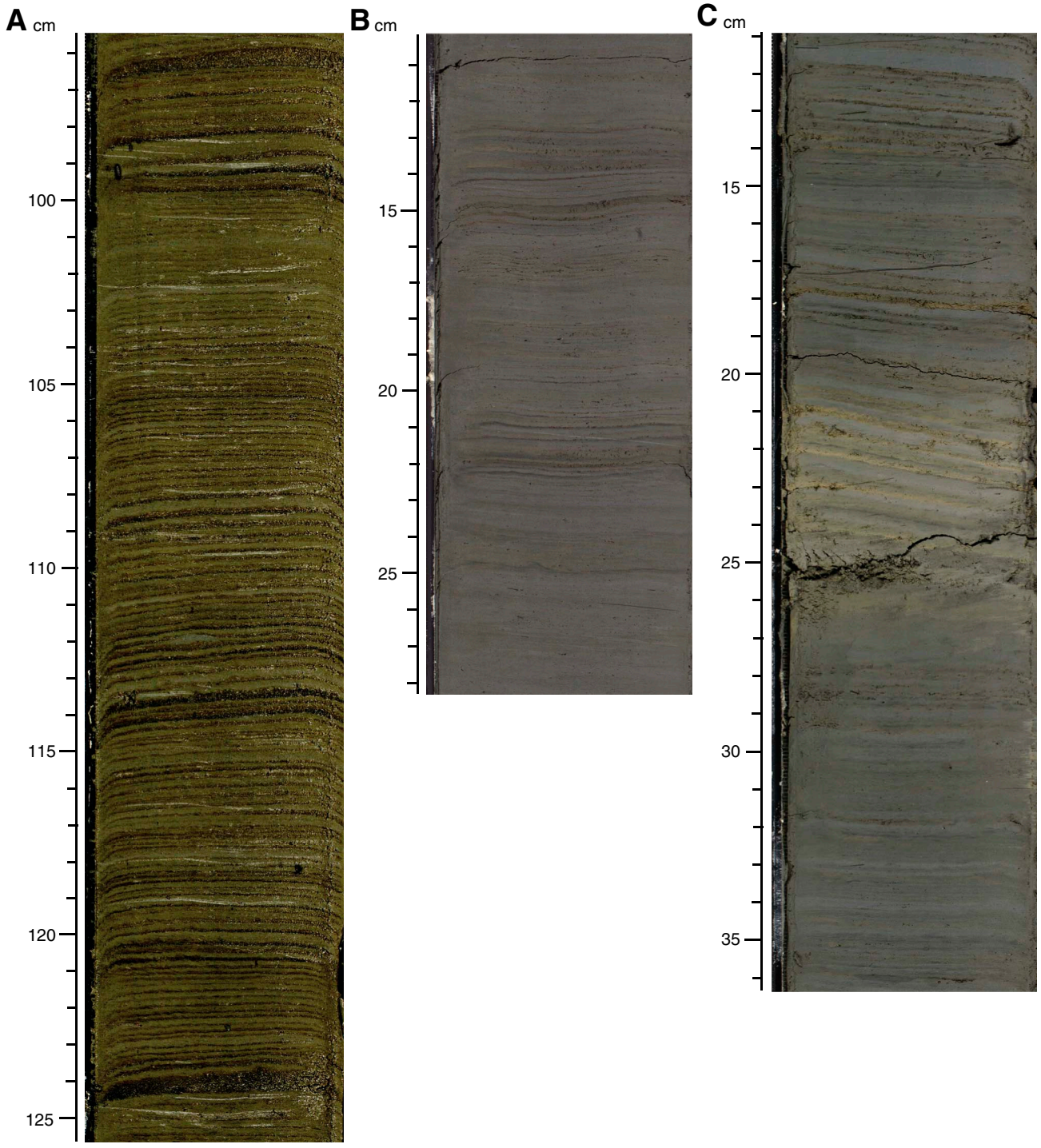

Figure F14. Age-depth plot for Site U1345 showing biostratigraphic datums based on radiolarians, diatoms, and silicoflagellates.

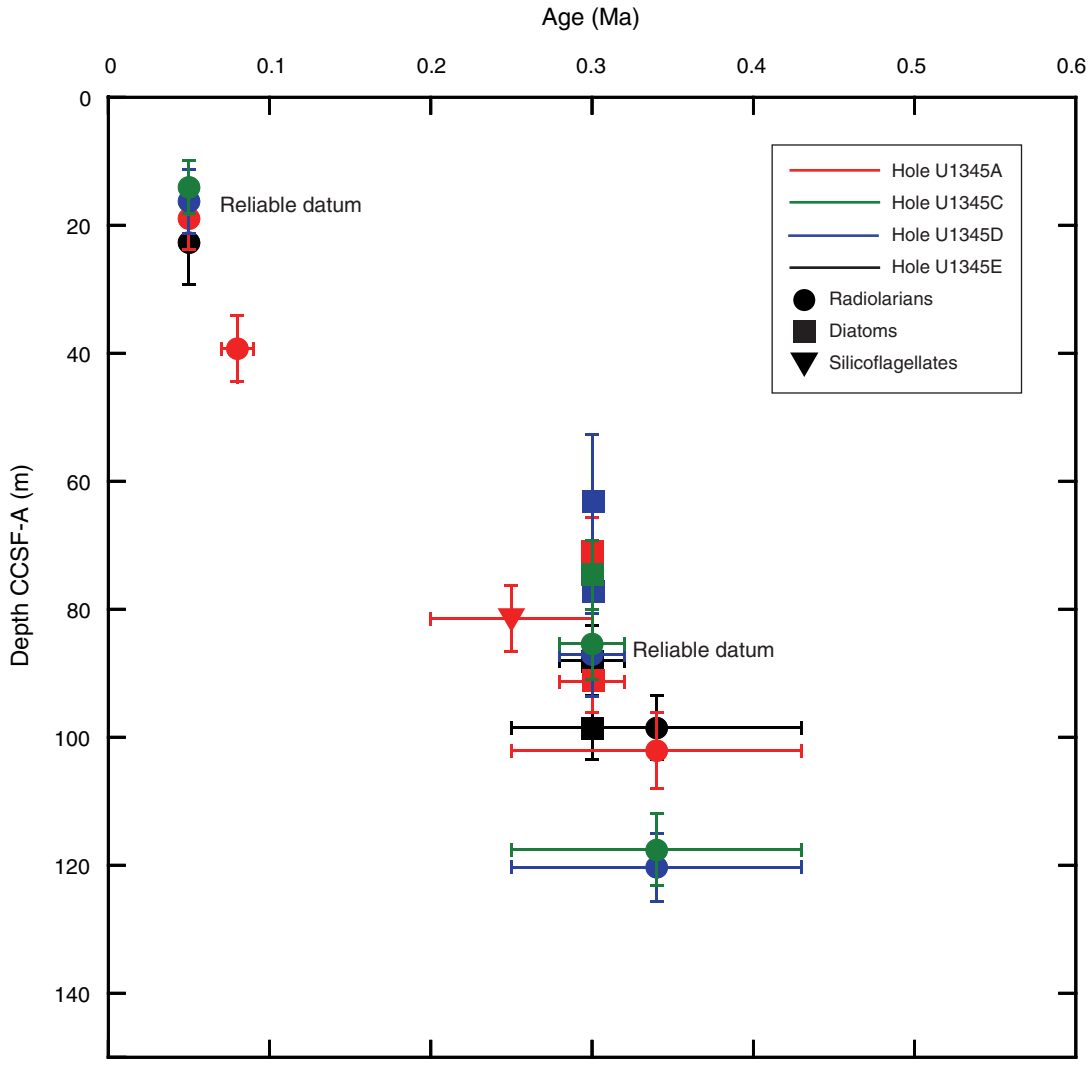

Figure F15. Microfossil abundances and selected species composition vs. composite depth, Site U1345. Gray bars = strongest interglacials (interpreted from all microfossil data). Calcareous nannofossil abundance: B = barren, R = rare, F = few, C = common, A = abundant. Planktonic foraminifer abundance: B = barren, P = present, R = rare, F = frequent, A = abundant, D = dominant. For benthic foraminifer abundance calculations, see **"Biostratigraphy"** in the "Methods" chapter.

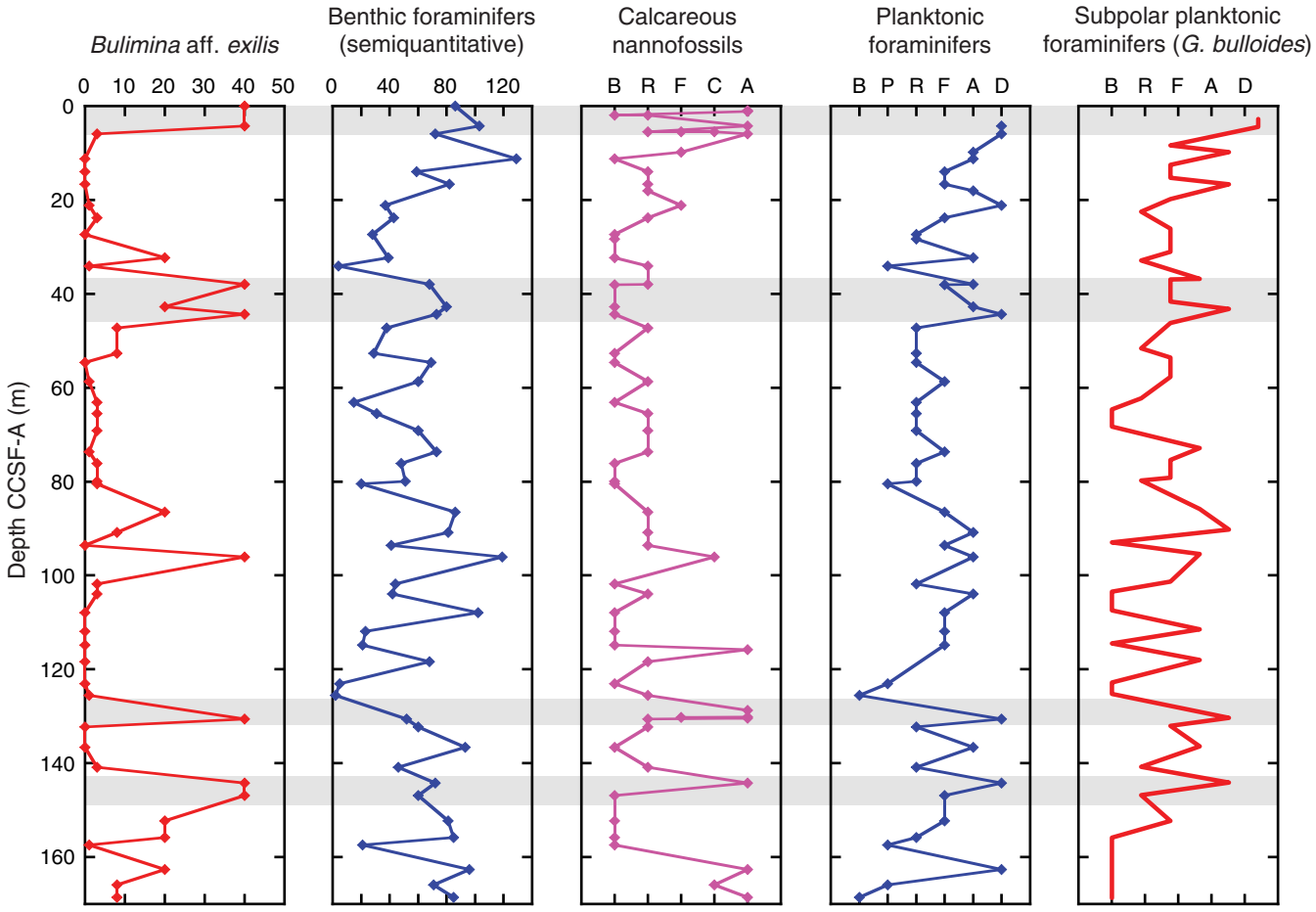

Figure F16. Organic microfossil abundances and selected species composition vs. composite depth, Site U1345. Gray bars = strongest interglacials (interpreted from all microfossil data).

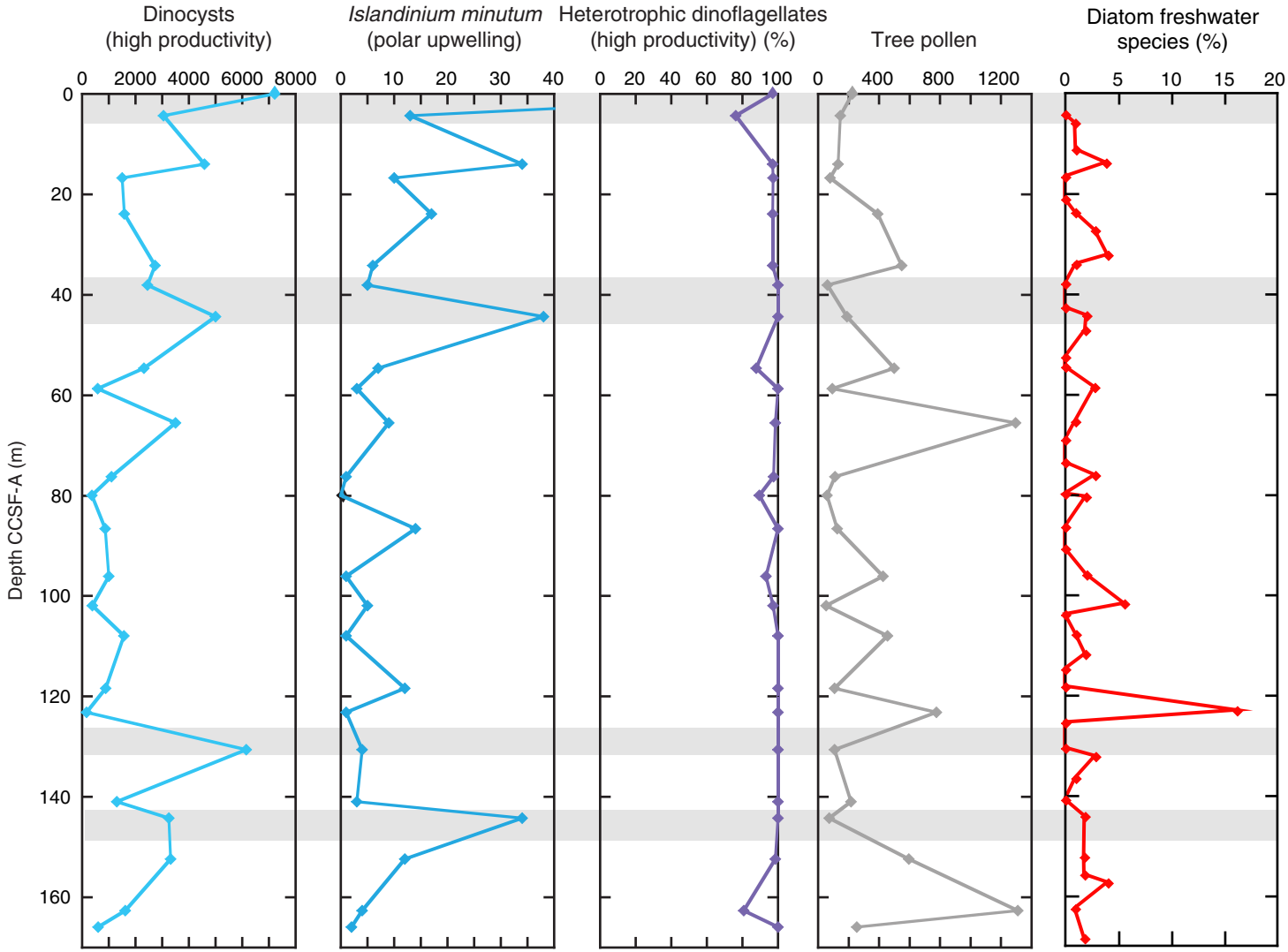

Figure F17. Siliceous microfossil abundances and selected species composition vs. composite depth, Site U1345. Gray bars = strongest interglacials (interpreted from all microfossil data). Diatom sea ice species include *Thalassiosira antarctica* spores, *Bacteriosira fragilis, Detonula confervacea, Thalassiosira hyalina, Porosira glacialis,* and *Fragilariopsis cylindrus*.

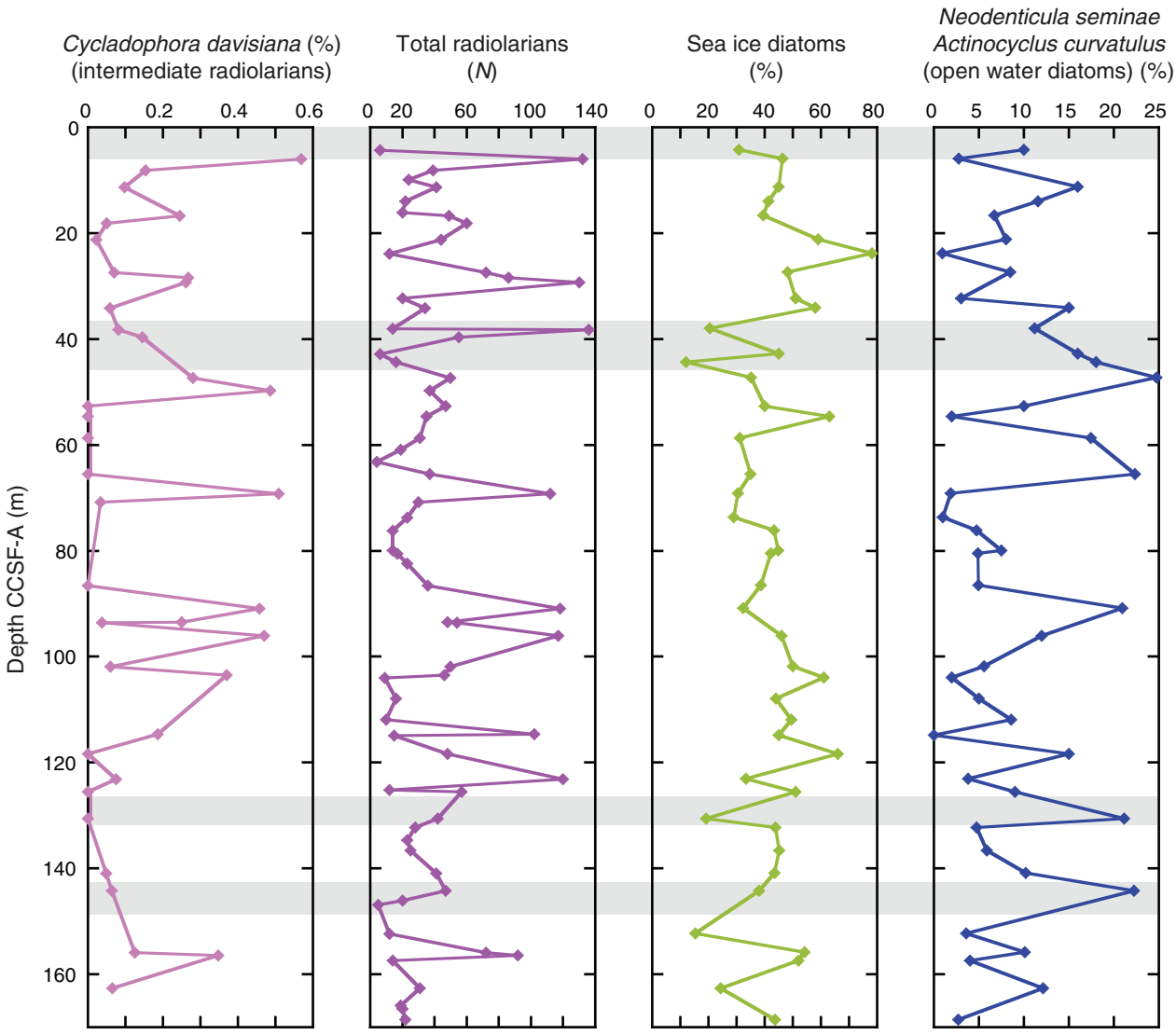

Figure F18. Inclination, declination, and intensity of remanent magnetization after 20 mT AF demagnetization ($Int_{20\ mT}$), Hole U1345A. Intensity data (black) are shown with STMSL magnetic susceptibility data (red).

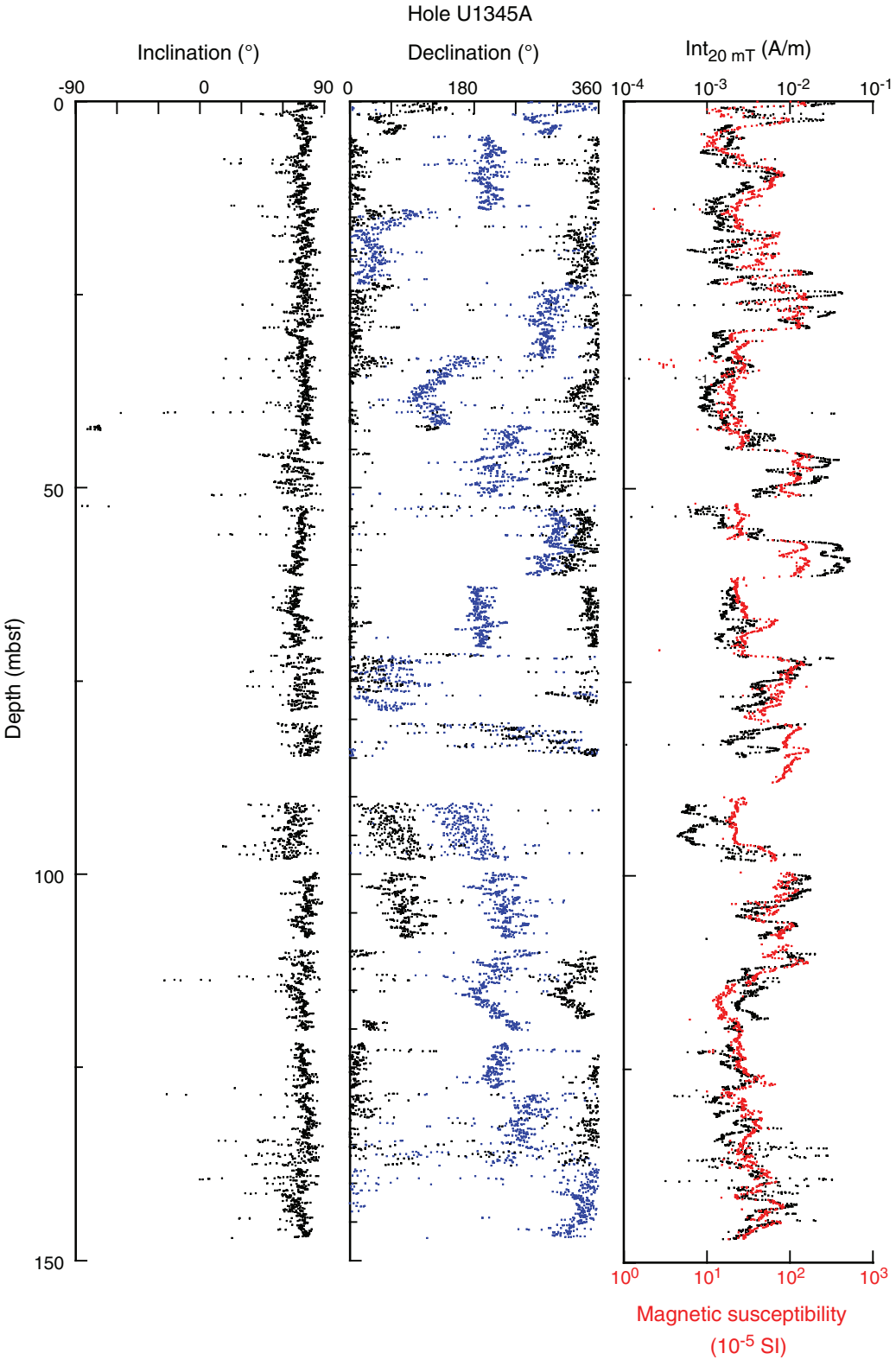

Figure F19. Inclination and intensity of remanent magnetization after 20 mT AF demagnetization ($Int_{20\ mT}$), Holes U1345C–U1345E. Intensity data (black) are shown with STMSL magnetic susceptibility data (red).

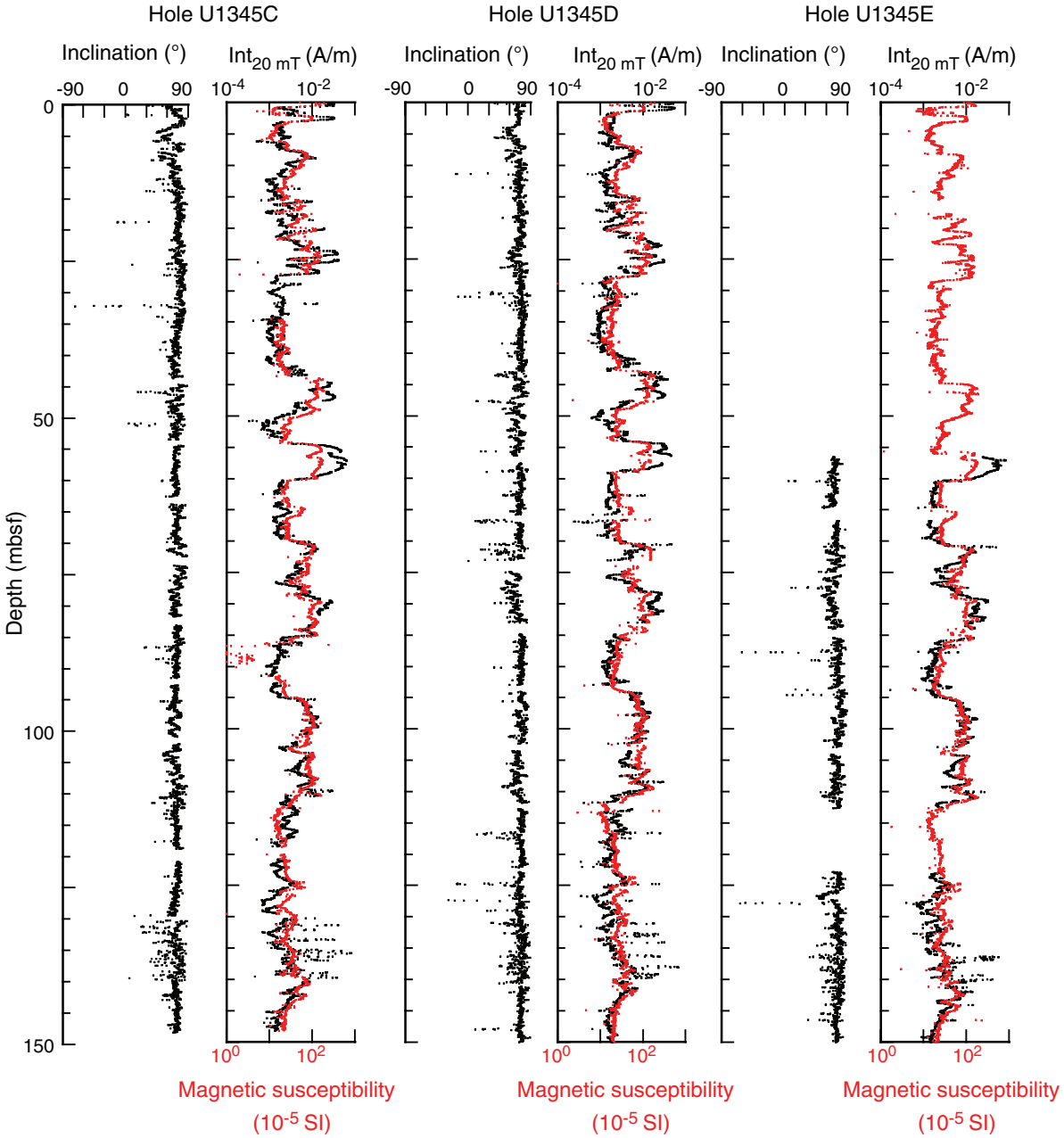

Figure F20. Magnetic susceptibility (top) and relative paleointensity (bottom) vs. depth, Hole U1345A. Relative paleointensity was estimated by normalizing remanent magnetization after 20 mT AF demagnetization ($Int_{20\ mT}$) by magnetic susceptibility. MIS 1–12 in the Brunhes Chron, numbered at top, were tentatively identified by correlating these features to other sites.

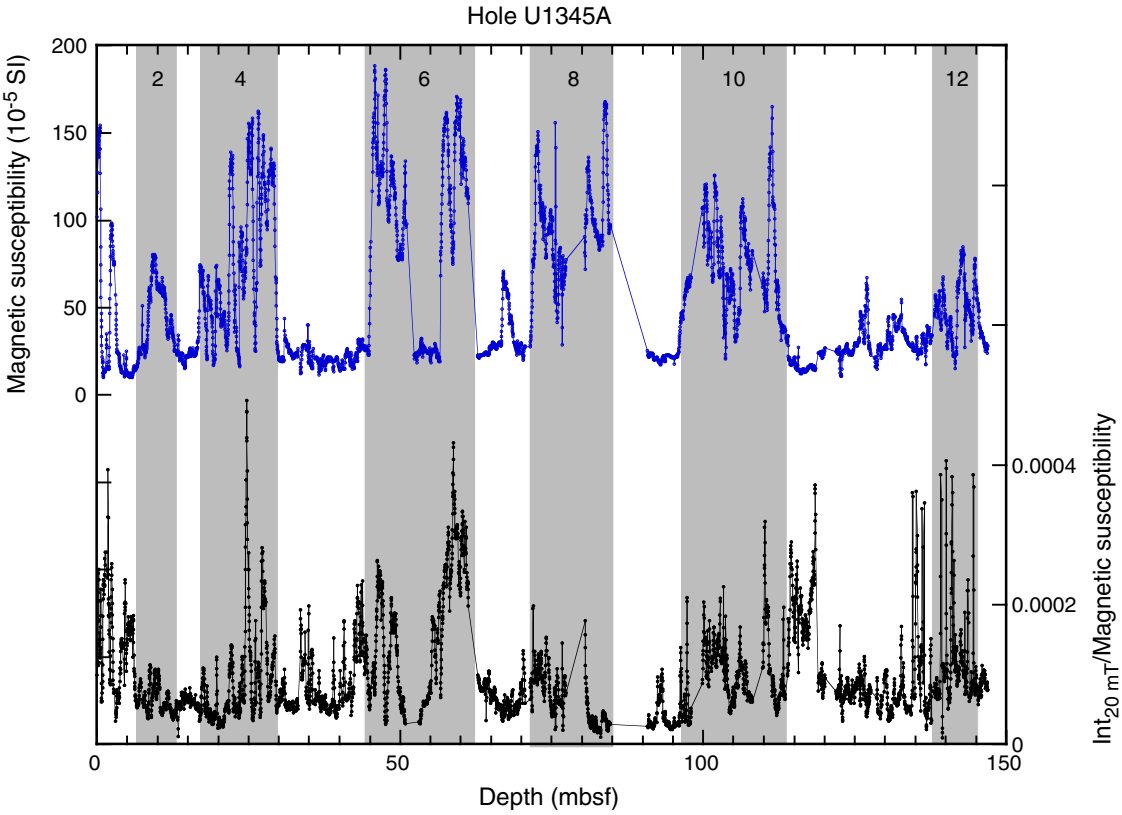

Figure F21. Dissolved chemical concentrations, Holes U1345A and U1345B. **A.** Dissolved inorganic carbon (DIC). **B.** pH. **C.** Alkalinity. **D.** Sulfate. **E.** Methane. **F.** Total hydrogen sulfide ($\Sigma H_2S = H_2S + HS^-$). **G.** Phosphate. **H.** Ammonium. **I.** Salinity. Note that SO_4^{2-}, CH_4, and ΣH_2S depth profiles are displayed only for the 0–15 mbsf interval.

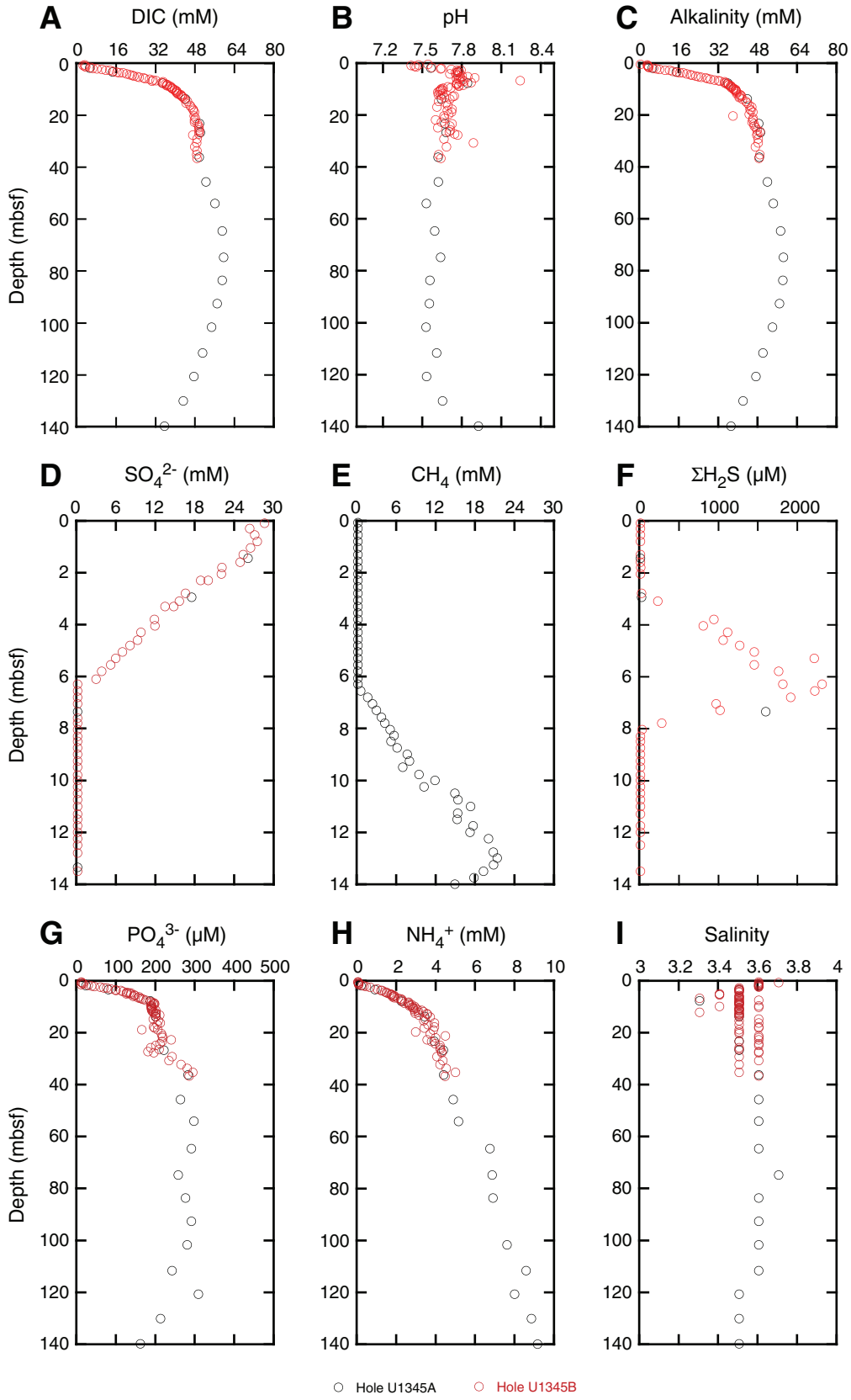

Figure F22. Dissolved chemical concentrations, Holes U1345A and U1345B. **A.** Calcium. **B.** Magnesium. **C.** Chloride. **D.** Sodium. **E.** Potassium. **F.** Strontium. **G.** Manganese. **H.** Iron. **I.** Lithium. **J.** Boron. **K.** Silica. **L.** Barium.

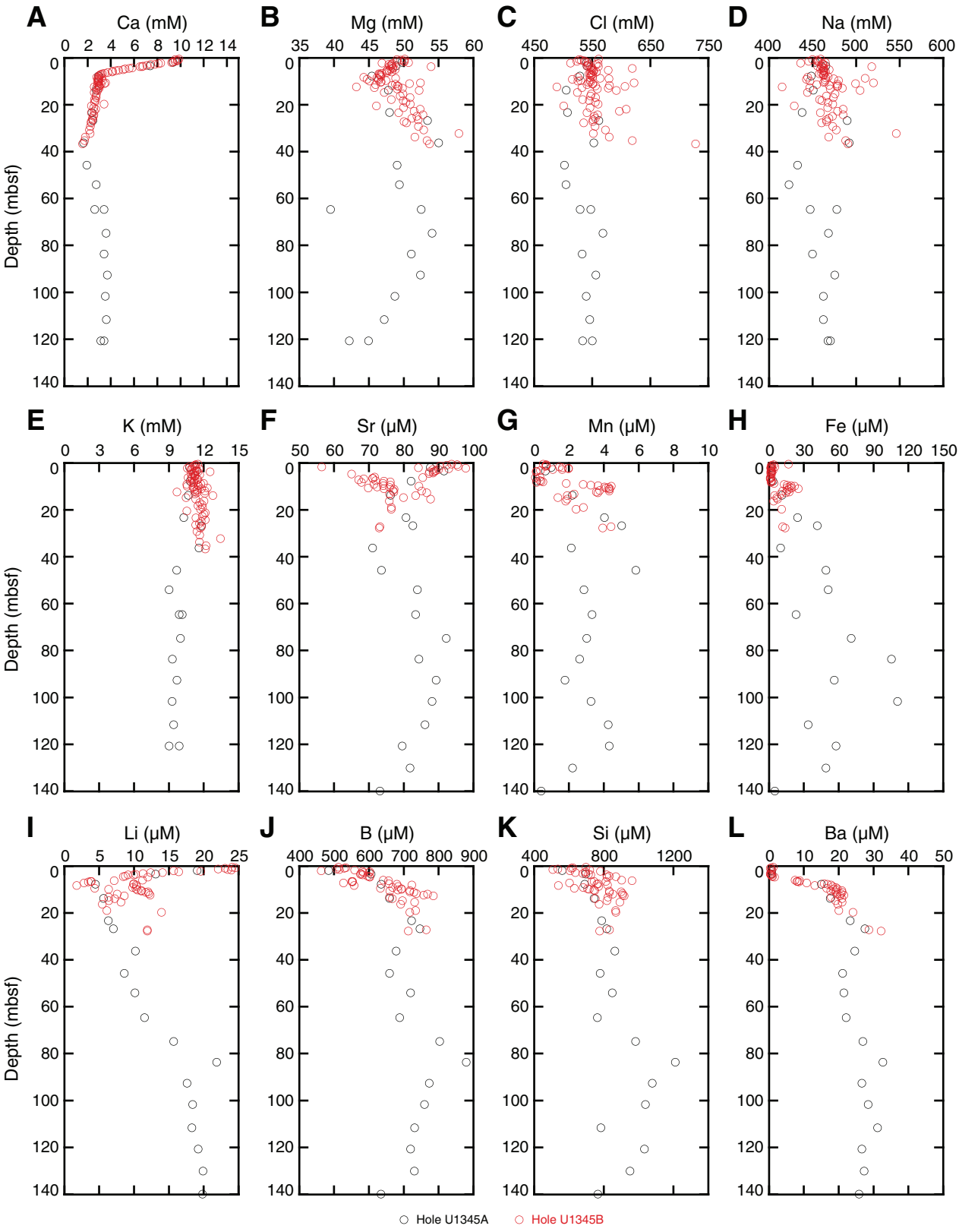

Figure F23. Solid-phase chemical concentrations, Hole U1345A. **A.** Calcium carbonate ($CaCO_3$). **B.** Total organic carbon (TOC). **C.** Total nitrogen (TN). **D.** Total sulfur (TS).

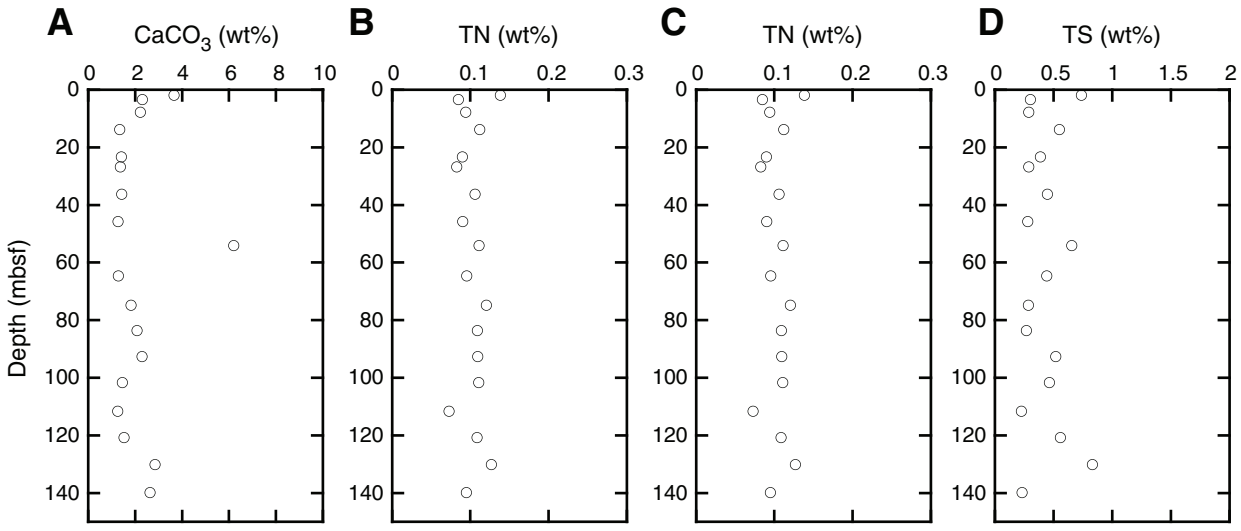

Figure F24. A. Downsection distribution of WRMSL gamma ray attenuation (GRA) wet bulk density measured on Hole U1345A cores. Open circles = plots of discrete-sample or MAD bulk density, also displayed in B. (**Continued on next page.**)

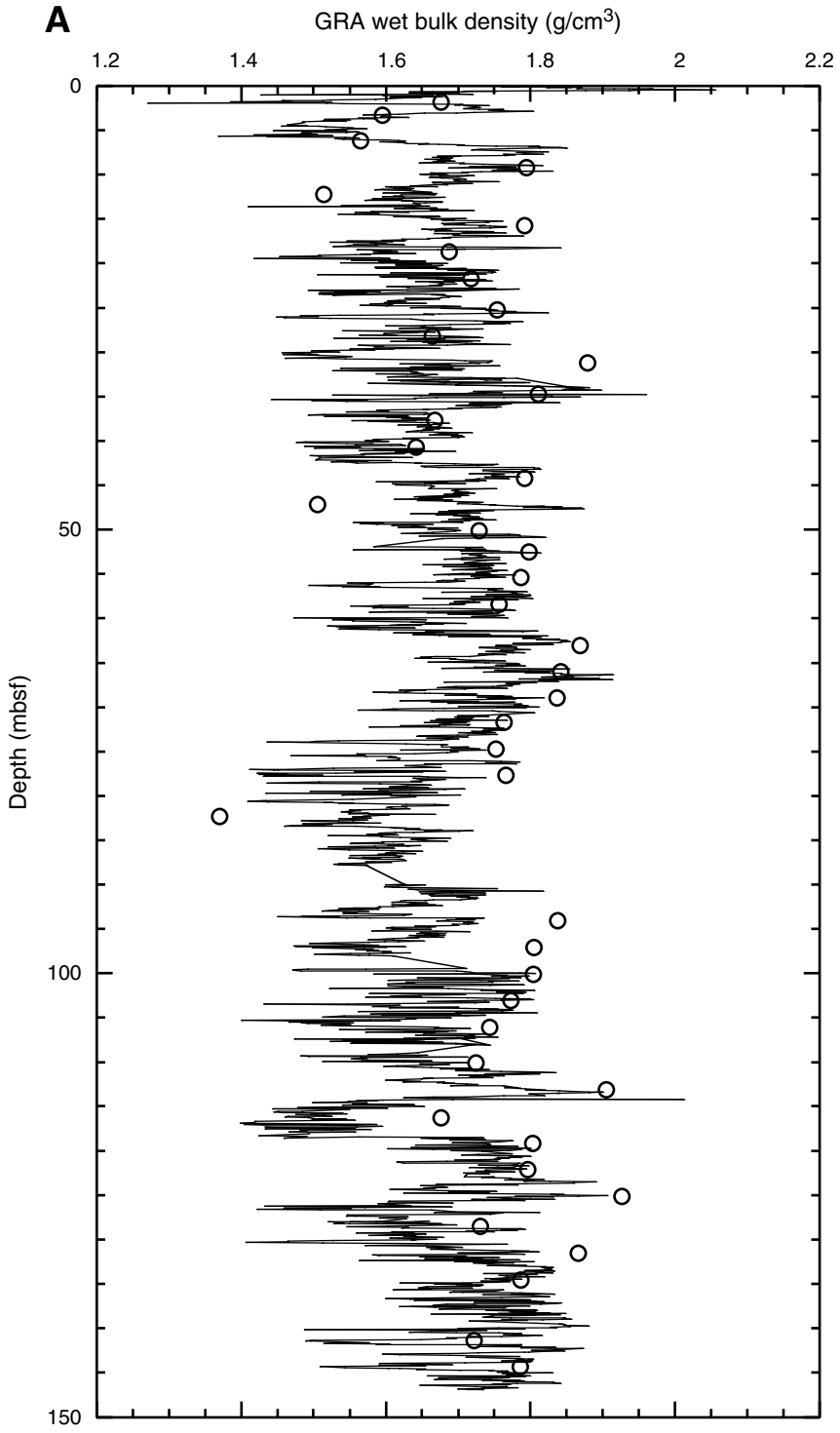

Figure F24 (continued). B. Downhole distribution of wet bulk density measured on discrete moisture and density (MAD) sediment samples collected from Hole U1345A cores.

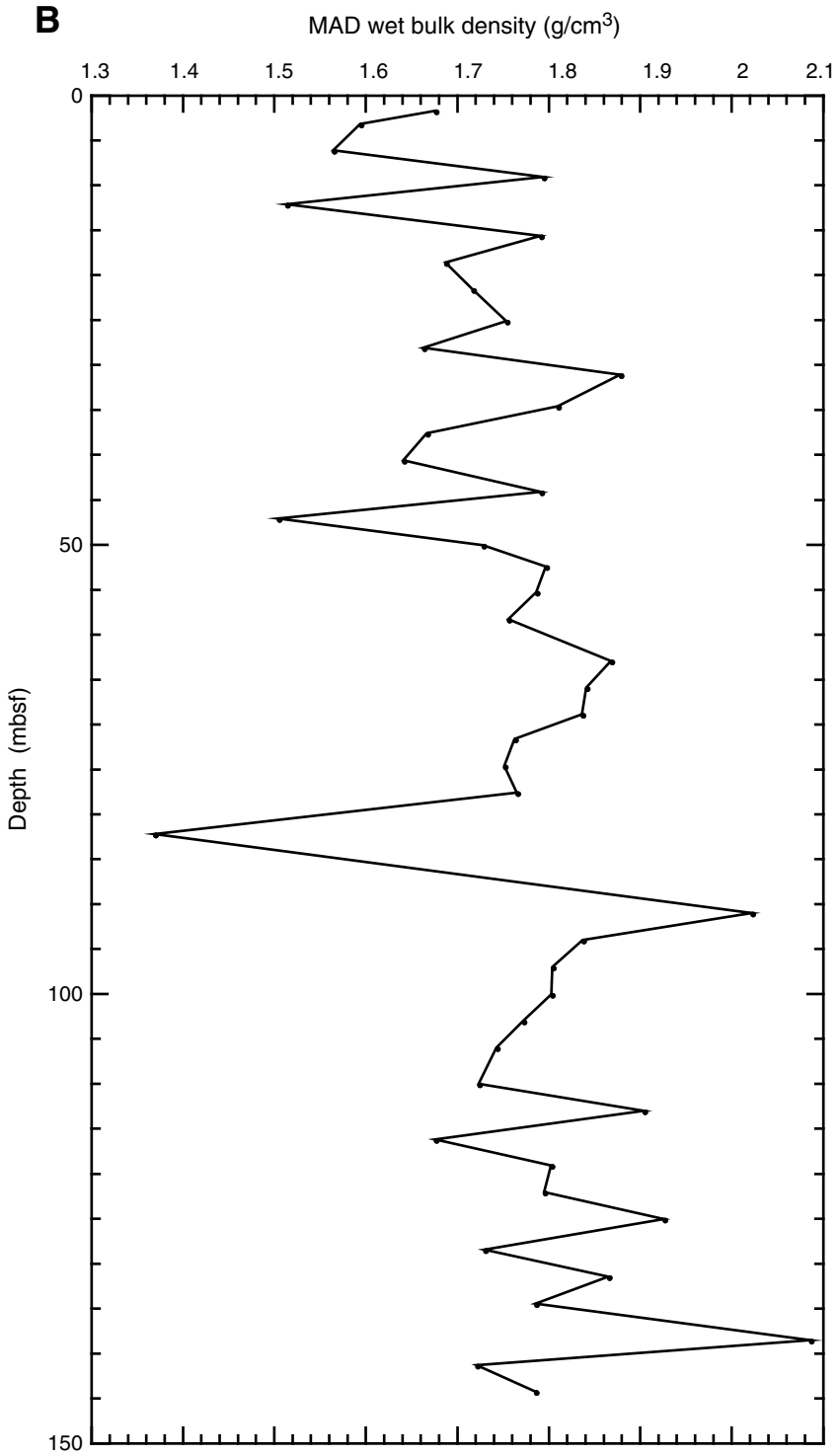

Figure F25. Downhole distribution of magnetic susceptibility recorded by the WRMSL scanner on core sections recovered from Hole U1345A.

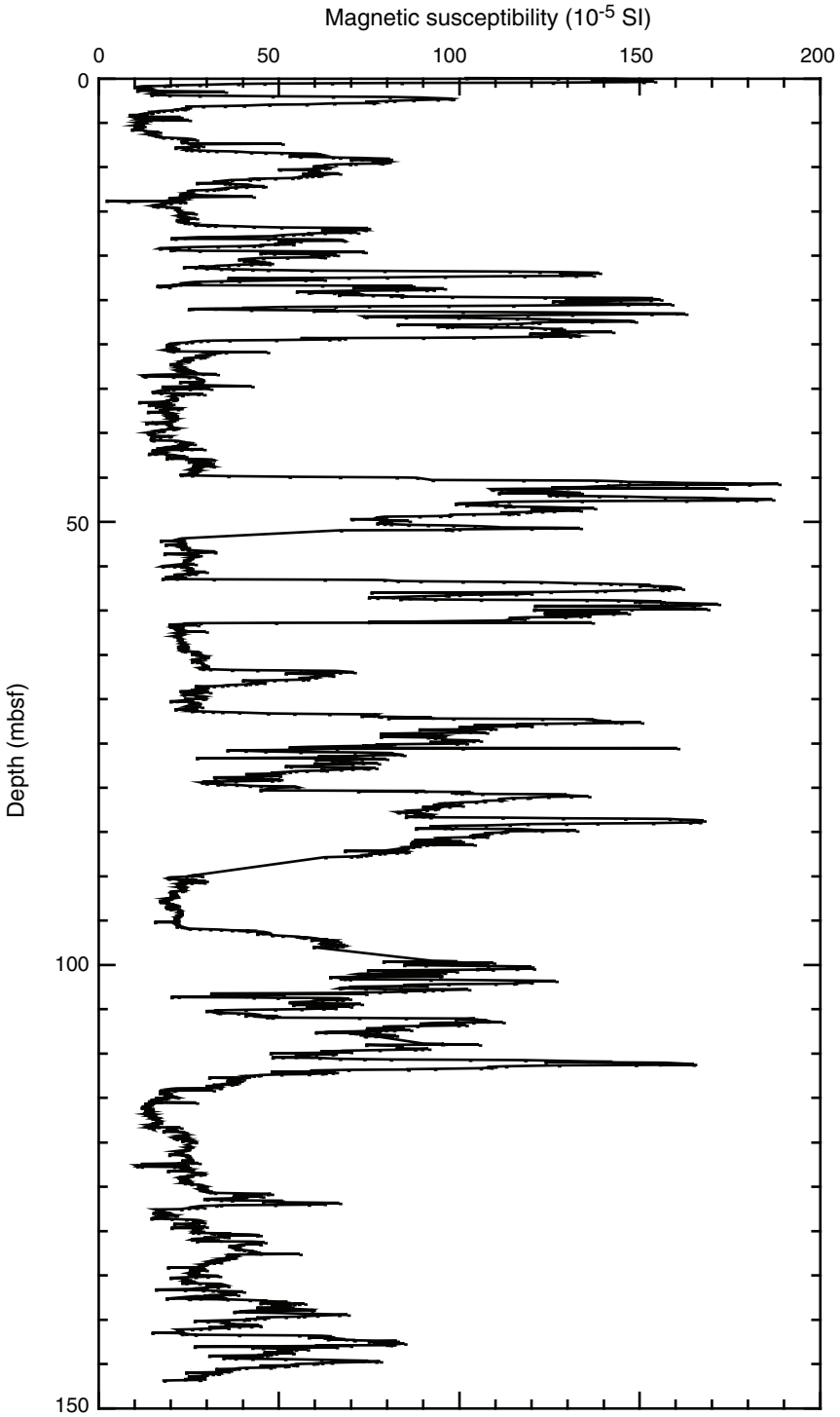

Figure F26. Downhole distribution of natural gamma ray (NGR) readings of total counts/s on core sections from Hole U1345A.

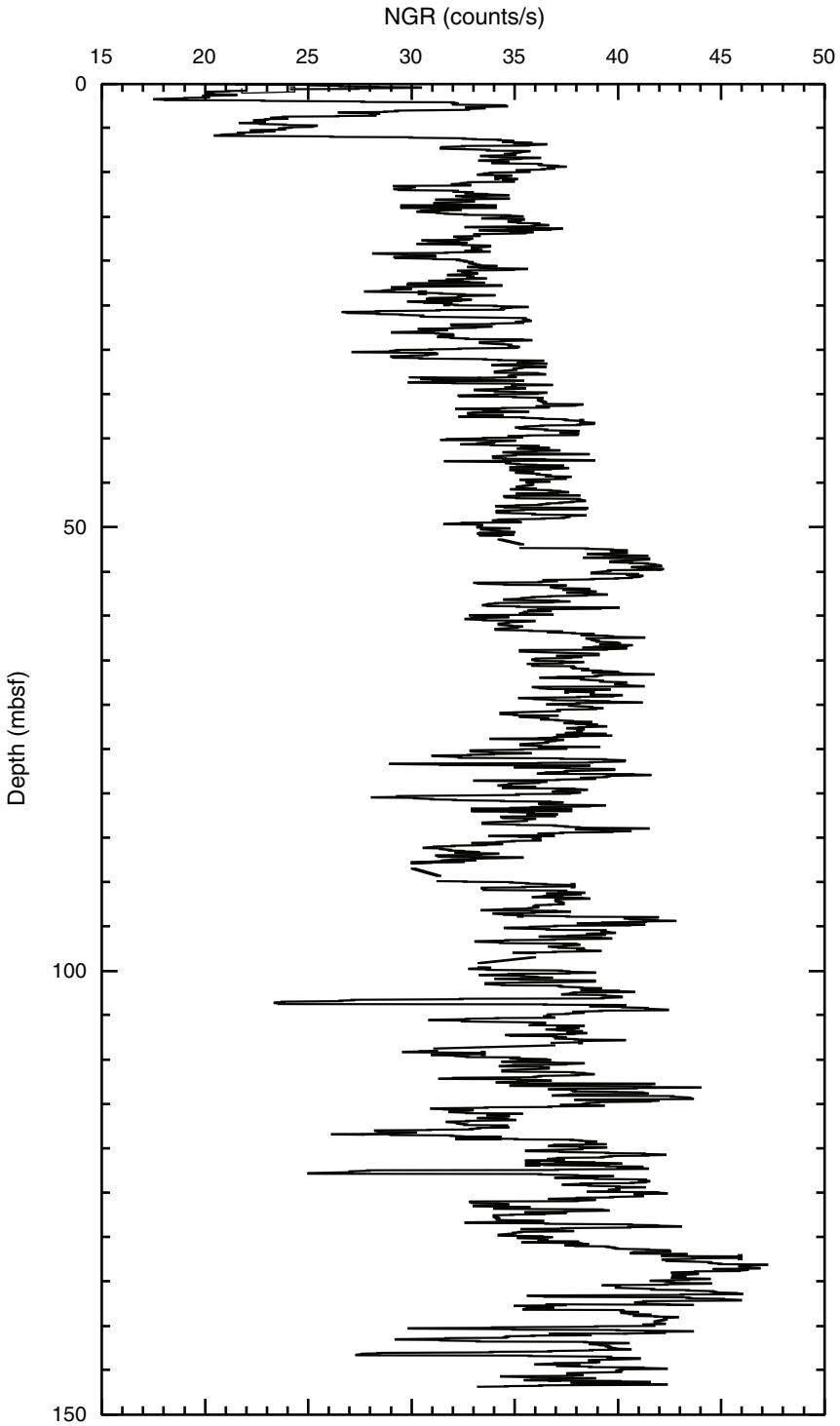

Figure F27. Downsection profiles of water content and porosity measured with MAD analyses of sediment samples taken from Holes U1345A cores.

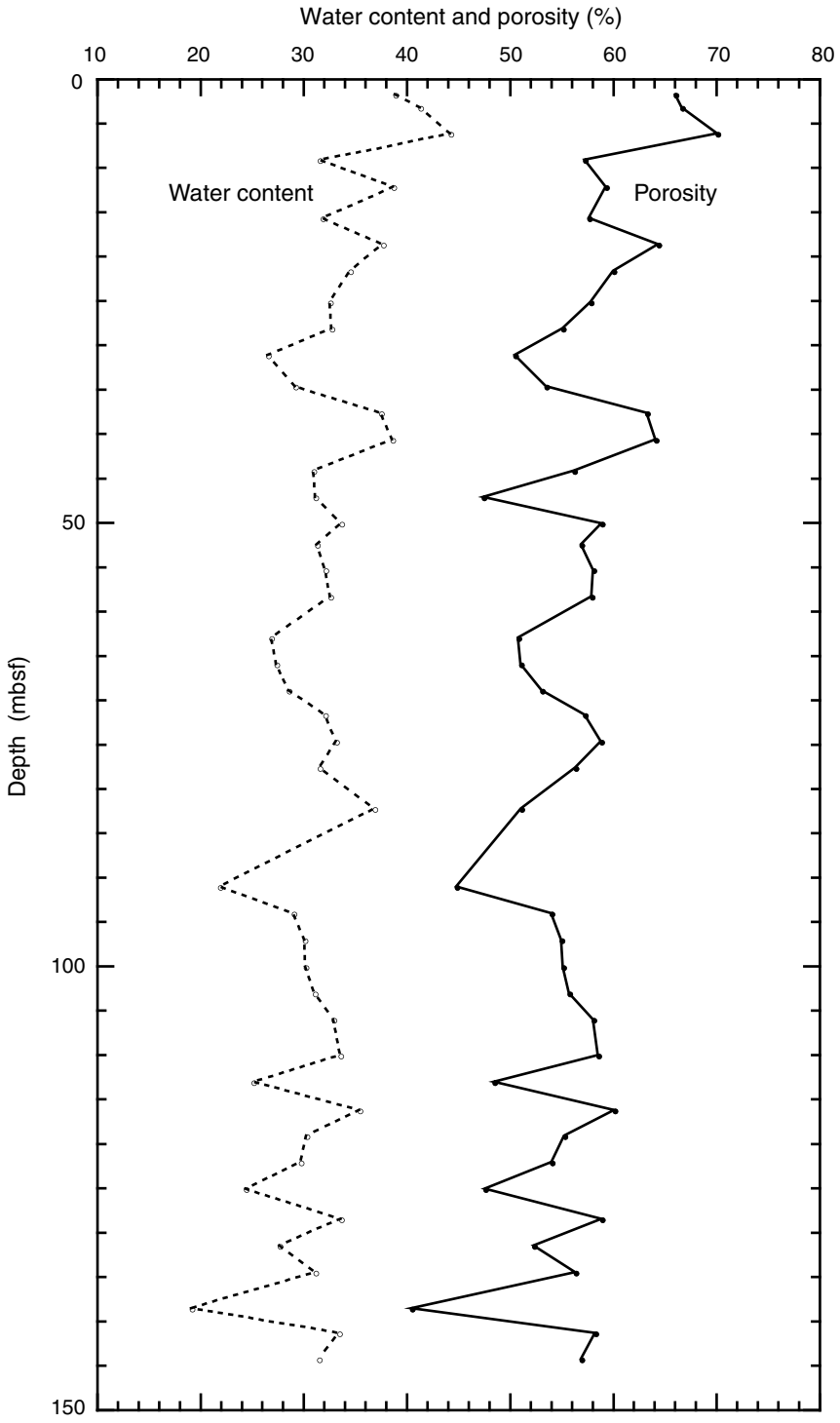

Figure F28. Downsection distribution of dry grain density measured by MAD analyses of sediment samples taken from Hole U1345A cores.

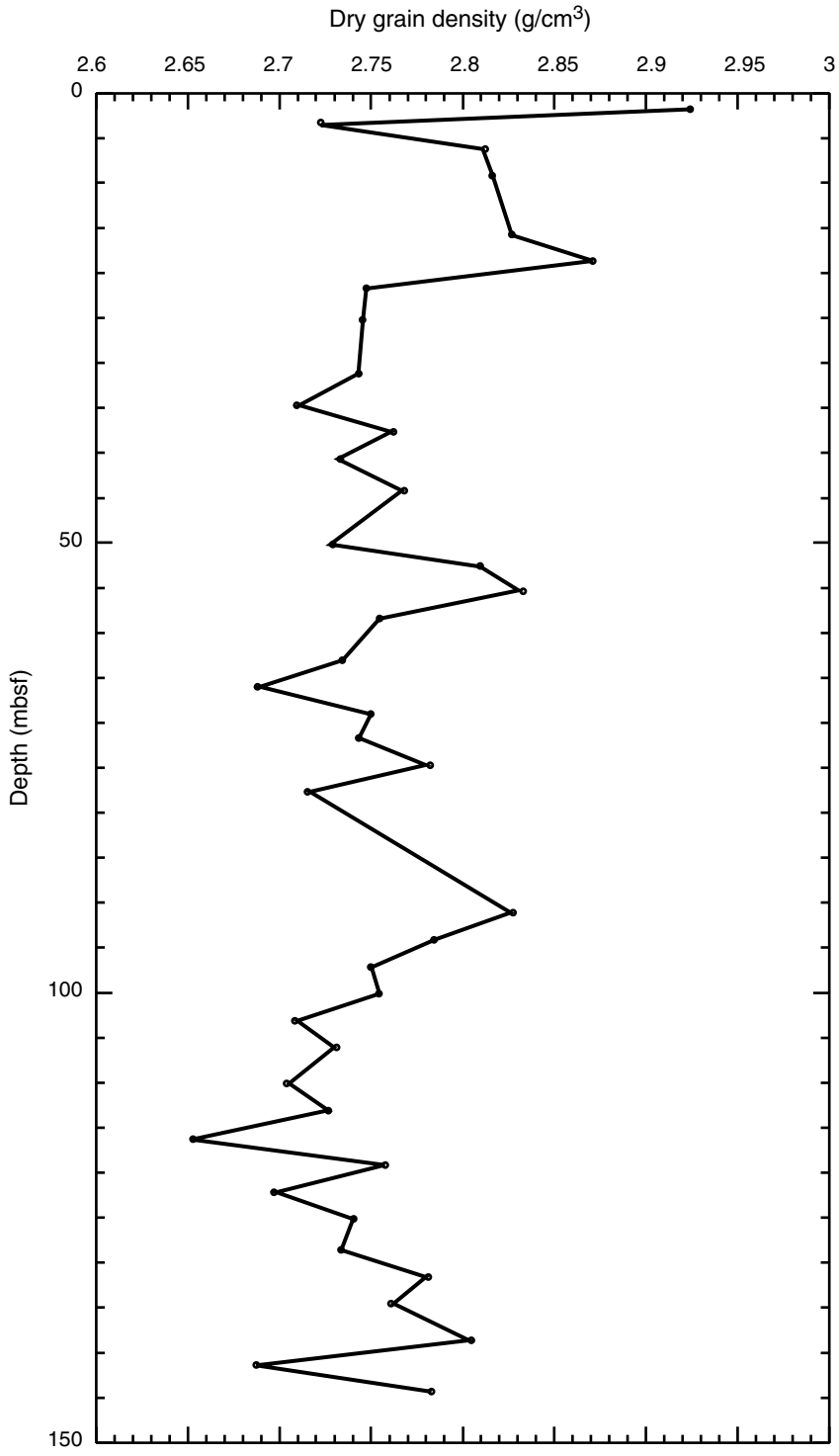

Figure F29. Downhole distribution of thermal conductivity measured mostly on Section 2 of cores retrieved from Hole U1345A.

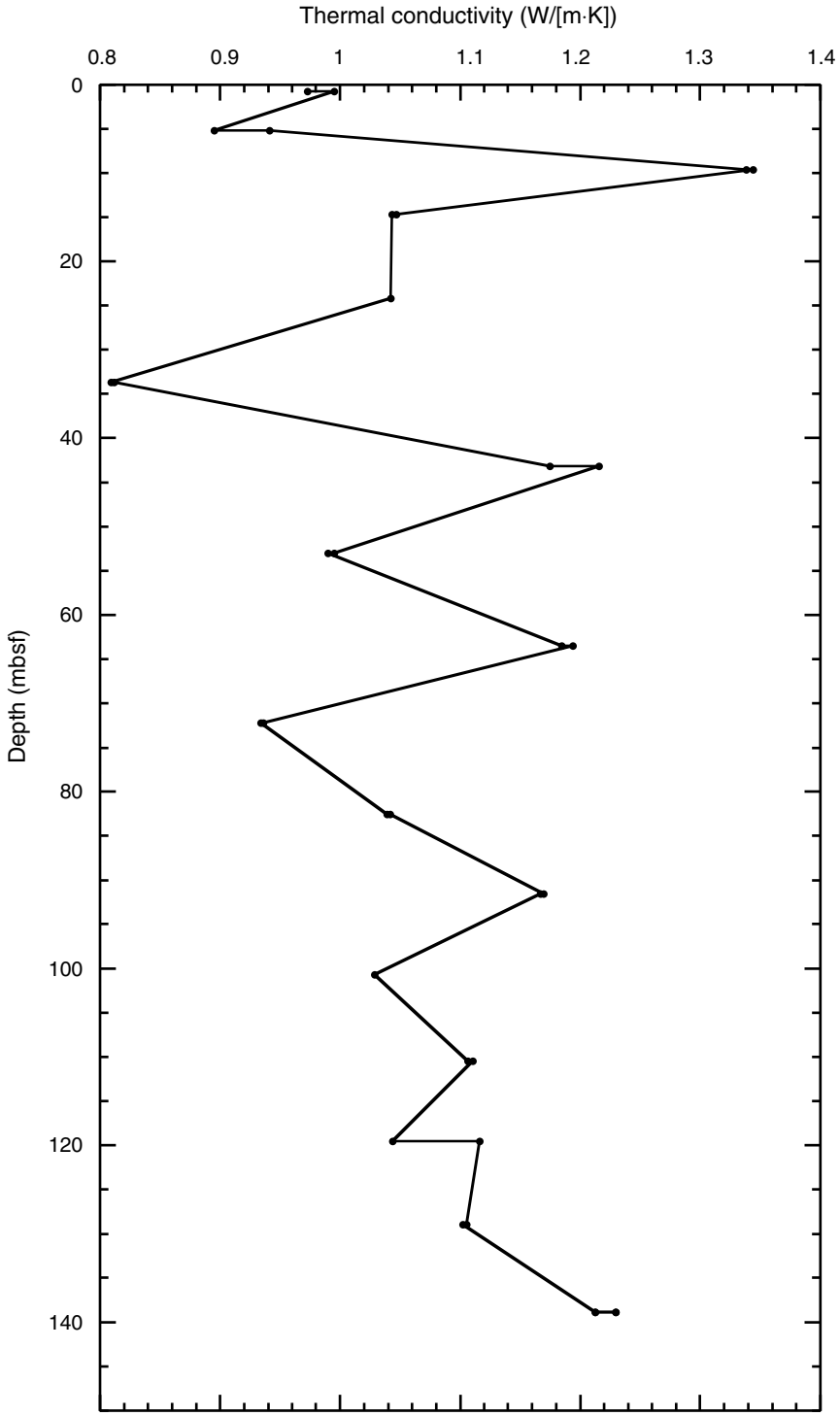

Figure F30. WRMSL magnetic susceptibility data vs. composite depth, Site U1345. STMSL magnetic susceptibility data are shown for Hole U1345B because cores from this microbiology-dedicated hole were not run through the WRMSL. For the primary splice record (top panel), depth on the CCSF-D scale is equivalent to depth on the CCSF-A scale. **A.** 0–85 m CCSF-A. (**Continued on next page.**)

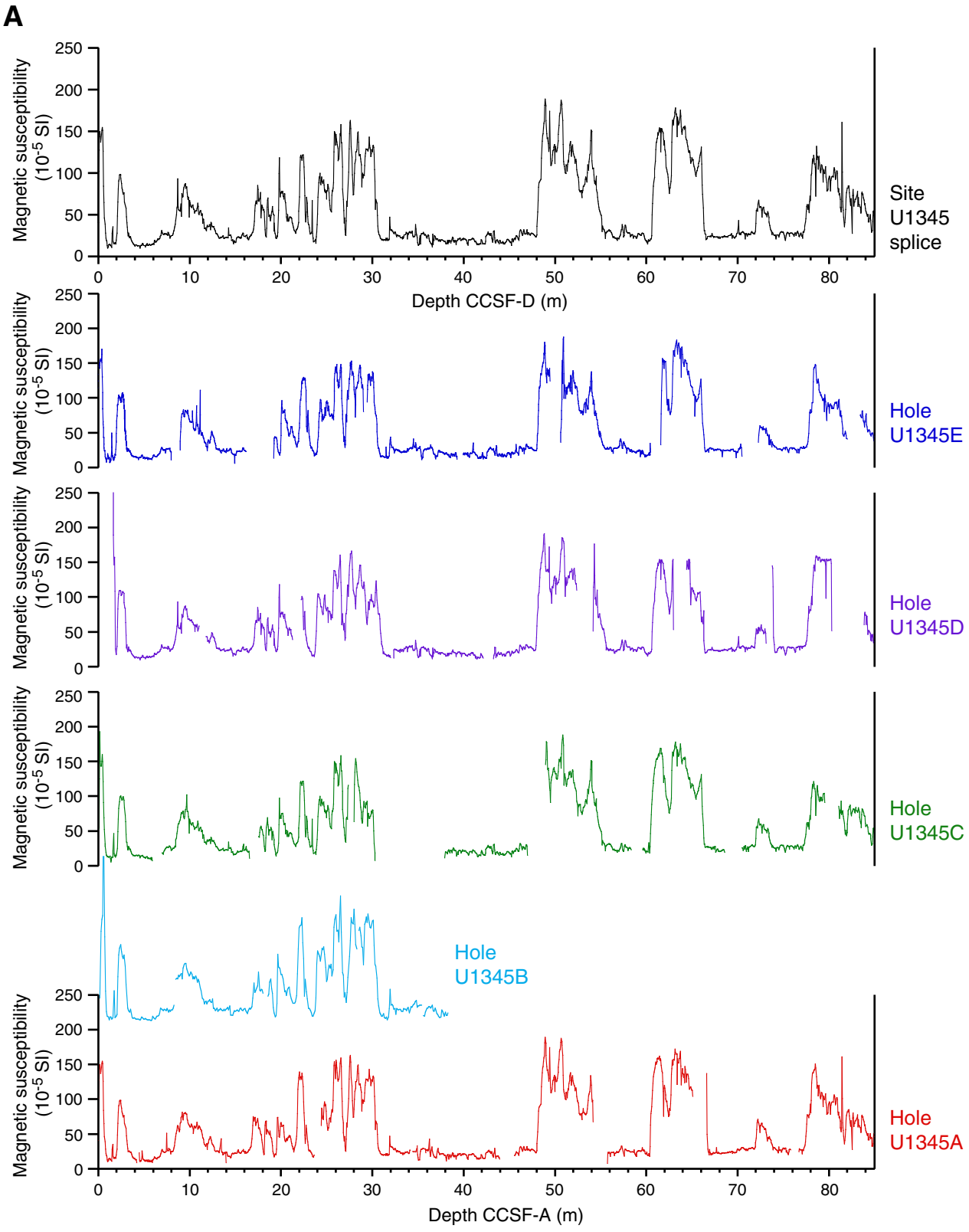

Figure F30 (continued). B. 80–170 m CCSF-A.

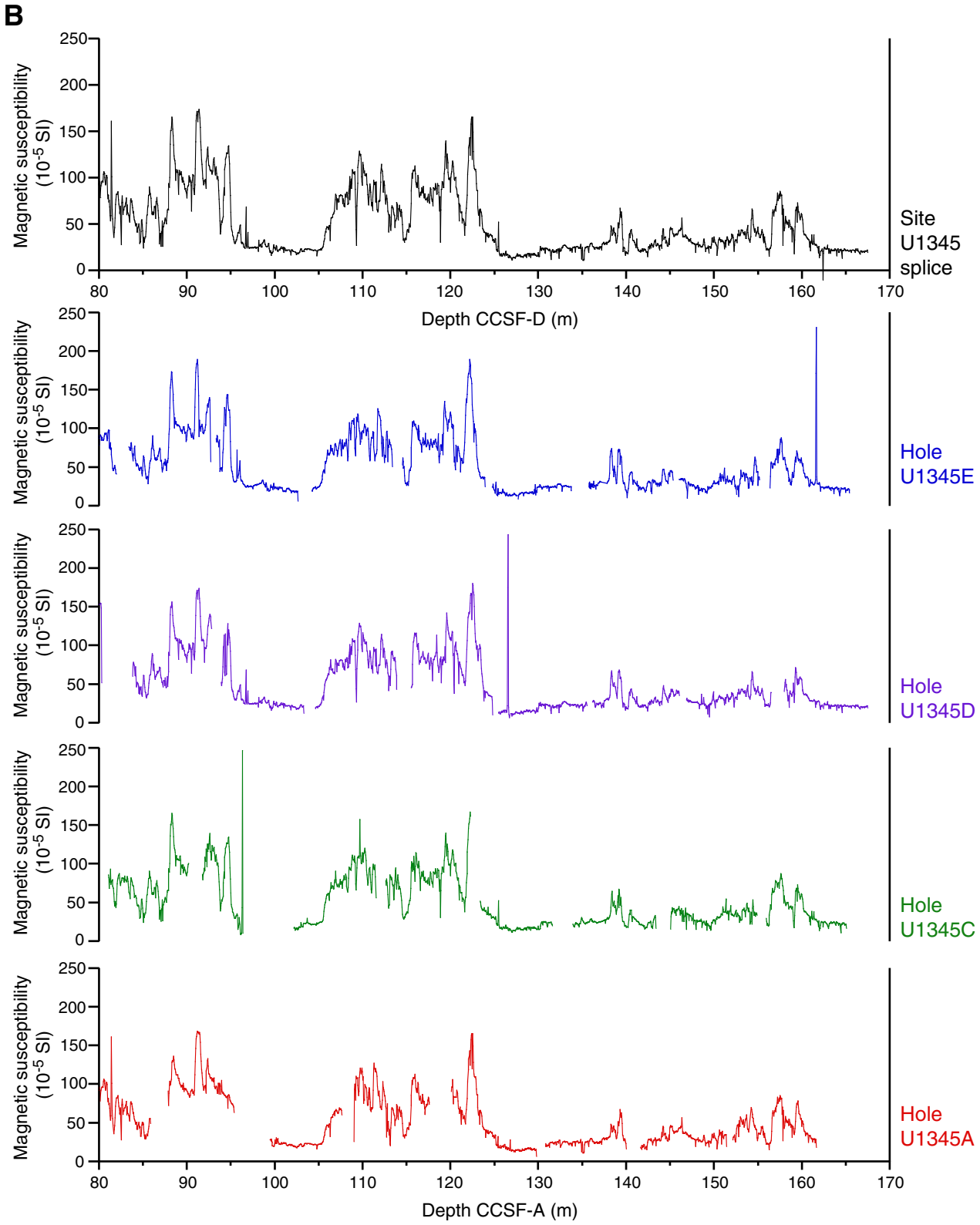

Figure F31. WRMSL gamma ray attenuation (GRA) bulk density vs. composite depth, Site U1345. STMSL GRA data are shown for Hole U1345B because cores from this microbiology-dedicated hole were not run through the WRMSL. For the primary splice record (top panel), depth on the CCSF-D scale is equivalent to depth on the CCSF-A scale. **A.** 0–85 m CCSF-A. (**Continued on next page.**)

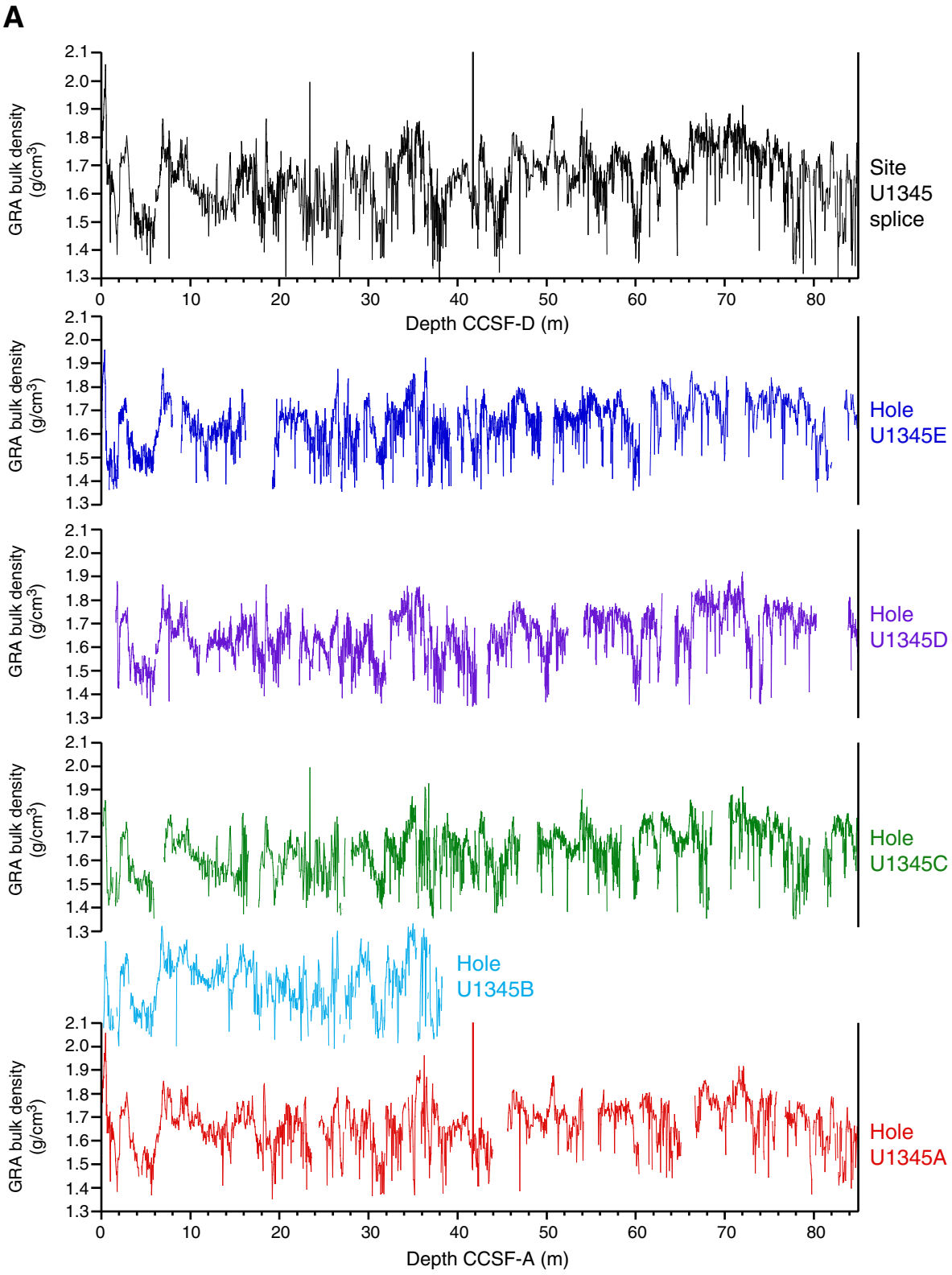

Figure F31 (continued). B. 85–170 m CCSF-A.

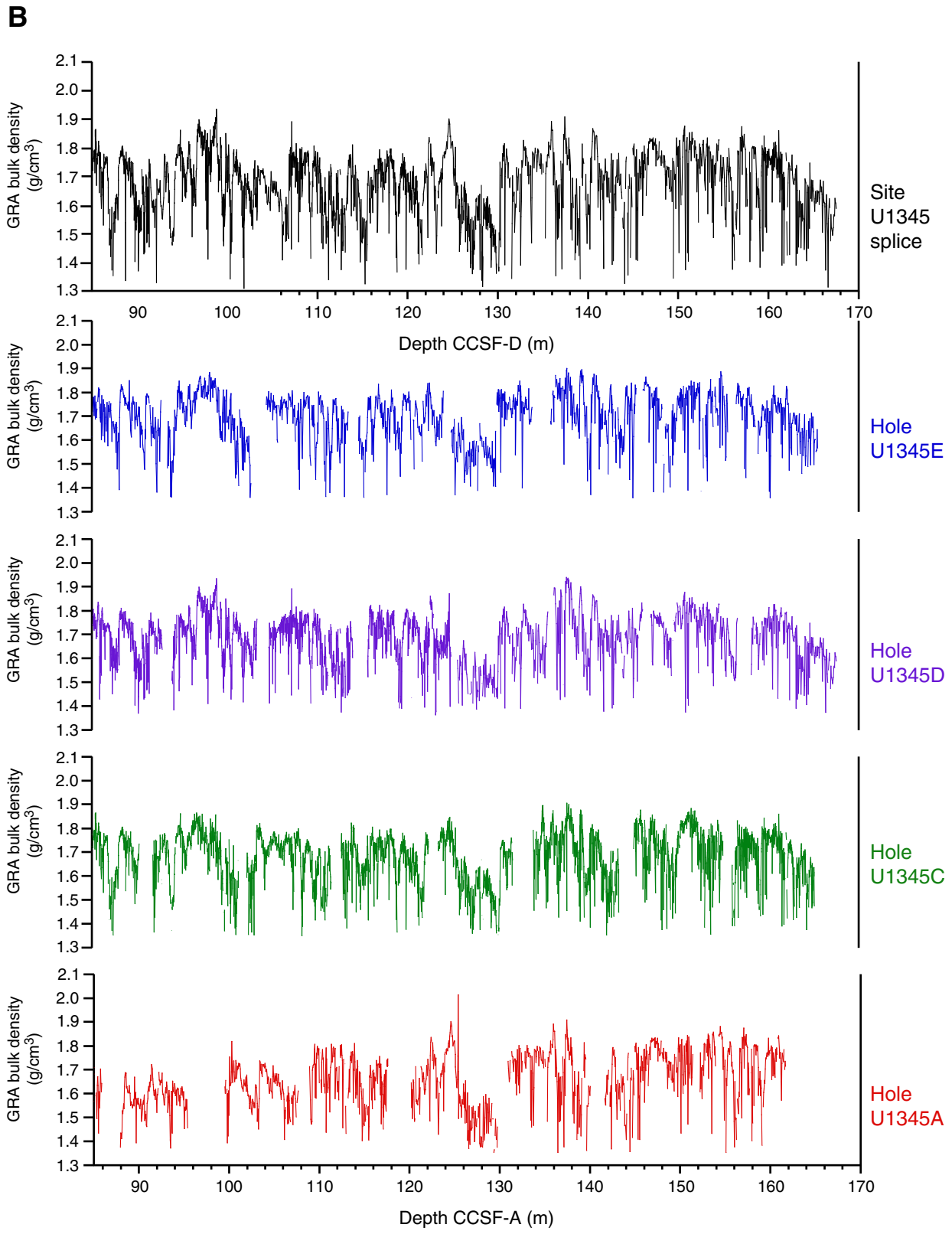

Figure F32. Natural gamma radiation (NGR) data collected with the NGRL vs. composite depth, Site U1345. No NGR data are available for Hole U1345B (microbiology-dedicated hole). For the primary splice record (top panel), depth on the CCSF-D scale is equivalent to depth on the CCSF-A scale. **A.** 0–85 m CCSF-A. (**Continued on next page.**)

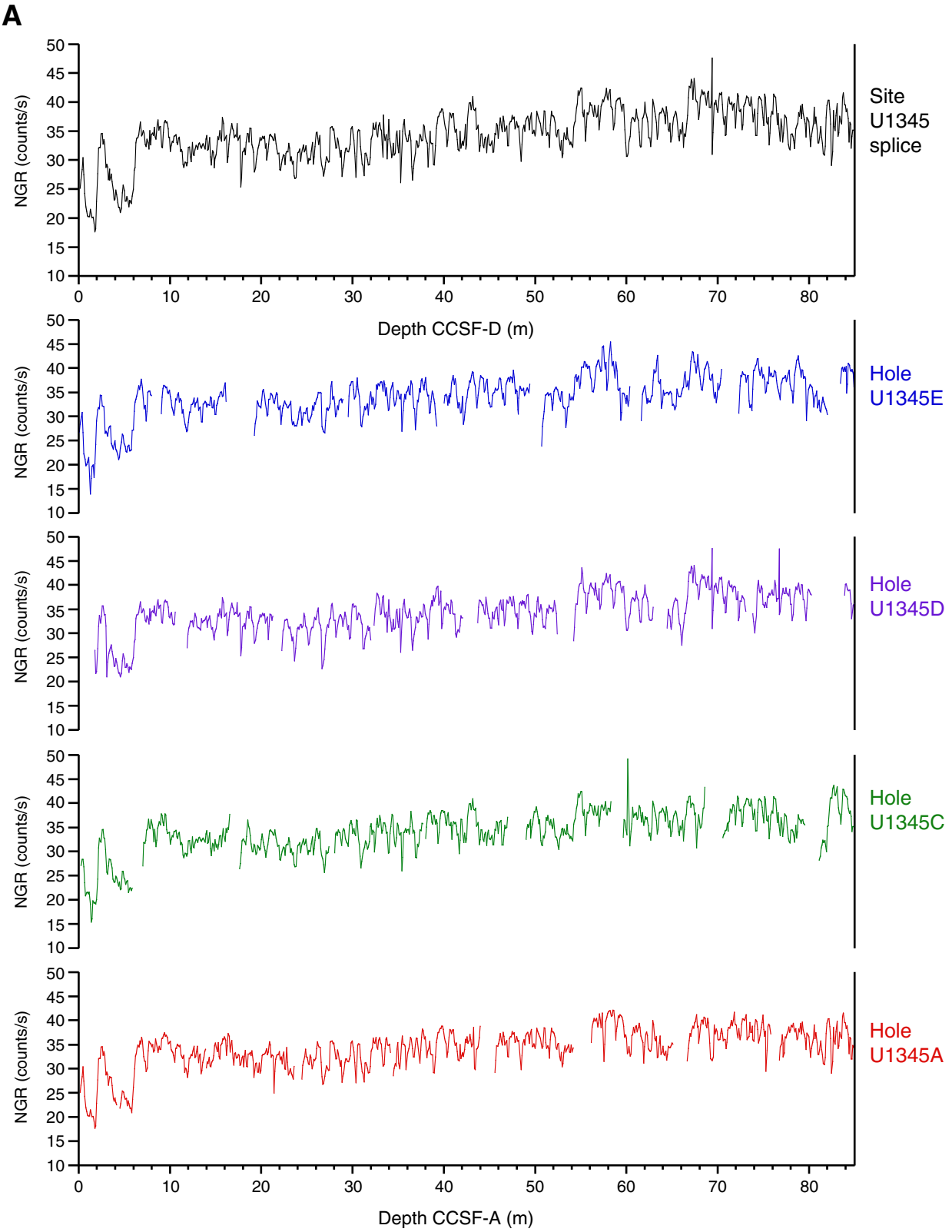

Figure F32 (continued). B. 85–170 m CCSF-A.

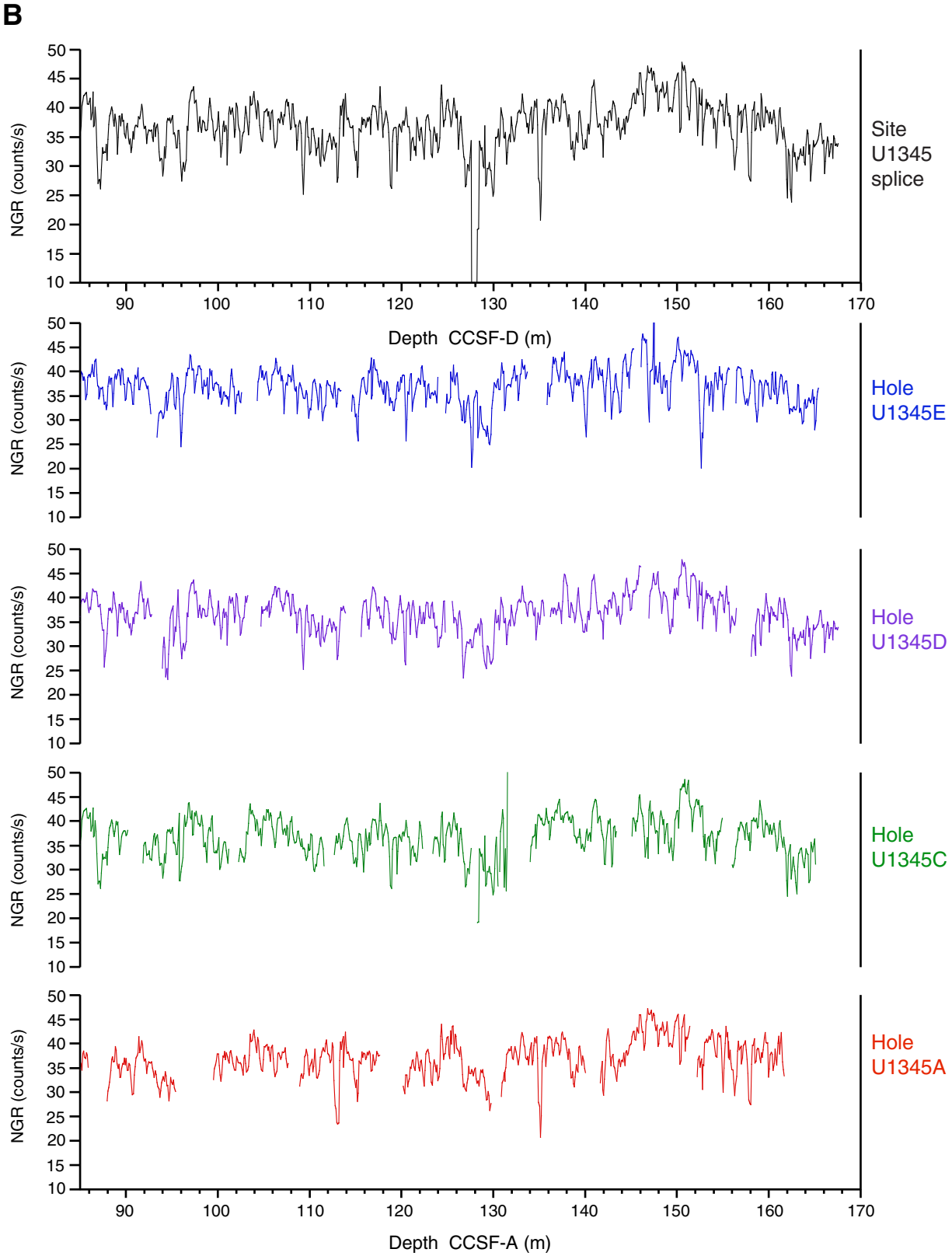

Figure F33. Color reflectance parameter b* data collected with the SHMSL vs. composite depth, Site U1345. No color reflectance data are available for Hole U1345B (microbiology-dedicated hole) or parts of Hole U1345E preserved as whole-round sections for postcruise study. For the primary splice record (top panel), depth on the CCSF-D scale is equivalent to depth on the CCSF-A scale. **A.** 0–85 m CCSF-A. (**Continued on next page.**)

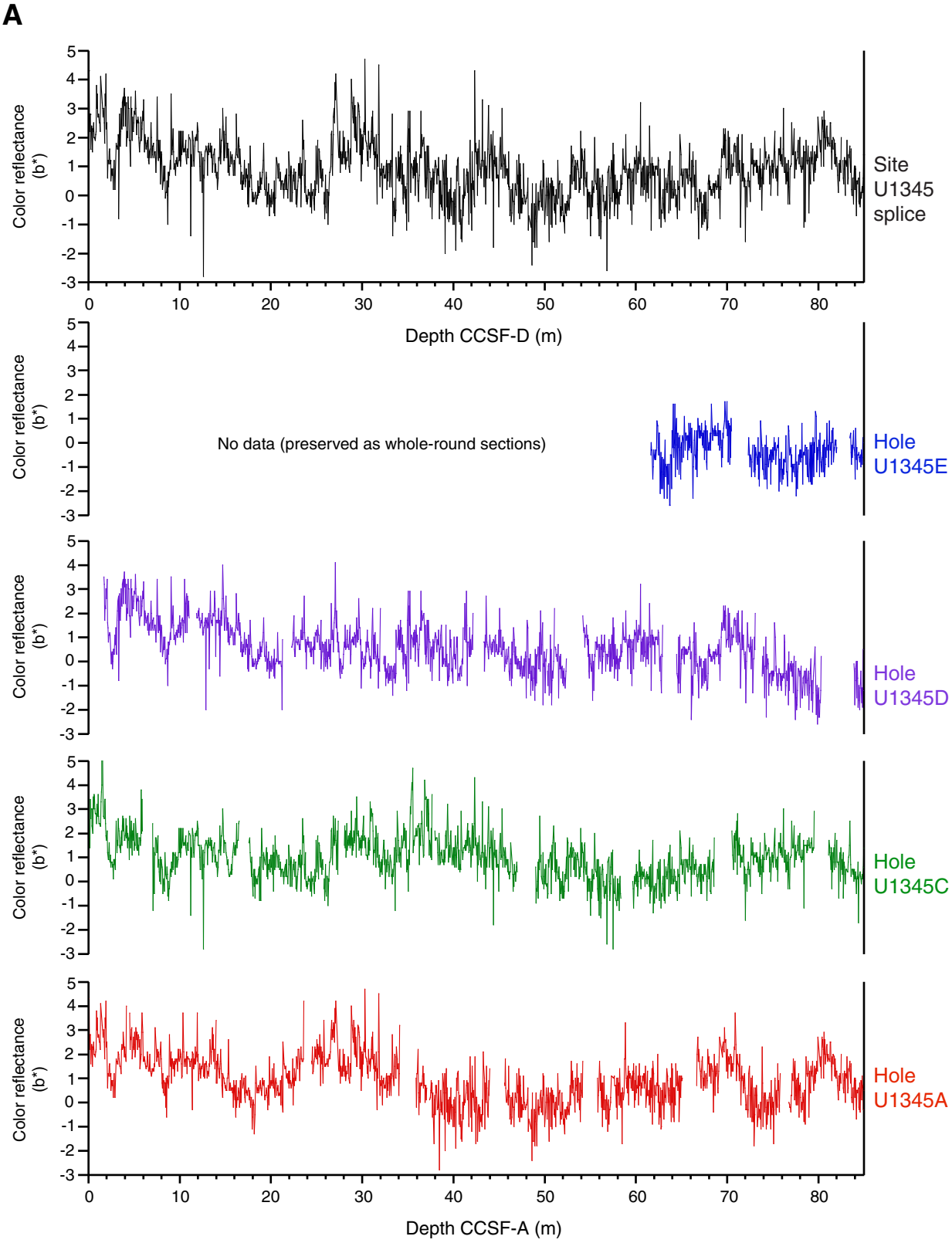

Figure F33 (continued). B. 85–170 m CCSF-A.

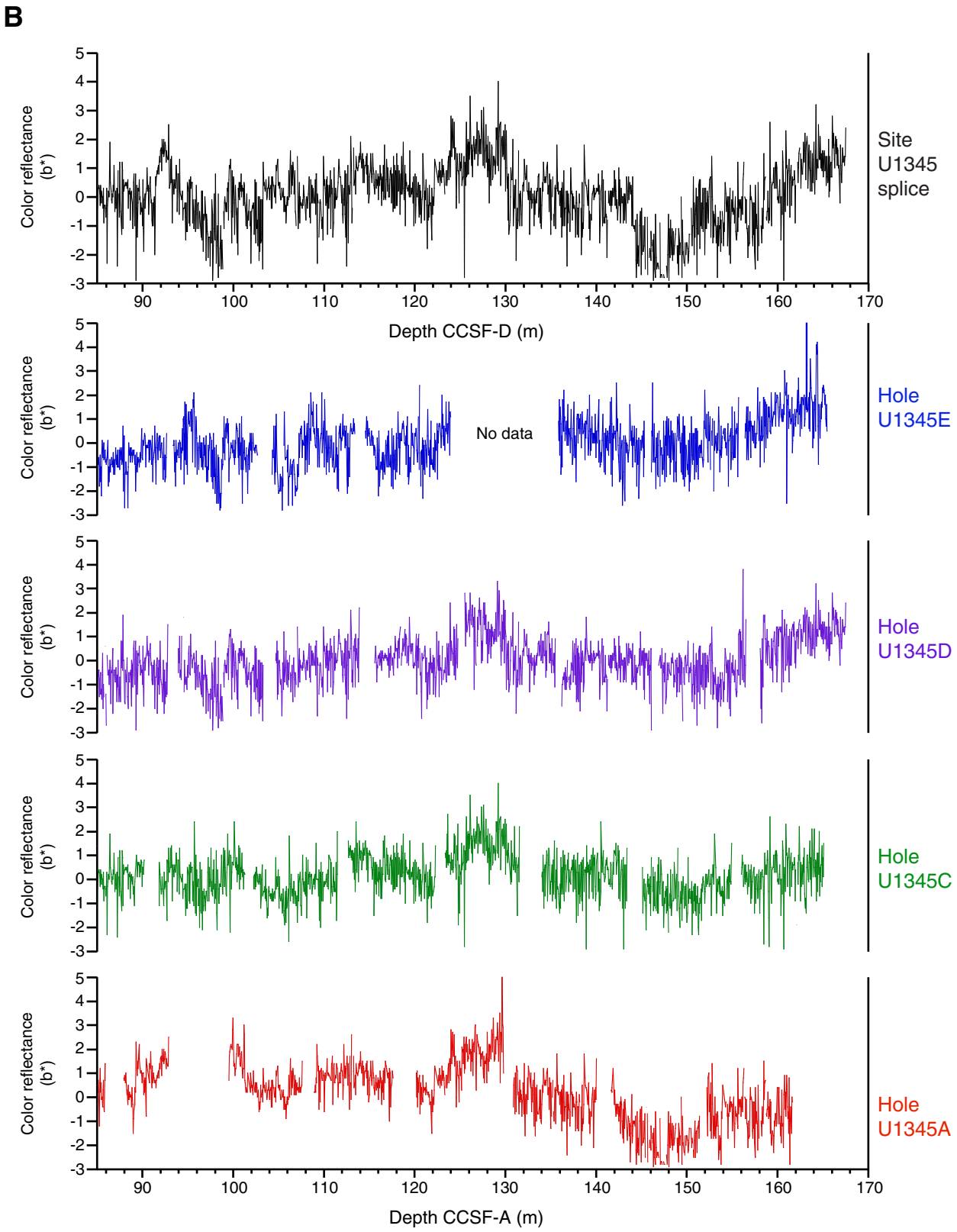

Figure F34. WRMSL magnetic susceptibility, gamma ray attenuation (GRA) bulk density, natural gamma radiation (NGR), and color reflectance parameter b* vs. composite depth in the primary splice, Site U1345. GRA, NGR, and b* data are smoothed.

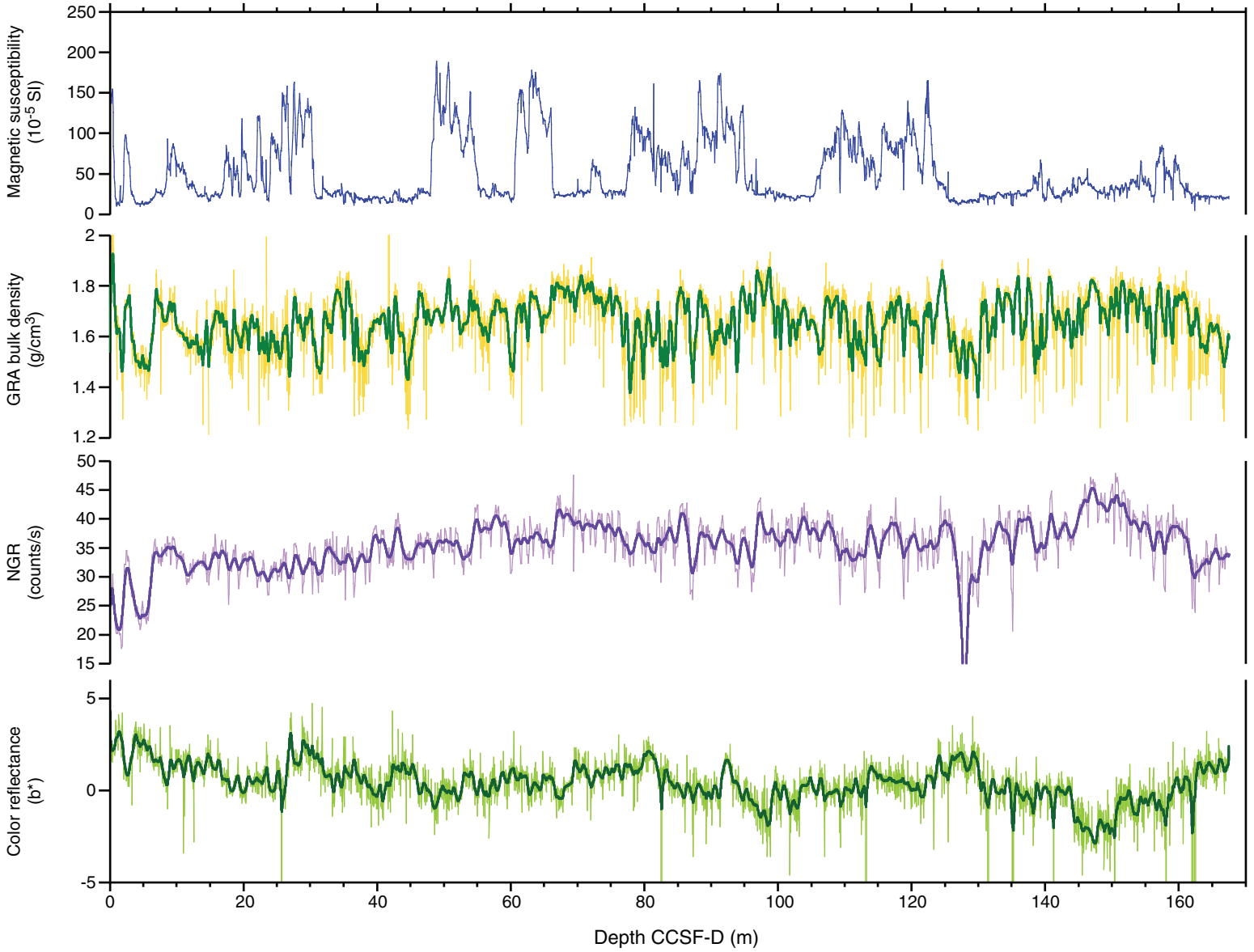

Figure F35. A. Mbsf vs. composite (CCSF-A) depth, Site U1345. **B.** Growth of cumulative depth offset (m) vs. mbsf in the splice. The affine growth factor is 1.11.

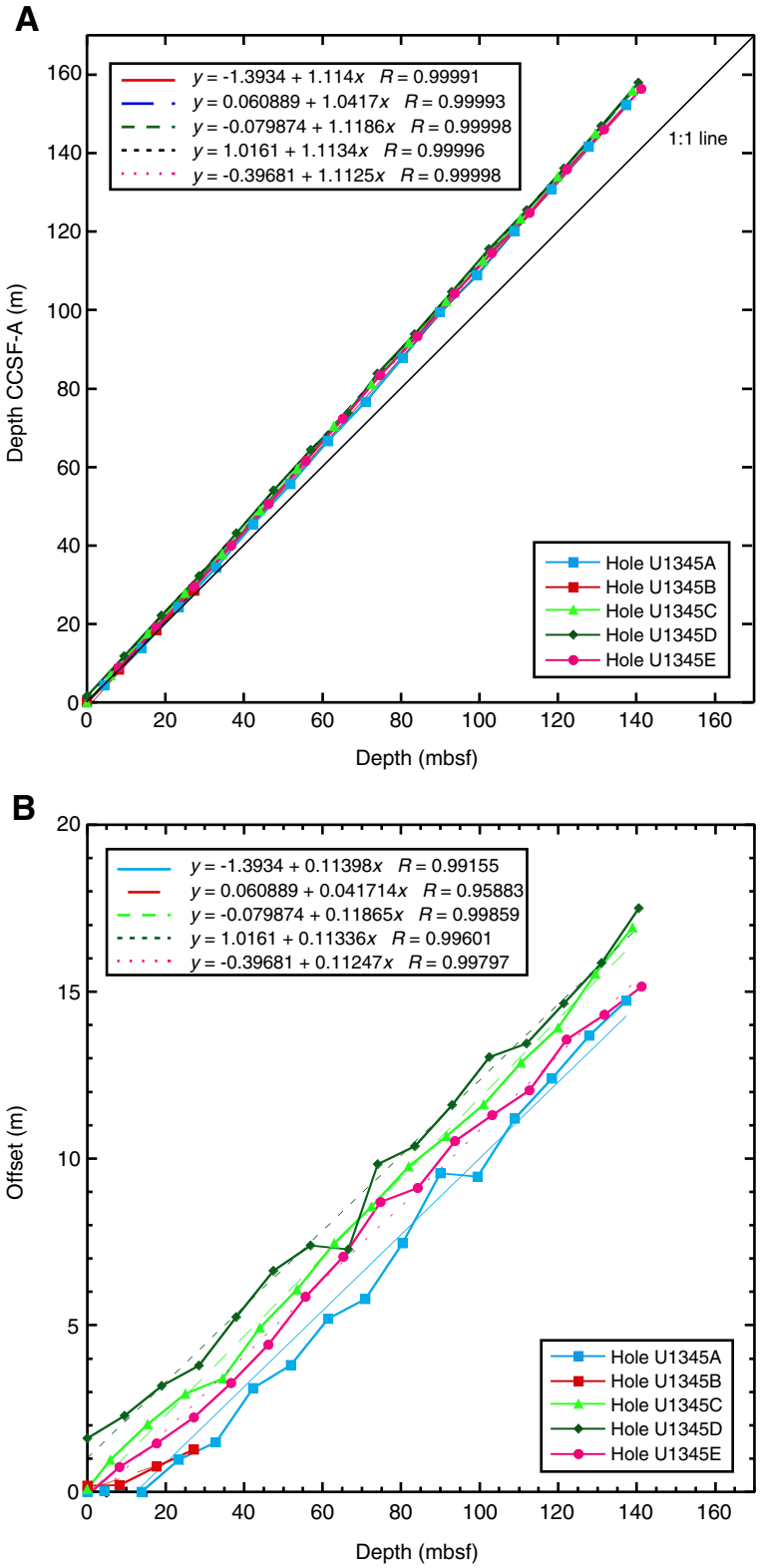

Figure F36. A. Records of the penetrations and temperature decays of the APCT-3 probe in Hole U1345A. **B.** The resulting temperature profile.

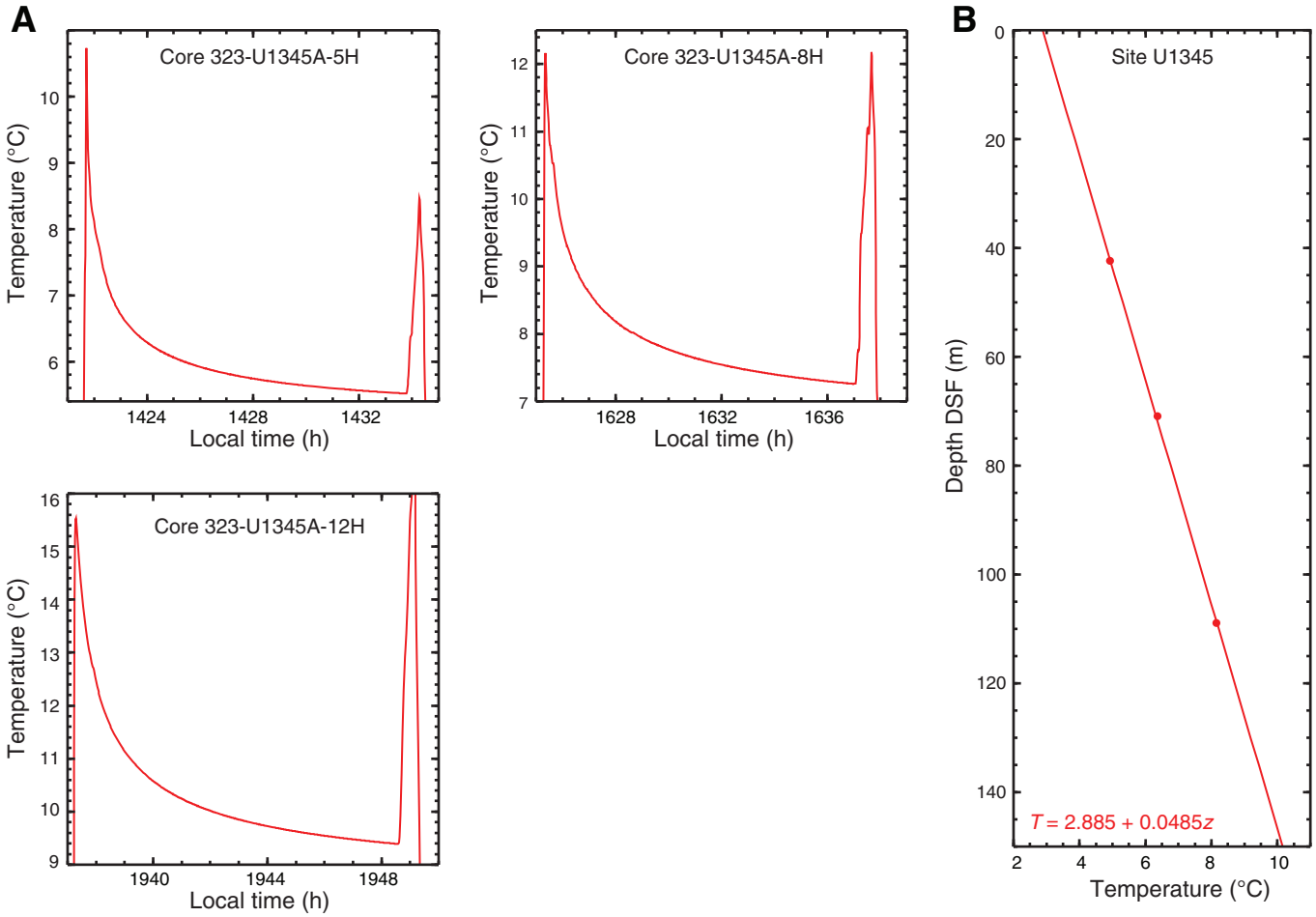

Table T1. Coring summary, Holes U1345A, U1345B, U1345C, U1345D, and U1345E. (See table notes.) (Continued on next two pages.)

Hole U1345A
Latitude: 60°9.1917′N
Longitude: 179°28.2036′W
Time on hole (h): 16.82
Seafloor (drill pipe measurement from rig floor, m DRF): 1019.00
Distance between rig floor and sea level (m): 11.7
Water depth (drill pipe measurement from sea level, m): 1007.3
Total depth (drill pipe measurement from rig floor, m DRF): 1166
Total penetration (mbsf): 146.9
Total length of cored section (m): 146.9
Total core recovered (m): 148.24
Core recovery (%): 101.1
Total number of cores: 16

Hole U1345B
Latitude: 60°9.2003′N
Longitude: 179°28.2127′W
Time on hole (h): 3.9
Seafloor (drill pipe measurement from rig floor, m DRF): 1019.25
Distance between rig floor and sea level (m): 11.7
Water depth (drill pipe measurement from sea level, m): 1007.5
Total depth (drill pipe measurement from rig floor, m DRF): 1056
Total penetration (mbsf): 36.7
Total length of cored section (m): 36.7
Total core recovered (m): 38.79
Core recovery (%): 105.7
Total number of cores: 4

Hole U1345C
Latitude: 60°9.2097′N
Longitude: 179°28.2229′W
Time on hole (h): 9.0
Seafloor (drill pipe measurement from rig floor, m DRF): 1020.5
Distance between rig floor and sea level (m): 11.7
Water depth (drill pipe measurement from sea level, m): 1008.8
Total depth (drill pipe measurement from rig floor, m DRF): 1169
Total penetration (mbsf): 148.5
Total length of cored section (m): 148.5
Total core recovered (m): 152.85
Core recovery (%): 102.9
Total number of cores: 16

Hole U1345D
Latitude: 60°9.2175′N
Longitude: 179°28.2283′W
Time on hole (h): 9.0
Seafloor (drill pipe measurement from rig floor, m DRF): 1020
Distance between rig floor and sea level (m): 11.7
Water depth (drill pipe measurement from sea level, m): 1008.3
Total depth (drill pipe measurement from rig floor, m DRF): 1170
Total penetration (mbsf): 150.0
Total length of cored section (m): 150.0
Total core recovered (m): 154.62
Core recovery (%): 103.1
Total number of cores: 16

Hole U1345E
Latitude: 60°9.2264′N
Longitude: 179°28.2407′W
Time on hole (h): 14.1
Seafloor (drill pipe measurement from rig floor, m DRF): 1018.8
Distance between rig floor and sea level (m): 11.7
Water depth (drill pipe measurement from sea level, m): 1007.1
Total depth (drill pipe measurement from rig floor, m DRF): 1168.8
Total penetration (mbsf): 150.0
Total length of cored section (m): 150.0
Total core recovered (m): 154.15
Core recovery (%): 102.8
Total number of cores: 16

Table T1 (continued). (Continued on next page.)

Core	Date (2009)	UTC (h)	Depth DSF (m) Top	Depth DSF (m) Bottom	Length (m) Cored	Length (m) Recovered	Recovery (%)	Comments
323-U1345A-								
1H	23 Aug	1155	0.0	4.4	4.4	4.39	100	Oriented nonmagnetic barrel
2H	23 Aug	1240	4.4	13.9	9.5	9.69	102	Oriented nonmagnetic barrel
3H	23 Aug	1320	13.9	23.4	9.5	10.02	105	Oriented nonmagnetic barrel
4H	23 Aug	1355	23.4	32.9	9.5	10.04	106	Oriented nonmagnetic barrel
5H	23 Aug	1445	32.9	42.4	9.5	10.05	106	APCT, oriented nonmagnetic barrel
6H	23 Aug	1520	42.4	51.9	9.5	9.21	97	Oriented nonmagnetic barrel
7H	23 Aug	1555	51.9	61.4	9.5	9.94	105	Oriented nonmagnetic barrel
8H	23 Aug	1650	61.4	70.9	9.5	9.71	102	APCT, oriented nonmagnetic barrel
9H	23 Aug	1730	70.9	80.4	9.5	9.74	103	Oriented nonmagnetic barrel
10H	23 Aug	1815	80.4	89.9	9.5	7.96	84	Oriented nonmagnetic barrel
11H	23 Aug	1905	89.9	99.4	9.5	8.59	90	Oriented nonmagnetic barrel
12H	23 Aug	2000	99.4	108.9	9.5	9.13	96	APCT, oriented nonmagnetic barrel
13H	23 Aug	2035	108.9	118.4	9.5	10.08	106	Oriented nonmagnetic barrel
14H	23 Aug	2115	118.4	127.9	9.5	9.72	102	Oriented nonmagnetic barrel
15H	23 Aug	2205	127.9	137.4	9.5	10.19	107	Oriented nonmagnetic barrel
16H	23 Aug	2240	137.4	146.9	9.5	10.03	106	Oriented nonmagnetic barrel
				Cored totals:	146.9	148.24	101	
323-U1345B-								
1H	24 Aug	0145	0.0	8.2	8.2	8.80	107	Nonmagnetic barrel
2H	24 Aug	0225	8.2	17.7	9.5	9.79	103	Nonmagnetic barrel
3H	24 Aug	0250	17.7	27.2	9.5	10.07	106	Nonmagnetic barrel
4H	24 Aug	0320	27.2	36.7	9.5	10.13	107	Nonmagnetic barrel
				Cored totals:	36.7	38.79	106	Nonmagnetic barrel
323-U1345C-								
1H	24 Aug	0440	0.0	6.0	6.0	5.96	99	Nonmagnetic barrel
2H	24 Aug	0510	6.0	15.5	9.5	9.82	103	Nonmagnetic barrel
3H	24 Aug	0540	15.5	25.0	9.5	10.16	107	Nonmagnetic barrel
4H	24 Aug	0610	25.0	34.5	9.5	10.14	107	Nonmagnetic barrel
5H	24 Aug	0635	34.5	44.0	9.5	9.54	100	Nonmagnetic barrel
6H	24 Aug	0700	44.0	53.5	9.5	9.87	104	Nonmagnetic barrel
7H	24 Aug	0725	53.5	63.0	9.5	9.71	102	Nonmagnetic barrel
8H	24 Aug	0755	63.0	72.5	9.5	9.60	101	Nonmagnetic barrel
9H	24 Aug	0820	72.5	82.0	9.5	9.64	101	Nonmagnetic barrel
10H	24 Aug	0850	82.0	91.5	9.5	9.91	104	Nonmagnetic barrel
11H	24 Aug	0930	91.5	101.0	9.5	9.83	103	Nonmagnetic barrel
12H	24 Aug	0955	101.0	110.5	9.5	10.08	106	Nonmagnetic barrel
13H	24 Aug	1025	110.5	120.0	9.5	8.66	91	Nonmagnetic barrel
14H	24 Aug	1055	120.0	129.5	9.5	9.85	104	Nonmagnetic barrel
15H	24 Aug	1125	129.5	139.0	9.5	10.55	111	Nonmagnetic barrel
16H	24 Aug	1155	139.0	148.5	9.5	9.53	100	Nonmagnetic barrel
				Cored totals:	148.5	152.85	103	
323-U1345D-								
1H	24 Aug	1355	0.0	9.5	9.5	9.76	103	Nonmagnetic barrel
2H	24 Aug	1420	9.5	19.0	9.5	9.73	102	Nonmagnetic barrel
3H	24 Aug	1445	19.0	28.5	9.5	10.19	107	Nonmagnetic barrel
4H	24 Aug	1530	28.5	38.0	9.5	10.18	107	Nonmagnetic barrel
5H	24 Aug	1555	38.0	47.5	9.5	9.54	100	Nonmagnetic barrel
6H	24 Aug	1620	47.5	57.0	9.5	9.22	97	Nonmagnetic barrel
7H	24 Aug	1645	57.0	66.5	9.5	9.36	99	Nonmagnetic barrel
8H	24 Aug	1715	66.5	74.0	7.5	6.82	91	Nonmagnetic barrel
9H	24 Aug	1745	74.0	83.5	9.5	9.52	100	Nonmagnetic barrel
10H	24 Aug	1815	83.5	93.0	9.5	9.97	105	Nonmagnetic barrel
11H	24 Aug	1845	93.0	102.5	9.5	9.77	103	Nonmagnetic barrel
12H	24 Aug	1910	102.5	112.0	9.5	9.53	100	Nonmagnetic barrel
13H	24 Aug	1935	112.0	121.5	9.5	10.65	112	Nonmagnetic barrel
14H	24 Aug	2000	121.5	131.0	9.5	10.31	109	Nonmagnetic barrel
15H	24 Aug	2025	131.0	140.5	9.5	10.06	106	Nonmagnetic barrel
16H	24 Aug	2050	140.5	150.0	9.5	10.01	105	Nonmagnetic barrel
				Cored totals:	150.0	154.62	103	Nonmagnetic barrel
323-U1345E-								
1H	24 Aug	2245	0.0	8.2	8.2	8.27	101	Nonmagnetic barrel
2H	24 Aug	2315	8.2	17.7	9.5	7.48	79	Nonmagnetic barrel
3H	24 Aug	2340	17.7	27.2	9.5	10.16	107	Nonmagnetic barrel
4H	25 Aug	0005	27.2	36.7	9.5	10.27	108	Nonmagnetic barrel
5H	25 Aug	0030	36.7	46.2	9.5	9.89	104	Nonmagnetic barrel
6H	25 Aug	0055	46.2	55.7	9.5	10.34	109	Nonmagnetic barrel

Table T1 (continued).

Core	Date (2009)	UTC (h)	Depth DSF (m) Top	Depth DSF (m) Bottom	Length (m) Cored	Length (m) Recovered	Recovery (%)	Comments
7H	25 Aug	0120	55.7	65.2	9.5	9.38	99	Nonmagnetic barrel
8H	25 Aug	0145	65.2	74.7	9.5	10.26	108	Nonmagnetic barrel
9H	25 Aug	0215	74.7	84.2	9.5	9.85	104	Nonmagnetic barrel
10H	25 Aug	0240	84.2	93.7	9.5	9.79	103	Nonmagnetic barrel
11H	25 Aug	0310	93.7	103.2	9.5	9.74	103	Nonmagnetic barrel
12H	25 Aug	0335	103.2	112.7	9.5	9.99	105	Nonmagnetic barrel
13H	25 Aug	0405	112.7	122.2	9.5	9.18	97	Nonmagnetic barrel
14H	25 Aug	0430	122.2	131.7	9.5	9.94	105	Nonmagnetic barrel
15H	25 Aug	0500	131.7	141.2	9.5	9.92	104	Nonmagnetic barrel
16H	25 Aug	0540	141.2	150.0	8.8	9.69	110	Nonmagnetic barrel
				Cored totals:	150.0	154.15	103	
				Site totals:	632.1	648.65	103	

Notes: DRF = drilling depth below rig floor, mbsf = meters below seafloor, DSF = drilling depth below seafloor. APCT = advanced piston corer temperature tool. UTC = Universal Time Coordinated.

Table T2. Datum events of radiolarians, silicoflagellates, and diatoms, Holes U1345A, U1345C, U1345D, and U1345E. (**See table notes.**)

Datum event	Taxon	Age (Ma)	Depth (mbsf) Hole U1345A	Depth (mbsf) Hole U1345C	Depth (mbsf) Hole U1345D	Depth (mbsf) Hole U1345E	Depth CCSF-A (m) Hole U1345A	Depth CCSF-A (m) Hole U1345C	Depth CCSF-A (m) Hole U1345D	Depth CCSF-A (m) Hole U1345E
LO *Lychnocanoma nipponica sakaii*	Radiolarian	0.05	19.0	10.9	14.5	21.8	19.0	14.1	16.3	22.8
LO *Amphimelissa setosa*	Radiolarian	0.08–0.10	38.2	—	—	—	39.3	—	—	—
LO *Distephanus octonarius*	Silicoflagellate	0.2–0.3	75.9	—	—	—	81.4	—	—	—
LO *Spongodiscus* sp.	Radiolarian	0.28–0.32	84.5	77.4	78.4	80.0	91.4	85.5	87.1	88.0
LO *Axoprunum acquilonium*	Radiolarian	0.25–0.43	93.4	106.2	107.4	89.3	102.1	117.6	120.3	98.6
LO *Proboscia curvirostris*	Diatom	0.3	66.25	67.7	69.8	89.1	70.9	74.6	77.2	98.6
LO *Thalassiosira jouseae*	Diatom	0.3	66.25	67.7	69.8	79.7	91.4	74.6	63.3	88.0

Notes: For last occurrences (LO), the depth was estimated as the midpoint between the depth at which the species was last observed and the depth of the next sample above. — = not applicable.

Table T3. Calcareous nannofossil range chart, Holes U1345A, U1345B, U1345C, and U1345D. (See table notes.) (Continued on next two pages.)

Core, section, interval (cm)	Martini (1971) zone	Abundance	Preservation	*Coccolithus braarudii*	*Coccolithus pelagicus*	*Cyclococcolithus leptoporus*	*Cyclococcolithus leptoporus* (small)	*Emiliania huxleyi*	*Gephyrocapsa* (medium)	*Gephyrocapsa* (small)	*Pseudoemiliania lacunosa*	*Reticulofenestra minuta*	*Reticulofenestra minutula*	Other taxa	Comments
323-U1345A-															
1H-1, 101.5		A	M	R	A			C	F						Sample from the sedimentology collection. Dark gray lamina. Large and small *Emiliania huxleyi*
1H-1, 102		A	G		A			C							Sample from the sedimentology collection. Light green lamina. Large and small *Emiliania huxleyi*
1H-1, 119.5		A	G	F	A			A							Sample from the sedimentology collection. Light gray lamina. Large and small *Emiliania huxleyi*
1H-2, 44.5		B													Sample from the sedimentology collection. Gray lamina
1H-2, 44.7		B													Sample from the sedimentology collection. Dark green lamina
1H-2, 45		R	M-G						R						Sample from the sedimentology collection. Light green lamina
1H-CC		A	G	F	A			D		F					Large (>4 µm) and small *Emiliania huxleyi* types are present and well preserved
2H-1, 113.5		R	M		R			R							Sample from the sedimentology collection. Gray lamina, coarse grains
2H-1, 113.6		F	G	R	F										Sample from the sedimentology collection. Dark gray lamina
2H-1, 114		C	MG	R	C			F							Sample from the sedimentology collection. Light green lamina. Large and small *Emiliania huxleyi*
2H-CC	NN21	R	M-G		R		R	R							
3H-CC		R	M						R	R					
4H-CC		R	M							R					Authigenic minerals, acicular shape, low birefringence
5H-CC		B													Reworked specimen (*Discoaster* spp.)
6H-CC		B													
7H-CC		R	M-G		R		R								
8H-CC		B													
9H-CC		R	M-G		R				R	R					
10H-CC		C	G						F	C					
11H-CC		B													
12H-CC		R	M-G		R				R	R					
13H-7, 121		A	G		C				C	A					Sample from the sedimentology collection. Laminated interval. Gephyrocapsids are *Gephyrocapsa caribbeanica* type
13H-CC		R	M-G		R					R					The core catcher was laminated
14H-CC		R	M		R										
15H-CC		B													
16H-CC		A	G		R	R			F	A					
323-U1345B-															
1H-CC	NN21	F	M		F			R							Large (>4 µm) and small *Emiliania huxleyi* types are present and well preserved
2H-CC		R	M-G		R				R						
3H-CC		B													
4H-CC		B													
323-U1345C-															
1H-CC	NN21	A	G	F	A			A	F	F					
2H-CC		R	M-G							R					
3H-CC		B													
4H-CC		R	G		R										
5H-CC		R	M							R					
6H-CC		R	M-G		R										
7H-CC		R	M-G			R	R		R						

Table T3 (continued). (Continued on next page.)

Core, section, interval (cm)	Martini (1971) zone	Abundance	Preservation	*Coccolithus braarudii*	*Coccolithus pelagicus*	*Cyclococcolithus leptoporus*	*Cyclococcolithus leptoporus* (small)	*Emiliania huxleyi*	*Gephyrocapsa* (medium)	*Gephyrocapsa* (small)	*Pseudoemiliania lacunosa*	*Reticulofenestra minuta*	*Reticulofenestra minutula*	Other taxa	Comments
8H-CC		B													
9H-CC		R	M		R										
10H-CC		B													
11H-CC		B													
12H-3, 22		A	G		C				A	A					Sample from the sedimentology collection. Laminated interval. Gephyrocapsids are *Gephyrocapsa caribbeanica* type
12H-CC		B													
13H-CC		R	M-G			R			R						
14H-CC		A	G							A					
15H-CC		B													
16H-CC		C	G						R	C					
323-U1345D-															
1H-CC		B													
2H-CC		F	M		F	R				R					Authigenic minerals, acicular shape, low birefringence. Overgrowth in *Coccolithus pelagicus*, etching in *Cyclococcolithus leptoporus*
3H-CC		B													
4H-CC		B													
5H-CC		B													
6H-CC		B													Coarse terrigenous grains
7H-CC		R	M				R								
8H-CC		B													
9H-CC		R	M-G							R					
10H-CC		R	M-G				R			R					
11H-CC		B													
12H-CC		R	P			R									
13H-3, 48		A	G						A	A					Sample from the sedimentology collection. Laminated interval. Gephyrocapsids are *Gephyrocapsa caribbeanica* type
13H-4, 45		F	M-G		F				F	F					Sample from the sedimentology collection. Laminated interval. Gephyrocapsids are *Gephyrocapsa caribbeanica* type
13H-4, 68		A	G		C				C	A					Sample from the sedimentology collection. Laminated interval. Gephyrocapsids are *Gephyrocapsa caribbeanica* type
13H-CC		B													
14H-CC		B													
15H-CC		B													
16H-CC		A	M-G		R				F	A					
1H-CC	NN21	A	G	F	A			A	F	F					
2H-CC		R	M-G							R					
3H-CC		B													
4H-CC		B													
5H-CC		B													
6H-CC		B													Coarse terrigenous grains
7H-CC		R	M				R								
8H-CC		B													
9H-CC		R	M-G							R					
10H-CC		R	M-G				R			R					

Table T3 (continued).

Core, section, interval (cm)	Martini (1971) zone	Abundance	Preservation	*Coccolithus braarudii*	*Coccolithus pelagicus*	*Cyclococcolithus leptoporus*	*Cyclococcolithus leptoporus* (small)	*Emiliania huxleyi*	*Gephyrocapsa* (medium)	*Gephyrocapsa* (small)	*Pseudoemiliania lacunosa*	*Reticulofenestra minuta*	*Reticulofenestra minutula*	Other taxa	Comments
11H-CC		B													
12H-CC		R	P			R									
13H-3, 48		A	G						A	A					Sample from the sedimentology collection. Laminated interval. Gephyrocapsids are *Gephyrocapsa caribbeanica* type
13H-4, 45		F	M-G		F				F	F					Sample from the sedimentology collection. Laminated interval. Gephyrocapsids are *Gephyrocapsa caribbeanica* type
13H-4, 68		A	G		C				C	A					Sample from the sedimentology collection. Laminated interval. Gephyrocapsids are *Gephyrocapsa caribbeanica* type
13H-CC		B													
14H-CC		B													
15H-CC		B													
16H-CC		A	M-G		R				F	A					

Notes: Abundance: D = dominant, A = abundant, C = common, F = few, R = rare. Preservation: G = good, M = moderate, P = poor.

Table T4. Planktonic foraminifer range chart, Holes U1345A, U1345B, U1345C, and U1345D. (See table notes.) (Continued on next page.)

Core, section	Abundance	Preservation	*Globigerina bulloides*	*Globigerina umbilicata*	*Neogloboquadrina pachyderma* (dex)	*Neogloboquadrina pachyderma* (sin)	*Turborotalia quinqueloba*	Other observations
323-U1345A-								
1H-CC	D	VG	D			D	R	Abundant siliciclastics
2H-CC	F	G	R			F		Dominant siliciclastics, pyrite
3H-CC	F	G	P			F		Dominant siliciclastics, pyrite
4H-CC	P	M	P			P		Dominant siliciclastics, pyrite, yellow foraminifer tests
5H-CC	D	M	A	R	P	D		Abundant siliciclastics, pyrite, mica, yellow foraminifer tests
6H-CC	R	M	R			R		Dominant siliciclastics, pyrite, mica
7H-CC	R	M				R		Dominant siliciclastics, pyrite, mica
8H-CC	R	G	R					Dominant siliciclastics, pyrite, mica
9H-CC	F	G	F			R		Few siliciclastics, pyrite, mica
10H-CC	A	G	F			A		Abundant siliciclastics, pyrite, mica, yellow foraminifer tests
11H-CC	F	G				F		Dominant siliciclastics, pyrite, mica
12H-CC		M	F			F		Abundant siliciclastics, pyrite, mica, yellow foraminifer tests
13H-CC	D	G	A	P		D		Abundant siliciclastics, mica, sponge spicules
14H-CC	R	G	P			R		Few siliciclastics, pyrite, mica
15H-CC	F	M	R			F		Abundant siliciclastics, pyrite, mica, yellow foraminifer tests
16H-CC	D	M				D		Abundant siliciclastics, pyrite, mica, yellow foraminifer tests
323-U1345B-								
1H-CC	A	G	R			A	P	Dominant siliciclastics, pyrite, mica
2H-CC	A	G	A			A		Dominant siliciclastics, pyrite, mica
3H-CC	R	G	R			R		Dominant siliciclastics, pyrite, mica, yellow foraminifer tests
4H-CC	F	G	R			F		Dominant siliciclastics, pyrite, mica
323-U1345C-								
1H-CC	D	VG	D			A		Dominant siliciclastics
2H-CC	F	G	R			F		Dominant siliciclastics, pyrite, mica, few yellow foraminifer tests
3H-CC	R	G	R			R		Dominant siliciclastics, pyrite, mica
4H-CC	A	G	F			A		Dominant siliciclastics, pyrite, mica
5H-CC	R	G	R			R		Dominant siliciclastics, pyrite, mica
6H-CC	F	G	R			F		Dominant siliciclastics, pyrite, mica
7H-CC	R	M				R		Dominant siliciclastics, pyrite, mica
8H-CC	R	M	R					Dominant siliciclastics, pyrite, mica
9H-CC	A	G	A			A		Dominant siliciclastics, pyrite, mica
10H-CC	R	G	R		P			Dominant siliciclastics, pyrite, mica
11H-CC	F	M	F			R		Abundant siliciclastics, pyrite, mica, yellow foraminifer tests
12H-CC	P	M				P		Abundant siliciclastics, pyrite, mica, yellow foraminifer tests
13H-CC	R	G	R	P				Abundant siliciclastics, pyrite, mica
14H-CC	D	G	A			D		Abundant siliciclastics, pyrite, mica
15H-CC	R	M				R		Abundant siliciclastics, pyrite, mica
16H-CC	P	M				P		Abundant siliciclastics, pyrite, mica
323-U1345D-								
Mudline	A	VG	R	P		A		
1H-CC	A	G	A			A		Abundant siliciclastics, mica
2H-CC	D	G	R			D		Abundant siliciclastics, pyrite, mica
3H-CC	A	G	R			A		Dominant siliciclastics, pyrite, mica
4H-CC	A	M	R			A		Dominant siliciclastics, pyrite, mica, yellow foraminifer tests
5H-CC	R	P	P		P			Abundant siliciclastics, pyrite, mica, yellow foraminifer tests
6H-CC	R	M	P			R		Dominant siliciclastics, pyrite, mica
7H-CC	F	G	F			F		Dominant siliciclastics, pyrite, mica
8H-CC	P	M	P		P	P		Dominant siliciclastics, pyrite, mica, yellow foraminifer tests
9H-CC	F	G			P	F		Dominant siliciclastics, pyrite, mica
10H-CC	A	G				A		Dominant siliciclastics, pyrite, mica
11H-CC	F	G				F		Dominant siliciclastics, pyrite, mica
12H-CC	B							
13H-CC	A	M	F			A		Abundant siliciclastics, pyrite, mica
14H-CC	F	M	P			F		Abundant siliciclastics, pyrite, mica

Table T4 (continued).

Core, section	Abundance	Preservation	*Globigerina bulloides*	*Globigerina umbilicata*	*Neogloboquadrina pachyderma* (dex)	*Neogloboquadrina pachyderma* (sin)	*Turborotalia quinqueloba*	Other observations
15H-CC	P	G					P	Dominant siliciclastics, pyrite, mica
16H-CC	B							

Notes: Abundance: D = dominant, A = abundant, F = few, R = rare, P = present. Preservation: VG = very good, G = good, M = moderate, P = poor. Dex = dextral, sin = sinistral.

Table T5. Benthic foraminifer range chart, Holes U1345A and U1345B. (**See table notes.**)

Core, section	Abundance	Preservation	*Alabaminella weddellensis*	*Brizalina earlandi*	*Brizalina pygmaea*	*Bulimina* aff. *exilis*	*Bulimina* sp.	*Cassidulina laevigata* var. *carinata*	*Cassidulina* sp.	*Cassidulinoides tenuis*	*Elphidium* cf. *batialis*	*Epistominella pulchella*	*Globobulimina pacifica*	*Globocassidulina* sp.	*Gyroidinoides soldanii*	*Islandiella norcrossi*	*Nodosaria* aff. *pyrula*	*Nonionella labradorica*	*Nonionella turgida*	*Nonionella turgida digitata*	*Planulina ariminensus*	*Procerolagena* cf. *gracillima*	*Pullenia* sp.	*Stainforthia* aff. *fusiformis*	*Trifarina angulosa*	*Uvigerina auberiana*	*Uvigerina* cf. *peregrina*	*Valvulineria* sp.	Siliciclastics	Other observations
323-U1345A-Mudline																													
1H-CC	D	VG		R	F	D							R						R	R				D			R		A	
2H-CC	A	G		P			P	F	P	F	R		R			R		A		R			R	P	R	P		R	D	Pyrite
3H-CC	F	G		F		R		P			P	R	F	P		R								R		R	F	P	D	Pyrite
4H-CC	P	M		P		P							P														P		D	Pyrite
5H-CC	D	M		A		D						P	F					R				P							A	Pyrite, mica, yellow foraminifers
6H-CC	D	M		P						R	R	R	R			F		D	P	R							R	P	D	Pyrite, mica
7H-CC	R	M		R		R				R	R		R	R		R		R				P					R	R	D	Pyrite, mica
8H-CC	A	G	P			R				F	P		F			F	P		P			P					F	F	D	Pyrite, mica
9H-CC	A	VG				A				R		F	A			R		R					P				A	F	F	Pyrite, mica
10H-CC	D	G		A		D						A	F					R									A	F	A	Pyrite, mica, yellow foraminifers
11H-CC	D	G						R		A			D			F		R									A	F	D	Pyrite, mica
12H-CC	D	M		D								F	F					P									R	F	A	Pyrite, mica, yellow foraminifers
13H-CC	D	G		F		D							R					P											A	Spicules, mica
14H-CC	A	M				R					F	R				R		A		R							R	R	F	Pyrite, mica
15H-CC	D	G				A				F		A	R			R	P				R					A		R	A	Pyrite, mica, yellow foraminifers
16H-CC	D	M				A				R	A	F	R		R	R		F									A	F	A	Pyrite, mica, yellow foraminifers
323-U1345B-																													
1H-CC	A	G				R				R	A	P	F			P		A					R	R			R		D	Pyrite, mica
2H-CC	A	G		A		A					R		F					F		F				F			R	R	D	Pyrite, mica
3H-CC	R	M						R				R	R			P		R				P				R			D	Pyrite, mica
4H-CC	A	M		R		A					R	R	R					F	P	R				R		R		R	D	Pyrite, mica

Notes: Abundance: D = dominant, A = abundant, F = few, R = rare, P = present. Preservation: VG = very good, G = good, M = moderate.

Table T6. Benthic foraminifer range chart, Hole U1345C. (See table notes.)

Core, section	Abundance	Preservation	*Alabaminella weddellensis*	*Brizalina earlandi*	*Bulimina* aff. *exilis*	*Cancris* cf. *philippinensis*	*Cassidulina laevigata* var. *carinata*	*Cassidulinoides tenuis*	*Cibicidoides mundulus*	*Cibicidoides* cf. *subhaidingeri*	*Elphidium* cf. *batialis*	*Epistominella pulchella*	*Fissurina* sp	*Fursenkoina* sp.	*Glandulina* sp.	*Globobulimina pacifica*	*Globocassidulina* sp.	*Gyroidinoides soldanii*	*Islandiella norcrossi*	*Lagena striata?*	*Nonionella labradorica*	*Nonionella turgida digitata*	*Planulina wuellerstorfi*	*Procerolagena* cf. *gracillima*	*Pullenia* sp.	*Pyrgo* sp.	*Stainforthia* aff. *fusiformis*	*Uvigerina* cf. *peregrina*	*Uvigerina* cf. *proboscidea*	*Valvulineria* sp.	Siliciclastics	Other observations
323-U1345C-																																
1H-CC	A	VG		F	R						F	A				R			R		R	F				F	F			D	
2H-CC	A	G		P							R	A	P			R			A	P	F	P			R		A		P	D	Pyrite, mica, few yellow foraminifers
3H-CC	F	G		R								P				F			P		F					R	R		P	D	Pyrite, mica
4H-CC	D	G		F	D		R									R					F					R	R			D	Pyrite, mica
5H-CC	F	G		P	F			R			F	R				F			P		R								R	D	Pyrite, mica
6H-CC	A	G		R	P			R		R						A			A		R			P			R		R	D	Pyrite, mica
7H-CC	A	G			R					P	A	R		P		R			R		A	R							R	D	Pyrite, mica
8H-CC	A	G			R			F								A					R						F	P	F	D	Pyrite, mica
9H-CC	D	G		D	F			R				R				F					R						F		F	D	Pyrite, mica
10H-CC	F	G			R			F		P	F	R			P	F	P				R	P			P		R		R	D	Pyrite, mica
11H-CC	F	M		P			P	F								F	P										P		R	A	Pyrite, mica
12H-CC	R	M						P								P											R			D	Pyrite, mica, few yellow foraminifers
13H-CC	D	G	P	R							A	R				R			R		F		R				F		F	A	Pyrite, mica
14H-CC	D	G	R	F	D	P										A														A	Pyrite, mica, spicules
15H-CC	A	G			A			R				F				A			R		F						A		R	A	Pyrite, mica, spicules
16H-CC	D	G			F			R	P		F	A						R									A		F	A	Pyrite, mica, shells

Notes: Abundance: D = dominant, A = abundant, F = few, R = rare, P = present. Preservation: VG = very good, G = good, M = moderate.

Table T7. Benthic foraminifer and ostracode range chart, Hole U1345D. (**See table notes.**)

Core, section	Abundance	Preservation	*Alabaminella weddellensis*	*Bolivina* sp.	*Brizalina* cf. *spathula*	*Brizalina earlandi*	*Bulimina* aff. *exilis*	*Bulimina* aff. *mexicana*	*Cancris* cf. *philippinensis*	*Cassidulina laevigata* var. *carinata*	*Cassidulina* sp.	*Cassidulinoides tenuis*	*Dentalina* sp.	*Eggerella* sp.	*Elphidium* cf. *batialis*	*Epistominella pulchella*	*Globobulimina pacifica*	*Islandiella norcrossi*	*Nodosaria* aff. *pyrula*	*Nonionella labradorica*	*Nonionella turgida*	*Nonionella turgida digitata*	*Planulina wuellerstorfi*	*Procerolagena* cf. *gracillima*	*Pullenia* sp.	*Pygmaeseistron* cf. *hispida*	*Pyrgo* sp.	*Rhabdammina* sp.	*Trilocullina* cf. *trihedra*	*Uvigerina* cf. *peregrina*	*Valvulineria* sp.	*Velereninoides jeffreysii*	*Cytheropteron* sp.	Siliciclastics	Other observations
323-U1345D-																																		
Mudline	D	G		A	F		D							R	R		R	R										P		F		P		D	Mica
1H-CC	D	G				F			P			F			D		A	F		F		R	R		R	P			R	A	R			A	Mica
2H-CC	F	G				R	P									F	F	R				R			R					F				A	Mica, pyrite
3H-CC	A	G				R	A	R							R			R		P		R								R				D	Mica, pyrite
4H-CC	A	G				R	A				R	R			F	R	A	R		F		R			R					R				D	Mica, pyrite, yellow foraminifers
5H-CC	F	M					F					R					F	R									P			R	R			A	Mica, pyrite, yellow foraminifers
6H-CC	F	M					R					F					P														R			D	Mica, pyrite
7H-CC	A	G				R	P					P				F	A	A				R			P					F	F			D	Mica, pyrite
8H-CC	F	M	P			P	R					R				P	R	P	P		P			P			P				R			D	Mica, pyrite, yellow foraminifers
9H-CC	F	M										R			F		F			P										A	P			D	Mica, pyrite
10H-CC	F	G	P				R					F	P		P	R	F	F	P	R					P					R	P			D	Mica, pyrite
11H-CC	F	G								P		F					F							P						R		P		D	Mica, pyrite, wood
12H-CC	P	G					P													P														D	Sand, wood
13H-CC	D	G				F						F				A	F	F		A										A	P			A	Mica, pyrite
14H-CC	D	G					D									R	R	R												F	R			A	Mica, pyrite
15H-CC	F	G					P					F			R			P												F				D	Mica, pyrite
16H-CC	D	G				R	F					R			P	A		P		P										D	F			A	Mica, pyrite

Notes: Abundance: D = dominant, A = abundant, F = few, R = rare, P = present. Preservation: G = good, M = moderate.

Table T8. Diatom range chart, Hole U1345A. (See table notes.)

Core, section	Depth (mbsf) Top	Depth (mbsf) Bottom	Abundance	Preservation	*Actinocyclus curvatulus*	*Actinocyclus ochotensis*	*Actinoptychus senarius*	*Asteromphalus robustus*	*Bacterosira fragilis*	*Chaetoceros furcellatum* spores	*Coscinodiscus marginatus*	*Coscinodiscus oculus-iridis*	*Cymbella* spp.	*Delphineis kippae*	*Delphineis surirella*	*Detonula confervacea*	*Diploneis* spp.	*Eunotia* spp.	*Fragilariopsis cylindrus*	*Fragilariopsis oceanica*	*Fragilariopsis* spp.	*Gomphonema* spp.	*Navicula distans*	*Navicula* spp.	*Neodenticula seminae*	*Nitzschia* spp.	*Odontella aurita*	*Paralia sol*	*Paralia sulcata*	*Pinnularia* spp.	*Porosira glacialis*	*Proboscia barboi*	*Proboscia curvirostris*	*Rhabdonema japonicum*	*Rhabdonema* spp.	*Rhizosolenia hebetata* f. *hebetata*	*Rhizosolenia hebetata* f. *hiemalis*	*Rhizosolenia hebetata* f. *semispina*	*Rhizosolenia* spp.	*Stephanopyxis* spp.	*Stephanopyxis turris*	*Stephanopyxis zabelinae*	*Tetracyclus* spp.	*Thalassionema nitzschioides*	*Thalassiosira antarctica* spores	*Thalassiosira eccentrica*	*Thalassiosira gravida*	*Thalassiosira hyalina*	*Thalassiosira jouseae*	*Thalassiosira lacustris*	*Thalassiosira latimarginata* s.l.	*Thalassiosira nordenskioeldii*	*Thalassiosira oestrupii*	*Thalassiosira* spp.	*Thalassiothrix longissima*	Diatom zone (NPD) in Yanagisawa and Akiba (1998)
323-U1345A-																																																				
1H-CC	4.25	4.39	A	G	F				C	C		R			C				C	C	F				C	C	R				F						R			R			F	C	R		C			C		F	C			
2H-CC	13.98	14.09	C	G	C		F		F	F					F		R			R	R		R	R	C	R	R	R	C	F					R		R				F	A			C		R	F	R				
3H-CC	23.61	23.92	C	G					A	C					F				R	R	F			R	R	F			F	R												A			C		R	R	F				*Neodenticula seminae* (NPD12)
4H-CC	33.2	33.44	F	M-G	F		R		C								R	R					R		C	F		R							R	F		R	R				A			C						R	
5H-CC	42.51	42.95	C	G	C				F				R			R				C					C	C			R	R	R												C		F	F			A			R	R
6H-CC	51.1	51.61	C	G	F				R						R	R	R												A														D				C						
7H-CC	61.33	61.84	C	M	C				C		C		R			R	R			C					C				F		R				R	F		C		R			A		R	R		C		C		
8H-CC	70.66	71.11	F	M	F				C	F							R			C	R				R	C	F	F	F	F		F			F	R	R			R		F	A			R	C		R		R	
9H-CC	80.14	80.64	R	M	F				R											R					R			F	A			R	F							R		R	A			C			R	F	
10H-CC	87.98	88.36	C	M-G	R				C											F		R			C	R			R	R	F		R						R			C	A		C	C	C		F	F		F	R	
11H-CC	98.1	98.49	C	M-G	C				F						R			R	R	C			F			R			C			R					R			F		R	F	A		R	F	F		C			F	R	
12H-CC	108.16	108.53	C	M-G	C				R						R										C			R	F				R	R									D		F				C				R	*Proboscia curvirostris* (NPD11)
13H-CC	118.62	118.98	A	G	C				C		F				F	R			C	C			F		F	C	F	F	C		F				R			R	R		F	F			F			C	R			R	R	
14H-CC	127.67	128.12	F	M-G	R	R			R					R	R				R	C					C	C	R		C							F			R			R	A			F			C		R	R	F	
15H-CC	137.76	138.09	F	M	F	R			C	C				F				R	F	F	R			R	R	F	R	F	A	R					R			F	R			C			C			R	F	R	
16H-CC	146.99	147.43	F	M	F		R		C	R	F				F		R			F					C	F		R	A	R						R						C	C						C		R	

Notes: Abundance: D = dominant, A = abundant, C = common, F = few, R = rare. Preservation: G = good, M = moderate.

Table T9. Diatom range chart, Hole U1345C. (See table notes.)

Core, section	Depth (mbsf) Top	Depth (mbsf) Bottom	Abundance	Preservation	*Actinocyclus curvatulus*	*Actinocyclus ochotensis*	*Actinoptychus senarius*	*Asteromphalus brookei*	*Aulacoseira* spp.	*Bacterosira fragilis*	*Chaetoceros furcellatum* spores	*Coscinodiscus marginatus*	*Coscinodiscus oculus-iridis*	*Cyclotella* spp.	*Cymbella* spp.	*Delphineis kippae*	*Delphineis surirella*	*Detonula confervacea*	*Diploneis* spp.	*Eunotia* spp.	*Fragilaria* spp.	*Fragilariopsis cylindrus*	*Fragilariopsis oceanica*	*Fragilariopsis* spp.	*Gomphonema* spp.	*Meridion* spp.	*Navicula* spp.	*Neodenticula seminae*	*Nitzschia* spp.	*Odontella aurita*	*Paralia sol*	*Paralia sulcata*	*Pinnularia* spp.	*Porosira glacialis*	*Proboscia barboi*	*Proboscia curvirostris*	*Rhizosolenia hebetata* f. *hebetata*	*Rhizosolenia hebetata* f. *hiemalis*	*Rhizosolenia hebetata* f. *semispina*	*Rhizosolenia* spp.	*Thalassionema nitzschioides*	*Thalassiosira antarctica* spores	*Thalassiosira* cf. *leptopus*	*Thalassiosira eccentrica*	*Thalassiosira gravida*	*Thalassiosira hyalina*	*Thalassiosira jouseae*	*Thalassiosira latimarginata* s.l.	*Thalassiosira leptopus*	*Thalassiosira nordenskioeldii*	*Thalassiosira oestrupii*	*Thalassiosira* spp.	*Thalassiothrix longissima*	Diatom zone (NPD) in Yanagisawa and Akiba (1998)
323-U1345C-																																																					
1H-CC	5.86	5.96	C	G						C	C		R		R	R	F	R				R	C					F	C	R			C							R	C	R		A	R		R			R		F			
2H-CC	15.59	15.82	F	M-G	F		F			F	F						F						F	R				F	F		F	A							F	A					C	R		R	R			
3H-CC	25.38	25.66	F	M-G	C					C	C		R				F		R		R		F				F	F	R	C	C	F								A				C	F		F			
4H-CC	34.77	35.14	C	M-G	C					C			F				C					F	F				R	R	F		A	C								R	C				R		C	F		R		*Neodenticula seminae* (NPD12)
5H-CC	43.62	44.04	C	M	C					F	F				R												R	C	R	R			R	F					R	A					A		F	R			
6H-CC	53.47	53.87	C	M	C					F													F						R		A	F								A					F					
7H-CC	62.54	63.21	C	M						C						F								F				F	C		A									A				R		F	R			
8H-CC	72.13	72.6	C	M-G	C		R			C	C	F	R					R										F	F	R	F	C		R	R	C	F		F		A		F			C		F	R			
9H-CC	81.73	82.14	C	M-G	C					C	F											F	C	C		R		C	F	F				F		F			F		F	A				C	F	F	F	R		
10H-CC	91.53	91.91	C	M-G						F				R									R					R	F			R								R		C		R			R						
11H-CC	101.23	101.33	C	M-G	C					R	R				R		F							F					F	C	R	C	C	R							F	A					F		F			
12H-CC	110.73	111.08	F	M	R				R	C		F	F	F	F				R		F	C	R	R				F	F	F	R	C	F	R		C	R		R	R	A			R	F	F	F		R	F		R	*Proboscia curvirostris* (NPD11)
13H-CC	118.77	119.16	F	M	F					F	C	R				F	R					R	C		F		R	F	C	R	R								C	A		R	F			F						
14H-CC	129.52	129.85	F	M	A	R		R		A	R						R			F		R	F					F	C	R					F					F	C			R		R	F			F		
15H-CC	139.46	140.05	C	M	C	R				C	R					F		R					F						C	C	F				F			R			A			R	F	F			F	F		

Notes: Abundance: A = abundant, C = common, F = few, R = rare. Preservation: G = good, M = moderate.

Table T10. Diatom range chart, Hole U1345D. (See table notes.)

Core, section	Depth (mbsf) Top	Depth (mbsf) Bottom	Abundance	Preservation	*Actinocyclus curvatulus*	*Actinocyclus oculatus*	*Amphora* spp.	*Aulacoseira* spp.	*Bacterosira fragilis*	*Cocconeis costata*	*Cocconeis vitrea*	*Coscinodiscus marginatus*	*Coscinodiscus oculus-iridis*	*Delphineis* cf. *angustata*	*Delphineis kippae*	*Delphineis surirella*	*Detonula confervacea*	*Diploneis* spp.	*Eunotia* spp.	*Fragilaria* sp.	*Fragilariopsis cylindrus*	*Fragilariopsis oceanica*	*Fragilariopsis* spp.	*Gonphonema* spp.	*Navicula distans*	*Navicula* spp.	*Neodenticula seminae*	*Nitzschia* spp.	*Odontella aurita*	*Paralia sol*	*Paralia sulcata*	*Pinnularia* spp.	*Porosira glacialis*	*Proboscia barboi*	*Proboscia curvirostris*	*Rhabdonema* spp.	*Rhizosolenia hebetata* f. *hebetata*	*Rhizosolenia hebetata* f. *hiemalis*	*Rhizosolenia hebetata* f. *semispina*	*Rhizosolenia* spp.	*Rhizosolenia styliformis*	*Stephanopyxis turris*	*Thalassionema nitzschioides*	*Thalassiosira antarctica* spores	*Thalassiosira gravida*	*Thalassiosira hyalina*	*Thalassiosira jouseae*	*Thalassiosira lacustris*	*Thalassiosira latimarginata* s.l.	*Thalassiosira nordenskioeldii*	*Thalassiosira* spp.	*Thalassiothrix longissima*	Diatom zone (NPD) in Yanagisawa and Akiba (1998)
323-U1345D-																																																						
1H-CC	9.47	9.76	C-A	M	F									F		C						R							C	C	R													A	F	R			C			F	
2H-CC	19.03	19.23	C	P-M	F				F												F	C			R	F	F		R	R	F				R								A	F	R			C				
3H-CC	28.85	29.19	F	P	R		F	R	F				R				R	R		R		C			R	R	F		F	F						F	R				R	A		F			C	R		R	*Neodenticula seminae* (NPD12)
4H-CC	38.37	38.68	C	M	F											C		R			F	C			R		C	R	C	C		R										A	R	F			C	R			
5H-CC	47.20	47.54	A	M-G	F				F			F					F	R			C	C				F	C	C	F			R					F		R	F	A	F	R			C			R	
7H-CC	65.78	66.36	C	M					C	R	R	F		F		F	R	R			F	C	C			R	R	F	C	C		R				F					C	R	R	F				F	R	
8H-CC	73.06	73.32	C	M	F				F	F					R	F					C	C	R		R	R	F		F	F	R	F		R		C	R				A			R		F	R	F	R	
10H-CC	93.00	93.47	C	P-M	F				F							R					R	C						F	R	F	F				R		F				A	R		F			C			R	
11H-CC	102.35	102.77	F-C	P					F							F	R					C			R			F	R	C	C				R		F	R	R	C				F	R		F	C	F	F	
12H-CC	111.81	112.03	C	M	C	R			R			R					R					F					F	R		F	C					R						A	C	R	C		C	R				*Proboscia curvirostris* (NPD11)
13H-CC	122.13	122.65	C	M	F				C					F		R	F		R		C	C					F	F		C	C				R		F				A	F	F	C		F				R	
15H-CC	131.48	141.06	C	M	F				R			F				F	R		F			F					R	R	F	F					F		R	R	R		A	F		R		C				R	
16H-CC	140.71	150.51	C	M-G	R				C					R	R	R			R		F	C	R				F	F	R		A			R						F	A			F		F	F	C			

Notes: Abundance: A = abundant, C = common, F = few, R = rare. Preservation: G = good, M = moderate, P = poor.

Table T11. Diatom range chart, Hole U1345E. (See table notes.)

Core, section	Depth (mbsf) Top	Depth (mbsf) Bottom	Abundance	Preservation	*Actinocyclus curvatulus*	*Amphora* spp.	*Aulacoseira* spp.	*Bacterosira fragilis*	*Coscinodiscus marginatus*	*Delphineis* cf. *angustata*	*Detonula confervacea*	*Eunotia* spp.	*Fragilariopsis cylindrus*	*Fragilariopsis oceanica*	*Neodenticula seminae*	*Nitzschia* spp.	*Odontella aurita*	*Paralia sol*	*Paralia sulcata*	*Porosira glacialis*	*Proboscia curvirostris*	*Rhizosolenia hebetata* f. *hebetata*	*Rhizosolenia styliformis*	*Stephanopyxis* spp.	*Stephanopyxis turris*	*Thalassionema nitzschioides*	*Thalassiosira antarctica* spores	*Thalassiosira gravida*	*Thalassiosira hyalina*	*Thalassiosira jouseae*	*Thalassiosira lacustris*	*Thalassiosira latimarginata* s.l.	*Thalassiosira nordenskioeldii*	*Thalassiosira* spp.	*Thalassiothrix longissima*	Diatom zone (NPD) in Yanagisawa and Akiba (1998)
323-U1345E-																																			
2H-CC	15.46	15.68	F	M	R	R		C						F	F	F			C							C	A				F				*Neodenticula seminae* (NPD12)
8H-CC	75.00	75.46	F	M	R	R		C				R	R	C	F	C	C		F			R					A		R		C	R	F		
9H-CC	84.02	84.55	C	M				C							C		R						R				A	F	R	A		C	R	F		
10H-CC	93.56	93.99	A	G	F			F		R	R			F	R		R		F	C	R				R	F	A	C		F		F		F	F	*Proboscia curvirostris* (NPD11)
11H-CC	102.92	103.44	C	M	C	F			R		R	R	R	C	C			C				F		F			A	R		R	R	C		R		
13H-CC	121.78	121.88	A	M-G				C		R	R		F	C	R	F			C	R			R			R	A	R	F	C	R	C		C		
15H-CC	141.41	141.62	A	M-G	F		R	F	R		R		F	F	F	R		R	C		R	R		R		F	A	C		R		C		F		

Notes: Abundance: A = abundant, C = common, F = few, R = rare. Preservation: G = good, M = moderate.

Table T12. Silicoflagellate range chart, Hole U1345A. (See table notes.)

Core, section	Depth (mbsf) Top	Depth (mbsf) Bottom	Abundances	Preservation	Silicoflagellates: Aberrant silicoflagellates	*Dictyocha subarctios*	*Distephanus medianoctisol*	*Distephanus medianoctisol**	*Distephanus octangulatus*	*Distephanus octonarius*	*Distephanus speculum*	*Distephanus speculum**	Zone in Ling (1992)
323-U1345A-													
1H-CC	4.25	4.39	A	G	R	R	T		C		C	R	
2H-CC	13.98	14.09	T	G						T			
3H-CC	23.61	23.92	B										
4H-CC	33.2	33.44	F	G							R	R	*Distephanus octangulatus*
5H-CC	42.51	42.95	C	G							C	R	
6H-CC	51.1	51.61	R	M						T	T		
7H-CC	61.33	61.84	B										
8H-CC	70.66	71.11	B										
9H-CC	80.14	80.64	R	M						R			
10H-CC	87.98	88.36	C	G			R		C	C	F	T	
11H-CC	98.1	98.49	T	G							T		
12H-CC	108.16	108.53	C	G	T		T		R	T	F	F	
13H-CC	118.62	118.98	A	G					F	F	C		*Distephanus octonarius*
14H-CC	127.67	128.12	R	G				T		R	T		
15H-CC	137.76	138.09	B										
16H-CC	146.99	147.43	C	G	T		C	R		R		R	

Notes: * = with short radial spines. Abundance: A = abundant, C = common, F = few, R = rare, T = trace, B = barren. Preservation: G = good, M = moderate.

Table T13. Radiolarian datum events, Holes U1345A, U1345B, U1345C, U1345D, and U1345E. (See table note.)

Zone	Marker species	Age (Ma)	Hole U1345A				Hole U1345B				Hole U1345C			
			Core, section		Depth (mbsf)		Core, section		Depth (mbsf)		Core, section		Depth (mbsf)	
			Top	Bottom	Top	Bottom	Top	Bottom	Top	Bottom	Top	Bottom	Top	Bottom
Botryostrobus aquilonaris	T *Lychnocanoma nipponica sakaii*	0.05	2H-CC	3H-CC	14.09	23.92	Top	1H-CC	0.00	9.75	1H-CC	2H-CC	5.96	15.82
	T *Amphimelissa setosa*	0.07–0.09	4H-CC	5H-CC	33.44	42.95								
	T *Spongodiscus* sp.	0.28–0.32	9H-CC	10H-CC	80.64	88.36					8H-CC	9H-CC	72.60	82.14
	T *Axoprunum acquilonium*	0.25–0.43	10H-CC	11H-CC	88.36	98.49					10H-CC	12H-CC	101.33	111.08

Note: T = top, B = bottom.

Zone	Marker species	Age (Ma)	Hole U1345D				Hole U1345E			
			Core, section		Depth (mbsf)		Core, section		Depth (mbsf)	
			Top	Bottom	Top	Bottom	Top	Bottom	Top	Bottom
Botryostrobus aquilonaris	T *Lychnocanoma nipponica sakaii*	0.05	1H-CC	2H-CC	9.76	19.23	2H-CC	3H-CC	15.68	27.86
	T *Amphimelissa setosa*	0.07–0.09								
	T *Spongodiscus* sp.	0.28–0.32	8H-CC	9H-CC	73.32	83.52	8H-CC	9H-CC	75.46	84.55
	T *Axoprunum acquilonium*	0.25–0.43	11H-CC	12H-CC	102.77	112.03	9H-CC	10H-CC	84.55	93.99

Table T14. Radiolarian range chart, Holes U1345A, U1345B, U1345C, U1345D, and U1345E. (See table notes.) (Continued on next page.)

Core, section	Depth (mbsf) Top	Depth (mbsf) Bottom	Abundance	Preservation	*Actinomma boreale*	*Actinomma medianum*	*Amphimelissa setosa*	*Axoprunum acquilonium*	*Botryostrobus aquilonaris*	*Ceratospyris borealis*	*Collosphaera pyloma*	*Cycladophora cornutoides*	*Cycladophora cosma*	*Cycladophora davisiana*	*Cycladophora sakaii*	*Cyrtocapsella japonica*	*Dendrospyris sakaii*	*Dictyophimus bullatus*	*Dictyophimus hirundo*	*Eucyrtidium asanoi*	*Eucyrtidium inflatum*	*Eucyrtidium matuyamai*	*Lamprocyrtis heteroporos*	*Larcopyle butschlii*	*Lipmanella redondoensis*	*Lithelius barbatus*	*Lychnocanoma magnacornuta*	*Lychnocanoma nipponica sakaii*	*Lychnocanoma parallelipes*	*Phormostichoartus fistula*	*Porodiscus circularis*	*Sphaeropyle langii-robusta* group	*Spongodiscus* sp.	*Spongopyle osculosa*	*Spongotrochus glacialis*	*Spongurus pylomaticus*	*Stichocorys delmontensis*	*Stichocorys peregrina*	*Stylatractus universus*	*Stylochlamydium venustum*	*Stylodictya validispina*	*Thecosphaera akitaensis*
323-U1345A-																																								
1H-CC	4.29	4.39	F	G						F				F																								F	F	
2H-CC	13.98	14.09	F	M						F																						F			F					F	
3H-CC	23.82	23.92	F	M						F																	F							F					F	F	
4H-CC	33.34	33.44	F	M					F	F				F									F				C												F	F	
5H-CC	42.85	42.95	F	M			F			F													F				F												F		
6H-CC	51.51	51.61	F	M						F													F				F						F						F	C	
7H-CC	61.74	61.84	F	M						F													F				F							F					F	F	
8H-CC	71.01	71.11	F	M						F				F									F				F														
9H-CC	80.54	80.64	F	M						C																	F													F	
10H-CC	88.26	88.36	C	M					F	C				A									F				F						F						F	F	
11H-CC	98.39	98.49	F	M	F			F		F																					F	C								F	
12H-CC	108.43	108.53	F	M	F				F	F																	F					C		F						F	
13H-CC	118.88	118.98	F	M		F	F			F																	F					F							F	F	
14H-CC	128.02	128.12	F	M	F			F		F				F																		C								F	
15H-CC	137.99	138.09	F	M	F			F																								F		F							
16H-CC	147.33	147.43	F	M	F			F		F				F					F					F									F	F	F						
323-U1345B-																																									
1H-CC	9.65	9.75	F	G	F					F				F					F								F							F					F	F	
2H-CC	17.84	17.99	C	G						C				F					F					F			C												F	F	
3H-CC	27.57	27.77	C	G						F				C										F			C							F					F	C	
4H-CC	37.08	37.33	C	G						C				C					F					F			A							F					F	C	
323-U1345C-																																									
1H-CC	5.86	5.96	C	G	C					C				A																									F	F	
2H-CC	15.72	15.82	F	M						C				C													C							F						F	
3H-CC	25.56	25.66	C	M						C				F					F								C													F	
4H-CC	35.04	35.14	F	M						F				F					F								F														
5H-CC	43.94	44.04	C	M						C				C					F								F													F	
6H-CC	53.77	53.87	F	M						C									F					F			F													F	
7H-CC	63.11	63.21	C	M						C				A					C					F			F												F	F	
8H-CC	72.5	72.6	F	M	F					F				F										F			F														
9H-CC	82.04	82.14	C	G						C				A					F					F			C													F	
10H-CC	91.81	91.91	C	M						C				F																			C							F	
11H-CC	101.23	101.33	F	M																													C							F	
12H-CC	110.98	111.08	C	M	F			F		F				C					F												F	A		F					F	
13H-CC	119.06	119.16	F	M	F					F				F																		C								
14H-CC	129.75	129.85	F	M	F					C				F																		C		F						
15H-CC	139.95	140.05	C	M	C					C				C																	F	C		F					F	
16H-CC	148.43	148.53	F	M	F					F																						F		F						

Table T14 (continued).

Core, section	Depth (mbsf) Top	Depth (mbsf) Bottom	Abundance	Preservation	*Actinomma boreale*	*Actinomma medianum*	*Amphimelissa setosa*	*Axoprunum acquilonium*	*Botryostrobus aquilonaris*	*Ceratospyris borealis*	*Collosphaera pyloma*	*Cycladophora cornutoides*	*Cycladophora cosma*	*Cycladophora davisiana*	*Cycladophora sakaii*	*Cyrtocapsella japonica*	*Dendrospyris sakaii*	*Dictyophimus bullatus*	*Dictyophimus hirundo*	*Eucyrtidium asanoi*	*Eucyrtidium inflatum*	*Eucyrtidium matuyamai*	*Lamprocyrtis heteroporos*	*Larcopyle butschlii*	*Lipmanella redondoensis*	*Lithelius barbatus*	*Lychnocanoma magnacornuta*	*Lychnocanoma nipponica sakaii*	*Lychnocanoma parallelipes*	*Phormostichoartus fistula*	*Porodiscus circularis*	*Sphaeropyle langii-robusta* group	*Spongodiscus* sp.	*Spongopyle osculosa*	*Spongotrochus glacialis*	*Spongurus pylomaticus*	*Stichocorys delmontensis*	*Stichocorys peregrina*	*Stylatractus universus*	*Stylochlamydium venustum*	*Stylodictya validispina*	*Thecosphaera akitaensis*
323-U1345D-																																								
1H-CC	9.66	9.76	F	M	F					C				F										F										F					F	F
2H-CC	19.13	19.23	F	M	F					F				F									F				C						F	F					F	C
3H-CC	29.09	29.19	F	M						F				F													F							F					F	F
4H-CC	38.58	38.68	F	M	F																		F				F													
5H-CC	47.44	47.54	F	M						F													F				F					F								C
6H-CC	56.62	56.72	F	M						F																	F													F
7H-CC	66.26	66.36	F	M	F					F				F									F				F							F						F
8H-CC	73.22	73.32	F	M	F					F				F									F																	
9H-CC	83.42	83.52	C	M						F				F																		C	F	F					F	C
10H-CC	93.37	93.47	F	M	F					F				F																		F								
11H-CC	102.67	102.77	F	M	F					F				F																		F								F
12H-CC	111.93	112.03	C	P	F			F	F	F														F			F					C		F					F	F
13H-CC	122.55	122.65	F	M	F			F		F																						C								
14H-CC	131.71	131.81	F	M	F																											F								
15H-CC	140.96	141.06	F	M	F					F																						F		F						
16H-CC	150.41	150.51	F	M						F																						F		F						F
323-U1345E-																																								
1H-CC	8.17	8.27	F	M						C				C					F																				F	F
2H-CC	15.58	15.68	F	M						C				F					F																				F	F
3H-CC	27.76	27.86	C	M						F				A					F					F				C						F					C	C
4H-CC	37.37	37.47	C	M						F				C					C					F				C							F					F	F
5H-CC	46.49	46.59	F	M						F				C														F						F					F	F
6H-CC	56.44	56.54	F	M						F				F					F									F							F					
7H-CC	64.98	65.08	F	M						F				F					F					F				C											F	F
8H-CC	75.36	75.46	F	M						F				F					F									F												F
9H-CC	84.45	84.55	F	M					F	F				C										F				F					C						F	F
10H-CC	93.89	93.99	F	M				F		F				C					F					F				F					C			F				F
11H-CC	103.34	103.44	C	M	F			F		F		F		C					C													F	A	F		F				C
12H-CC	113.09	113.19	F	M					F																			F					F						F	
13H-CC	121.78	121.88	F	M						F				F					F														C							
14H-CC	132.04	132.14	F	M	F														F														F							
15H-CC	141.52	141.62	C	M						C		F		A					C														C		F					F
16H-CC	150.79	150.89	F	M						F				F										F									F		F					

Notes: Abundances: A = abundant, C = common, F = few, R = rare. Preservation: G = good, M = moderate, P = poor.

Table T15. Dinoflagellate cyst, pollen, and palynomorph range chart, Holes U1345A, U1345B, and U1345C. (See table notes.)

	Depth (mbsf)			Marine		Pollen and spores								Fresh water			Dinoflagellate cyst assemblages																	
Core, section	Top	Bottom	Preservation	Dinoflagellate cysts	Organic lining of foraminifers	*Picea*	*Pinus*	Pollen (herbs)	Pollen (shrubs)	Pollen (trees)	Total pollen	Spores of *Sphagnum*	Spores of pteridophytes	*Botryococcus* + *Pediastrum*	*Hallodinium*	Reworked palynomorphs	*Bitectatodinium tepikiense*	*Brigantedinium cariacoense*	*Brigantedinium simplex*	*Brigantedinium* spp.	*Echinidinium aculeatum*	*Impagidinium* spp.	*Islandinium* cf. *brevispinosum*	*Islandinium imnutum*	*Islandinium* morphotype *cesare*	*Operculodinium centrocarpum*	*Operculodinium centrocarpum* - Arctic morphotype	*Operculodinium centrocarpum* var. short processes	*Pentapharsodinium dalei*	*Polykrikos* - Arctic morphotype	*Polykrikos schwartzii*	*Protoperidinium americanum*	*Quinquecuspis concreta*	*Spiniferites elongatus*
323-U1345A-																																		
1H-CC	4.3	4.4	G	A	F	F		R	R	F	C	C	F	F		R		R	A	D		R		A		A		R				R		R
2H-CC	14.0	14.1	G	A	C	R	R	R		F	F	R	F	F		R		R	A	D	R			A	R	R								
3H-CC	23.8	23.9	G	C	F	C	R	R	R	C	C	F	C	F		R		F	A	D				A		R	R				R			
4H-CC	33.3	33.4	G	A	R	C	R		R	C	C	R	C			R	R	R	A	D				A		R								
5H-CC	42.9	43.0	G	A	C	F				C	C	R	R	F		R		R	F	A			R	D	R									
6H-CC	51.5	51.6	G	A	F	C	R	R	F	C	C	C	C	C		R		R	A	D				A		F		R						R
7H-CC	61.7	61.8	M	A	R	C	F			C	C	C	C	C		F		R	A	D				A		R								
8H-CC	71.0	71.1	G	C	R	R	R		R	F	F	F	R	R		R		R	A	D				R				R					R	
9H-CC	80.5	80.6	G	C	R	F			R	F	F	F		R		R		F	A	D			R	A										
10H-CC	88.3	88.4	G	C	C	C	R	R	R	C	C	F	C	C		R		R	D	D				R					R					R
11H-CC	98.4	98.5	M	C	R	C				C	C		R	F		R		R	A	D				R										
12H-CC	108.4	108.5	G	C	R	F			R	F	F	R	R	R				R	A	D				D									R	
13H-CC	118.9	119.0	G	A		F		R		F	C	C	F	F				F	D	D				R									R	
14H-CC	128.0	128.1	M	C	R	C				C	C		F	R		R		R	A	D				A										
15H-CC	138.0	138.1	G	A	F	C				C	C	C	F	F				F	A	D				A		R							F	
16H-CC	147.3	147.4	G	C	C	C	R			C	C		F	F		C			A	D				F		F	R	R						
323-U1345B-																																		
Mudline			G	A	C	C		R	R	C	C	R	R	R	C			R	R	A	R			D		R	R					R		
323-U1345C-																																		
2H-CC	15.7	15.8	G	C	F	R				R	R	R	R	R		R	R		A	D				A						F				
4H-CC	35.0	35.1	G	A	C	R				R	R		R	F		R		R	A	D				A									F	
6H-CC	53.8	53.9	G	C	R	R			R	R	F		R	R		R		R	F	D				A										
8H-CC	72.5	72.6	M	C	R	R				R	R		R			R			A	D		R				F								
10H-CC	91.8	91.9	G	C	R	R	R		R	R	R	R	R	R			R	F	A	D			R	A										
12H-CC	111.0	111.1	M	F	R	C	F		R	C	C	C	R	F		R		F	A	D				A										
14H-CC	129.8	129.9	G	A		R				R	R	R	R	R		C			F	A				D									R	
16H-CC	148.4	148.5	M	C	R	C			R	C	C	F		R		F		F	A	D				A										

Notes: Absolute abundance: A = abundant (>2000/cm^3), C = common (>200/cm^3), F = few (>100/cm^3), R = rare (<100/cm^3). Relative abundance of dinoflagellate cysts: D = dominant (>30%), A = abundant (>10%), F = few (>5%), R = rare (<5%), P = occurrence (when counts are <20). Preservation: G = good, M = moderate, P = poor.

Table T16. Moisture and density, Hole U1345A. (See table note.)

Core, section	Depth (mbsf)	Density (g/cm^3)			Void ratio	Water content (%)	Porosity (%)
		Dry grain	Wet bulk	Dry bulk			
323-U1345A-							
1H-2	1.8	2.92	1.68	1.02	1.94	66.04	38.92
1H-3	3.3	2.72	1.59	0.94	2.00	66.72	41.34
2H-2	6.2	2.81	1.57	0.87	2.35	70.11	44.26
2H-4	9.2	2.82	1.79	1.23	1.34	57.30	31.55
2H-6	12.2	NM	1.51	0.93	1.46	59.32	38.71
3H-2	15.7	2.83	1.79	1.22	1.37	57.73	31.84
3H-4	18.7	2.87	1.69	1.05	1.81	64.42	37.71
3H-6	21.7	2.75	1.72	1.12	1.50	60.04	34.53
4H-2	25.2	2.75	1.75	1.18	1.37	57.85	32.58
4H-4	28.2	2.45	1.66	1.12	1.23	55.15	32.75
4H-6	31.2	2.74	1.88	1.38	1.02	50.51	26.56
5H-2	34.7	2.71	1.81	1.28	1.15	53.56	29.23
5H-4	37.7	2.76	1.67	1.04	1.73	63.31	37.52
5H-6	40.7	2.73	1.64	1.01	1.79	64.16	38.62
6H-2	44.2	2.77	1.79	1.24	1.28	56.23	31.00
6H-4	47.2	NM	1.51	1.04	0.90	47.47	31.16
6H-6	50.2	2.73	1.73	1.15	1.44	58.94	33.69
7H-2	52.6	2.81	1.80	1.23	1.32	56.97	31.32
7H-4	55.4	2.83	1.79	1.21	1.39	58.13	32.14
7H-6	58.4	2.75	1.76	1.18	1.38	57.97	32.61
8H-2	63.0	2.73	1.87	1.37	1.03	50.84	26.88
8H-4	66.0	2.69	1.84	1.34	1.04	51.08	27.40
8H-6	69.0	2.75	1.84	1.31	1.13	53.15	28.59
9H-2	71.7	2.74	1.76	1.20	1.34	57.28	32.10
9H-4	74.7	2.78	1.75	1.17	1.43	58.87	33.20
9H-6	77.7	2.72	1.77	1.21	1.29	56.39	31.55
10H-2	82.3	NM	1.37	NM	1.05	51.14	36.88
11H-2	91.1	2.83	2.02	1.58	0.81	44.86	21.92
11H-4	94.1	2.78	1.84	1.30	1.18	54.04	29.05
11H-6	97.1	2.75	1.80	1.26	1.22	55.03	30.13
12H-2	100.1	2.75	1.80	1.26	1.23	55.20	30.24
12H-4	103.1	2.71	1.77	1.22	1.26	55.79	31.09
12H-6	106.1	2.73	1.74	1.17	1.39	58.12	32.94
13H-2	110.1	2.70	1.72	1.15	1.41	58.58	33.57
13H-4	113.1	2.73	1.90	1.43	0.94	48.49	25.15
13H-6	116.3	2.65	1.68	1.08	1.51	60.17	35.46
14H-2	119.2	2.76	1.80	1.26	1.24	55.32	30.31
14H-4	122.2	2.70	1.80	1.26	1.18	54.09	29.76
14H-6	125.2	2.74	1.93	1.46	0.91	47.65	24.44
15H-2	128.6	2.73	1.73	1.15	1.44	58.95	33.66
15H-4	131.6	2.78	1.87	1.35	1.10	52.35	27.72
15H-6	134.6	2.76	1.79	1.23	1.29	56.38	31.19
16H-2	138.6	2.80	2.09	1.69	0.68	40.51	19.18
16H-4	141.4	2.69	1.72	1.15	1.40	58.30	33.46
16H-6	144.3	2.78	1.79	1.22	1.32	56.96	31.51

Note: NM = no measurement.

Table T17. Affine table indicating the amount that each core in each hole needs to be offset in order to construct a continuous record, Site U1345. (**Continued on next page.**)

Core	Depth (mbsf) Top	Depth (mbsf) Bottom	Offset (m)	Depth CCSF-A (m) Top	Depth CCSF-A (m) Bottom	Recovered (m)	Recovery (%)
323-U1345A-							
1H	0.00	4.39	0.00	0.00	4.39	4.39	100
2H	4.40	14.09	0.04	4.44	14.13	9.69	102
3H	13.90	23.92	0.01	13.91	23.93	10.02	105
4H	23.40	33.44	0.98	24.38	34.42	10.04	106
5H	32.90	42.95	1.49	34.39	44.44	10.05	106
6H	42.40	51.61	3.12	45.52	54.73	9.21	97
7H	51.90	61.84	4.11	56.01	65.95	9.94	105
8H	61.40	71.11	5.54	66.94	76.65	9.71	102
9H	70.90	80.64	5.79	76.69	86.43	9.74	103
10H	80.40	88.36	7.46	87.86	95.82	7.96	84
11H	89.90	98.49	9.57	99.47	108.06	8.59	90
12H	99.40	108.53	9.46	108.86	117.99	9.13	96
13H	108.90	118.98	11.20	120.10	130.18	10.08	106
14H	118.40	128.12	12.40	130.80	140.52	9.72	102
15H	127.90	138.09	13.68	141.58	151.77	10.19	107
16H	137.40	147.43	15.00	152.40	162.43	10.03	106
323-U1345B-							
1H	0.00	8.25	0.20	0.20	8.45	8.25	101
2H	8.20	17.99	0.21	8.41	18.20	9.79	103
3H	17.70	27.77	0.78	18.48	28.55	10.07	106
4H	27.20	37.33	1.27	28.47	38.60	10.13	107
323-U1345C-							
1H	0.00	5.96	0.09	0.09	6.05	5.96	99
2H	6.00	15.82	0.97	6.97	16.79	9.82	103
3H	15.50	25.66	2.03	17.53	27.69	10.16	107
4H	25.00	35.14	2.96	27.96	38.10	10.14	107
5H	34.50	44.04	3.41	37.91	47.45	9.54	100
6H	44.00	53.87	4.93	48.93	58.80	9.87	104
7H	53.50	63.21	6.08	59.58	69.29	9.71	102
8H	63.00	72.60	7.46	70.46	80.06	9.60	101
9H	72.50	82.14	8.55	81.05	90.69	9.64	101
10H	82.00	91.91	9.76	91.76	101.67	9.91	104
11H	91.50	101.33	10.67	102.17	112.00	9.83	103
12H	101.00	111.08	11.62	112.62	122.70	10.08	106
13H	110.50	119.16	12.86	123.36	132.02	8.66	91
14H	120.00	129.85	13.92	133.92	143.77	9.85	104
15H	129.50	140.05	15.53	145.03	155.58	10.55	111
16H	139.00	148.53	16.93	155.93	165.46	9.53	100
323-U1345D-							
1H	0.00	9.76	1.61	1.61	11.37	9.76	103
2H	9.50	19.23	2.28	11.78	21.51	9.73	102
3H	19.00	29.19	2.75	21.75	31.94	10.19	107
4H	28.50	38.69	4.22	32.72	42.91	10.18	107
5H	38.00	47.54	5.47	43.47	53.01	9.54	100
6H	47.50	56.72	6.63	54.13	63.35	9.22	97
7H	57.00	66.36	7.40	64.40	73.76	9.36	99
8H	66.50	73.32	7.27	73.77	80.59	6.82	91
9H	74.00	83.52	9.83	83.83	93.35	9.52	100
10H	83.50	93.47	10.36	93.86	103.83	9.97	105
11H	93.00	102.77	11.60	104.60	114.37	9.77	103
12H	102.50	112.03	13.04	115.54	125.07	9.53	100
13H	112.00	122.65	13.44	125.44	136.09	10.65	112
14H	121.50	131.81	14.64	136.14	146.45	10.31	109
15H	131.00	141.06	15.85	146.85	156.91	10.06	106
16H	140.50	150.51	17.49	157.99	168.00	10.01	105
323-U1345E-							
1H	0.00	8.27	–0.09	–0.09	8.18	8.27	101
2H	8.20	15.68	0.75	8.95	16.43	7.48	79
3H	17.70	27.86	1.00	18.70	28.86	10.16	107
4H	27.20	37.47	2.24	29.44	39.71	10.27	108
5H	36.70	46.59	3.49	40.19	50.08	9.89	104
6H	46.20	56.54	4.76	50.96	61.30	10.34	109
7H	55.70	65.08	6.02	61.72	71.10	9.38	99
8H	65.20	75.46	7.34	72.54	82.80	10.26	108

Table T17 (continued).

Core	Depth (mbsf) Top	Depth (mbsf) Bottom	Offset (m)	Depth CCSF-A (m) Top	Depth CCSF-A (m) Bottom	Recovered (m)	Recovery (%)
9H	74.70	84.55	8.50	83.20	93.05	9.85	104
10H	84.20	93.99	9.12	93.32	103.11	9.79	103
11H	93.70	103.44	10.52	104.22	113.96	9.74	103
12H	103.20	113.19	11.29	114.49	124.48	9.99	105
13H	112.70	121.88	12.04	124.74	133.92	9.18	97
14H	122.20	132.14	13.56	135.76	145.70	9.94	105
15H	131.70	141.62	14.31	146.01	155.93	9.92	104
16H	141.20	150.89	15.50	156.70	166.39	9.69	110

Table T18. Primary splice table, Site U1345.

Hole, core, section, interval (cm)	Depth mbsf	Depth CCSF-D (m)		Hole, core, section, interval (cm)	Depth mbsf	Depth CCSF-D (m)
323-				323-		
U1345A-1H-3, 30.7	3.31	3.31	Tie to	U1345D-1H-2, 19.7	1.70	3.31
U1345D-1H-6, 75.7	8.26	9.87	Tie to	U1345C-2H-2, 140.0	8.90	9.87
U1345C-2H-6, 41.1	13.91	14.88	Tie to	U1345D-2H-3, 9.4	12.59	14.88
U1345D-2H-6, 143.1	18.43	20.72	Tie to	U1345C-3H-3, 18.2	18.68	20.72
U1345C-3H-7, 55.3	25.05	27.09	Tie to	U1345A-4H-2, 120.7	26.11	27.09
U1345A-4H-6, 99.3	31.89	32.87	Tie to	U1345D-4H-1, 57.2	29.07	32.87
U1345D-4H-4, 131.4	34.31	38.11	Tie to	U1345A-5H-3, 72.9	36.63	38.11
U1345A-5H-6, 41.3	40.81	42.30	Tie to	U1345C-5H-3, 139.3	38.89	42.30
U1345C-5H-6, 61.3	42.61	46.02	Tie to	U1345A-6H-1, 50.0	42.90	46.02
U1345A-6H-6, 3.0	49.89	53.01	Tie to	U1345C-6H-4, 47.3	48.08	53.01
U1345C-6H-7, 28.8	52.40	57.32	Tie to	U1345D-6H-3, 19.7	50.70	57.32
U1345D-6H-6, 99.0	55.93	62.56	Tie to	U1345C-7H-3, 65.1	56.48	62.56
U1345C-7H-6, 18.7	60.39	66.46	Tie to	U1345D-7H-3, 4.7	59.07	66.46
U1345D-7H-6, 103.2	64.49	71.89	Tie to	U1345C-8H-2, 70.4	64.42	71.89
U1345C-8H-6, 141.2	71.10	78.57	Tie to	U1345A-9H-2, 136.4	72.77	78.57
U1345A-9H-7, 49.0	79.32	85.11	Tie to	U1345C-9H-4, 8.0	76.56	85.11
U1345C-9H-6, 84.2	80.24	88.79	Tie to	U1345D-9H-4, 114.8	78.97	88.79
U1345D-9H-6, 114.7	81.90	91.72	Tie to	U1345A-10H-3, 99.4	84.26	91.72
U1345A-10H-4, 48.8	85.23	92.69	Tie to	U1345C-10H-1, 93.0	82.93	92.69
U1345C-10H-3, 117.3	85.71	95.47	Tie to	U1345D-10H-2, 28.5	85.10	95.47
U1345D-10H-7, 54.5	92.65	103.02	Tie to	U1345A-11H-3, 115.4	93.45	103.02
U1345A-11H-6, 23.9	97.04	106.60	Tie to	U1345D-11H-2, 98.0	95.00	106.60
U1345D-11H-7, 5.7	101.48	113.08	Tie to	U1345A-12H-4, 80.2	103.62	113.08
U1345A-12H-6, 138.2	107.14	116.60	Tie to	U1345C-12H-3, 148.4	104.98	116.60
U1345C-12H-7, 67.7	110.07	121.68	Tie to	U1345A-13H-2, 69.8	110.49	121.68
U1345A-13H-4, 126.8	114.06	125.25	Tie to	U1345C-13H-2, 55.6	112.40	125.25
U1345C-13H-5, 96.8	117.29	130.15	Tie to	U1345D-13H-4, 97.7	116.71	130.15
U1345D-13H-8, 83.0	122.06	135.50	Tie to	U1345A-14H-4, 125.0	123.10	135.50
U1345A-14H-7, 88.3	127.23	139.64	Tie to	U1345D-14H-3, 65.9	125.00	139.64
U1345D-14H-7, 4.0	130.60	145.50	Tie to	U1345A-15H-4, 6.0	137.32	145.00
U1345A-15H-7, 91.2	136.67	150.36	Tie to	U1345D-15H-3, 50.2	134.50	150.36
U1345D-15H-7, 72.0	138.66	156.51	Tie to	U1345C-16H-2, 0.0	139.58	156.51
U1345C-16H-5, 117.8	145.21	162.14	Tie to	U1345D-16H-4, 55.4	144.64	162.14

Table T19. Secondary splice table indicating tie points between holes, Site U1345. Sampling along the splice should be used to construct a continuous record.

Hole, core, section, interval (cm)	Depth mbsf	Depth CCSF-A (m)		Hole, core, section, interval (cm)	Depth mbsf	Depth CCSF-A (m)
323-				323-		
U1345C-1H-2, 54.5	2.05	2.14	Tie to	U1345E-1H-2, 63.1	2.13	2.04
U1345E-1H-6, 39.7	7.90	7.80	Tie to	U1345A-2H-3, 36.5	7.77	7.80
U1345A-2H-5, 24.7	10.65	10.68	Tie to	U1345E-2H-2, 23.0	9.93	10.68
U1345E-2H-5, 86.1	15.06	15.82	Tie to	U1345A-3H-2, 40.7	15.81	15.82
U1345A-3H-4, 44.1	18.84	18.85	Tie to	U1345E-3H-1, 14.7	17.85	18.85
U1345E-3H-7, 21.8	26.92	27.92	Tie to	U1345D-3H-5, 17.0	25.17	27.92
U1345D-3H-6, 130.3	27.80	30.55	Tie to	U1345E-4H-1, 111.5	28.32	30.55
U1345E-4H-7, 33.9	36.54	38.78	Tie to	U1345D-4H-5, 6.0	34.56	38.78
U1345D-4H-6, 77.2	36.77	40.99	Tie to	U1345E-5H-2, 11.	37.50	40.99
U1345E-5H-7, 100	45.88	49.37	Tie to	U1345D-5H-5, 100.9	43.90	49.37
U1345D-5H-7, 103.1	46.92	52.39	Tie to	U1345E-6H-2, 16.4	47.63	52.39
U1345E-6H-6, 132.7	54.80	59.56	Tie to	U1345A-7H-4, 33.3	55.44	59.56
U1345A-7H-6, 41.4	58.52	62.64	Tie to	U1345E-7H-2, 12.0	56.62	62.64
U1345E-7H-6, 135	63.85	69.87	Tie to	U1345A-8H-3, 8.8	64.33	69.87
U1345A-8H-5, 142.7	68.67	74.20	Tie to	U1345E-8H-2, 16.8	66.87	74.20
U1345E-8H-7, 55.9	74.74	82.08	Tie to	U1345C-9H-2, 4.4	73.52	82.08
U1345C-9H-3, 49.7	75.48	84.03	Tie to	U1345E-9H-2, 7.3	75.52	84.03
U1345E-9H-7, 120.4	83.93	92.44	Tie to		GAP	92.44
	GAP	93.38	Tie to	U1345E-10H-1, 5.4	84.25	93.38
U1345E-10H-7, 70.1	93.50	102.62	Tie to	U1345C-11H-1, 45.0	91.95	102.62
U1345C-11H-4, 8.3	95.65	106.33	Tie to	U1345E-11H-2, 60.5	95.81	106.33
U1345E-11H-7, 29.4	102.69	113.21	Tie to	U1345C-12H-1, 59.6	101.60	113.21
U1345C-12H-3, 134.9	104.85	116.47	Tie to	U1345E-12H-2, 114.3	105.17	116.47
U1345E-12H-7, 125.3	112.64	123.94	Tie to	U1345C-13H-1, 57.8	111.08	123.94
U1345C-13H-2, 72.1	112.56	125.42	Tie to	U1345E-13H-2, 4.0	113.38	125.42
U1345E-13H-7, 89.5	121.60	133.63	Tie to	U1345A-14H-3, 88.3	121.23	133.63
U1345A-14H-4, 48.2	122.33	134.73	Tie to	U1345C-14H-2, 4.4	120.81	134.73
U1345C-14H-4, 42.5	124.13	138.04	Tie to	U1345E-14H-3, 20.1	124.48	138.04
U1345E-14H-8, 50.7	131.74	145.30	Tie to	U1345C-15H-1, 26.8	129.77	145.30
U1345C-15H-3, 53.8	132.19	147.72	Tie to	U1345E-15H-2, 17.7	133.41	147.72
U1345E-15H-6, 137.8	140.61	154.92	Tie to	U1345A-16H-3, 39.5	139.93	154.92
U1345A-16H-5, 111.7	143.44	158.43	Tie to	U1345E-16H-2, 23.3	142.93	158.43

Table T20. Temperature data, Site U1345. (See table note.)

Core	Depth (mbsf)	Thermal resistance (m^2K/W)	T (°C)	T_s (°C)
323-U1345A-				
5H	42.4	42.02	4.92	3.10
8H	70.9	69.30	6.36	3.15
12H	108.9	105.41	8.15	3.10

Note: T = formation temperature, T_s = seafloor temperature.